ナノ粉砕とバイオディーゼル製造用固体塩基触媒の開発に関する研究

Study on Nano-grinding and Development of Solid Base Catalyst for Biodiesel Production

Frisda Rimbun Panjaitan

Muroran Institute of Technology

2016

Contents

Chapter 1

Introduction

1-1 Biodiesel and challenges in green production

In the era of industrial development and rapid population growth, global energy consumption has increased dramatically. Accordingly, in 2015, 85.76% of the global energy consumption came from natural gas (24.36%), coal (28.93%) and liquids (32.45%, mainly oil, biofuels, gas-to-liquids and coal-to-liquids). The global energy consumption, which is reported by Portal in **Fig.1**, will keep rising till 2035, it is predicted that the use of these resources will reduce to 81.27%, among which 26.11% is supplied by natural gas, 26.14% by coal and 29.01% by liquid sources [**1**]. It should be highlighted that the use of biofuel will increase from 5.26% in 2015 to 13.02% in 2035 as shown in **Fig.2** [**2**]. According to International Energy Agency's (US EIA, Eurostat), among the biofuel, biodiesel, a mixture of methyl esters or ethyl esters of fatty acids, is the most popular alternative energy resource. Biodiesel can fulfill energy security needs without sacrificing engine`s operational performance. Currently, global biodiesel production has increased ten folds in the last decade [**3, 4**].

In particular, Indonesia government has announced the introduction of the Indonesia’s Biodiesel Mandate on late 2013, that by 2016 the proportion of biodiesel blending in gasoil is to be 20 % [**Table 1**]. It was applied to gasoil sold (price-subsidized and price-non subsidized) to transport, industries, and commercial sectors. Indonesia continues to revise the regulation to better intensify this huge biodiesel industry. Even more, Indonesian government has financed the mandate with a $50/MT levy imposed on crude palm oil (CPO) oil and palm oil product exports. The blending mandate may be supporting the local biodiesel industry in Indonesia.

Now on, Indonesia’s biodiesel sector is growing with total production capacity of 877 million liters in 2016 [**Table 2**] by increasing and intensified production and usage of palm oil-renewable energy source.

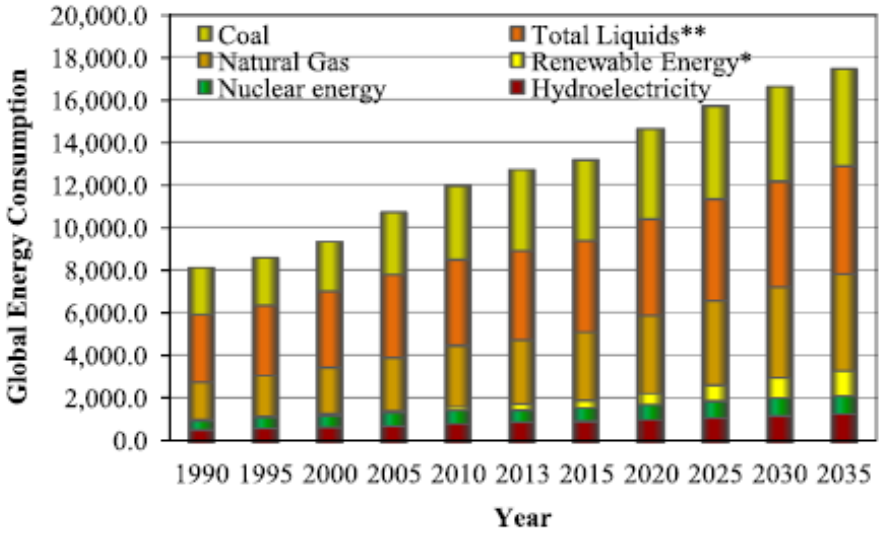

Fig.1 World energy consumption by source (1990-2035; MT of oil equivalent); *Includes oil, biofuels, gas-to-liquids and coal-to-liquids; **Includes wind power, solar electricity, and other renewables. Taken from **[1]**.

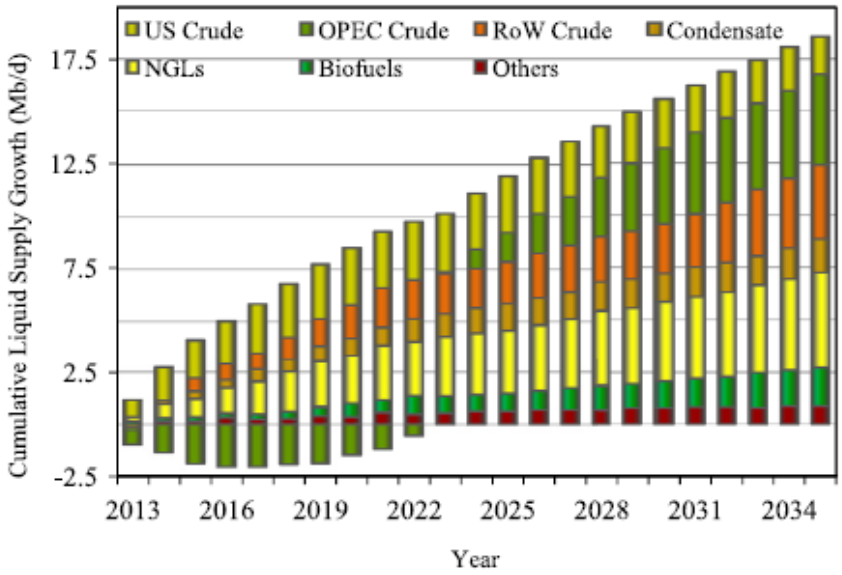

Fig.2 World liquid energy supply growth till 2035; *Includes gas-to-liquids, coal-to-liquids and refinery volume gain. Taken from **[2]**.

Table 1 Indonesia Biodiesel Mandatory Target as stated in Regulation 12/2015

Biodiesel (Minimum, %)				
Sector	2015	2016	2020	2025
Transportation, Public service obligation (PSO)	15	20	30	30
Transportation, Non-PSO	15	20	30	30
Industry	15	20	30	30
Electricity	25	30	30	30

Source: MEMR Regulation 12/2015 in [**5**].

Note: Public Service Obligation (PSO) refers to subsidized fuel for road vehicles. It is uniquely sold through Pertamina (Indonesian state-owned company). Non-PSO refers to unsubsidized fuel sold through private sector shops.

Amongst the renewable fuels, biodiesel has a significant position. It can be produced from widespread bio sources, such as vegetable oils, animal fats and algal lipids. Biodiesel is renewable, biodegradable, less environmental toxicity, superior combustion efficiency, and contributes to the reduction of most regulated exhaust emissions are the main advantages of biodiesel [**4, 6, 7**]. Moreover, biodiesel can either be used directly without major modification in diesel engines or blended with fossil diesel. Typically biodiesel blends are B-2, B-5, B-7, B-20 and B-100 where the number denotes the percentage of biodiesel in the blend e.g. B-2 indicates 2% biodiesel and 98% fossil diesel [**8**].

Generally, more than 95% of the world biodiesel is produced from edible oil. Rapeseed (84%) is the primary source of edible oil followed by sun flower oil (13%), palm oil (1%), soybean oil and others (2%). However, edible oils high raw material prices and competition with food caused the commercialization of biodiesel is difficult

due to its final cost, representing between 70% and 85% of the overall production cost of this energetic input [**7, 9**].

Table 2 Indonesia Biodiesel Production and Supply Statistics

Biodiesel (million Liters)								
Year	2009	2010	2011	2012	2013	2014	2015	2016
Production	330	740	1,800	2,200	2,800	3,000	1,180	2,450
Production capacity								
No. of biorefineries	20	22	22	26	26	26	27	28
Nameplate capacity	3,528	3,936	4,281	4,881	5,670	5,670	6,750	7,286
Capacity use (%)	9	19	42	45	49	53	17	34
Feedstock Use for Fuel (1,000 MT)								
CPO	304	680	1,656	2,024	2,576	2,760	1,086	2,254
Market Penetration (million Liters)								
Biodiesel Transportation	48	176	286	637	996	1,520	817	2,093
Diesel Transportation	22,877	25,172	24,772	27,714	27,950	26,437	26,142	26,220
Blend Rate (%)	0.2	0.7	1.2	2.3	3.6	5.7	3.1	8.0
Diesel Total Use	29,237	32,052	33,712	34,314	34,150	32,767	32,472	32,569

Source: Indonesia Biofuels Annual 2016 in [**5**].

Amongst the different possible options known for the conversion of oils to biodiesel, transesterification/esterification process has been frequently utilized, even applied in industry. The catalysts used for the transesterification process could be divided into two categories based on their active site: acid and base catalysts [**10**]. The mostly applied technologies for biodiesel production are based homogeneous base catalysis. Nonetheless, this process has some drawbacks such as highly sensitive to free fatty acids (FFA), and water content. In addition, homogeneous catalysts are usually difficult to be removed from the product stream and this will charge extra purification cost.

Nowadays, the use of heterogeneous catalysts is gaining attention due to non-toxic nature, ease of separation, reusability and the reaction conditions could be less drastic than the methanol supercritical process [**11, 12**]. In the past, the Institute Français du Petrole (IFP) developed great research in biodiesel commercial plant (160,000 t/y) based on the Hesterfip-H technology. The catalyst is mixed oxide of zinc and aluminum and operates at 200–250 °C. The catalyst does not require catalyst recovery and methyl ester yield very high, close to the theoretical value. The glycerol, as a side product, produced in high purity and is free from any salts contaminants [**11, 13**]. However, such a high temperature operation, the pressure operation also high, consequently the cost very high. Therefore, great research efforts have been underway recently to find the right catalysts without this severe operating conditions.

Generally, heterogeneous catalyst conversion rate is lower compared to homogeneous catalyst [**14**]. The main limitation of heterogeneous catalyst is the surface area to serve the reaction is not sufficient enough. This phenomenon raises some drawbacks such low reaction rate, requires long time to achieve the maximal biodiesel production, and requirement of high methanol to oil ratio. These limitations became a

bottleneck in their commercial application [**15, 16, 17**].

Many of studies reported in developing high catalytic activity of heterogeneous catalyst for transesterification reaction. Also many reviews which propose a lot of constructive suggestions and recommendations to improve the transesterification processes. CaO catalyst was the most emphasized to assess for the future perspectives of its use [**7, 10**]. CaO catalyst has high basicity, low solubility in organic solvents, available in a wide variety of sources, long service lifetime, and effective under mild reaction conditions [**18**]. From the environmental point of view, CaO catalyst has big potential as green catalyst. Green catalysis by solid base is a chemical philosophy that encourages the design of products and processes that reduce or eliminate the use and generation of hazardous substances [**19**].

1-2 Review of Preview Works

1-2-1 Transesterification of oil feedstock catalyzed by CaO

CaO transesterification catalyzed reaction contains a liquid-liquid-solid system reaction and reaction occurs on the surface of CaO [**16**]. A key point in this fact was mass transfer limitation in the initial stage of transesterification. This was the main reason why reaction rate of CaO inferior to homogeneous base catalyst. The transesterification reaction can be significantly enhanced by improving physicochemical properties of CaO, such as specific surface area (SSA), high basicity of the active sites on surface of catalyst and particle size. The larger SSA determines the number of molecules which are able approach the surface of catalyst and also improved mass-transfer characteristics for both reactants and products in the catalytic reaction. High basicity of the active sites of reaction (*or active phases on the surface of the catalyst*), easily accessible of reactants to functional of catalyst to start the reaction.

Catalyst particle size, provides shorter paths to access active sites for molecules, which reduces the internal diffusion significantly [**16**].

It is important to understanding the kinetic study and mechanism on the CaO-catalyzed transesterification. At the beginning of reaction, the transesterification depends on a rate on mass transfer of the reactants, because vegetable oil and methanol immiscible under the transesterifying condition. Latter, an increase in the reaction rate causes the shift in the rate determining step toward the chemical reaction controlled regime [**20, 21**].

When neat CaO is employed on transesterification, CaO is turned into calcium glyceroxide (CaDg) by combining with glycerol of the by-product. Kouzu et al. [**21, 22, 23, 24, 25**] reported only at the initial stage of the reaction CaO-based catalyst take a role as the solid base catalyst. Hence, mass transfer limitation determines by the physicochemical properties of CaO. In the later stage of transesterification, once the glycerol is formed, CaO-based catalyst is transformed into CaDg which is the true catalyst to govern the chemical reaction. Hence, how fast the transformation of CaO into CaDg determine the chemical reaction controlled regime. Leon-Reina and co-workers [**26**] later reported that CaDg catalyst has high catalytic activity compared to CaO-based catalyst as the presence of basic oxygen anion, formed due to the interruption of crystal structure at surface which can easily abstract proton from OH group of methanol and forms methoxide ion on the surface.

The particle size of the catalyst is one of the most important factors for their catalytic activity. When the particle is small the chemical reaction rate is increased since the diffusion forces would only be able to carry the product away from the surface of the catalyst particle. Many studies have confirmed that catalysts with a lower particle size and higher surface area accelerate reaction rates, due to an increased number of

molecules that have the minimum required energy for the reaction to occur. Zhao *et al*. [**16**] utilized a higher surface area (HSA) nano-CaO with 89.52 m^2/g of SSA, at 65 ^oC, 99.85% biodiesel yield was obtained at 2 h when 3 wt.% catalyst was used with 1 : 9 molar ratio oil to methanol. Buasri *et al*. [**27**] derived CaO from mussel shells (S_{BET} = 89.91 m^2/g), cockle shells (S_{BET} = 59.87 m^2/g), and scallop shells (S_{BET} = 74.96 $m^2/$ g) for biodiesel synthesis from palm oil. Tan *et al*. [**28**] utilized CaO that was synthesized from waste chicken-eggshell with S_{BET} = 54.6 m^2/g and from calcined ostrich-eggshell with S_{BET} = 71.0 m^2/g for the transesterification of waste cooking oil. A simple method used to increase the S_{BET} is thermal activation-calcination-milling techniques.

The basic sites on surface of CaO were found in increasing the reaction rates. By activation by methanol and glycerol, several active phases can be formed on surface of catalysts. Calcium methoxide/ethoxide/glyceroxide has a moderate surface area, relative broader particle size distribution, narrower pore size distribution, strong basicity, long narrower pore size distribution, strong basicity, long catalyst lifetime and better stability in organic solvent [**29, 22, 26, 30**]. The catalytic behavior in the transesterification reaction is also determined as a function of the adsorbate coverage at surface of the catalyst [**31**]. Kouzu et al. [**22**] and Refaat [**32**] stated that reactivity order of active phases was $CaCO_3<Ca(OH)_2<CaO<Ca(OCH_3)_2$. Mass transfer resistance highly controls the overall rate of heterogeneous methanolysis reaction because of the immiscibility of nonpolar triglyceride phase and the polar methanol phase. Lukic *et al*. [**33**] reported CaDg creates an emulsifier action in suppressing the mass transfer resistance due to increased value of interface area between methanol and oil. During the methanolysis reaction, CaO catalyst was transformed into CaDg by combining with glycerol [**33**].

The synthesis or design of those catalysts that mentioned above was conducted in several ways: thermal decomposition [**34, 27**], impregnation [**35, 36, 37, 38**], mixing [**39, 40, 41**], and coprecipitation [**42**]. In fact, these catalysts synthesis which in most cases involve multi-step processes, heating and addition of expensive and hazardous reagents. Green catalysis appears to be an achievable and promising approach that may overcome many of the environmental problems associated with current industrial chemical processes as well as permitting economic manufacture of products with a conversion rate [**19**].

1-2-2 Nano-grinding

Dry Grinding based on mechanochemical activation has been emerged as a highly promising and methodology applied in the synthesis of advanced nanomaterials with a wide range of uses and applications [**43, 44**]. Furthermore, the nature of the grinding process may compete with traditional synthetic protocols for catalysts synthesis which in most cases involve multi-step processes, heating and addition of expensive and hazardous reagents. Despite the great potential practical applications, James *et al*. [**45**] provided evidences of notable benefit of using mechanochemical synthesis in terms of cost, sustainability and reproducibility. Mechanochemical approaches for catalysts preparation with improved catalyst activity and selectivity aroused over the past 5-10 years [**45**]. The synthesis of CaO.ZnO catalyst by mechanochemical process for transesterification reaction to biodiesel synthesis, was recently reported [**46**]. Other works also have been published on development catalysts based mechanochemical treatment: $La_{1-x}Sr_xMnO_3$, Cu/ZnO, $LaCrO_3$, $CuO\text{-}CeO_2$, $CaCO_3\text{-}TiO_2$, perovskite-type $La_{0.8}Sr_{0.2}MnO_3$ and the spinel-type Li-Mn-O, kaolin, calcined limestone and zinc oxide [**47-55**].

Nano-grinding is chosen method in this research dissertation for designing high catalytic activity of CaO, namely SSA, increased-basicity and decreased-particle size. Mechanochemical reaction during the nano grinding can created several active sites and high SSA at the surface of CaO at one-step process.

1-3 Scope of Thesis

Due to the promising potential of using CaO–based catalysts as heterogeneous catalysts in biodiesel production, this research dissertation was conducted in attempt to obtain CaO catalyst which near the practical level. Two issues of CaO catalyst are needed to overcome in this research dissertation. The primary issue is the CaO catalytic activity inferior to homogeneous base catalyst for biodiesel production. Some fundamentals of understanding, such as the catalytically active site, reaction mechanism, drastically change in CaO structures during transesterification reaction were still important to study in deeply in order to get enough information to design the CaO catalyst. The secondary issue is to protect CaO catalyst from the ambient CO_2 and H_2O and also FFA, which deteriorates the catalytically basic sites.

Scope of this thesis were as follows below:

1. To investigate of the changes of physicochemical properties of CaO catalyst during alcohol-assisted nano-grinding.
2. To investigate the art of CaO transesterification catalyzed in focusing on true active site catalytic. The CaO-based catalyst was which treated by alcohol-assisted nano-grinding. The effect of physicochemical properties of CaO catalyst during alcohol-assisted nano-grinding on mechanism reaction will deeply investigate.
3. To investigate the tolerance of CaO catalyst during alcohol-assisted nano-

grinding towards the FFA and water content.

In this research dissertation, **Scheme 1** and **2** was design considerations for CaO physicochemical properties for the high rate conversion of transesterification.

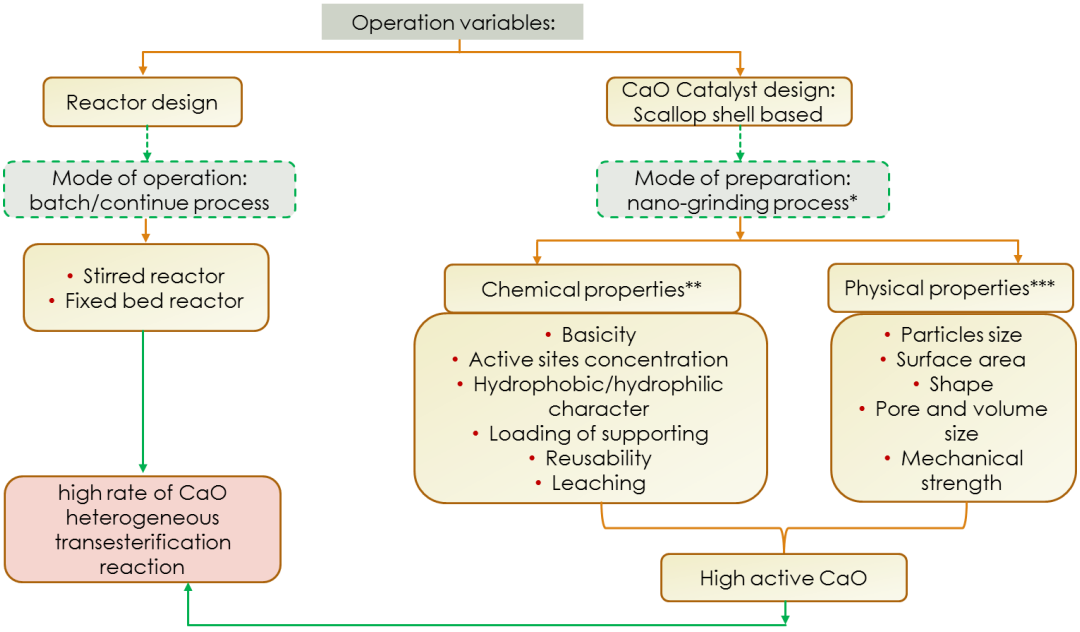

Scheme 1 Design considerations of the thesis experiments

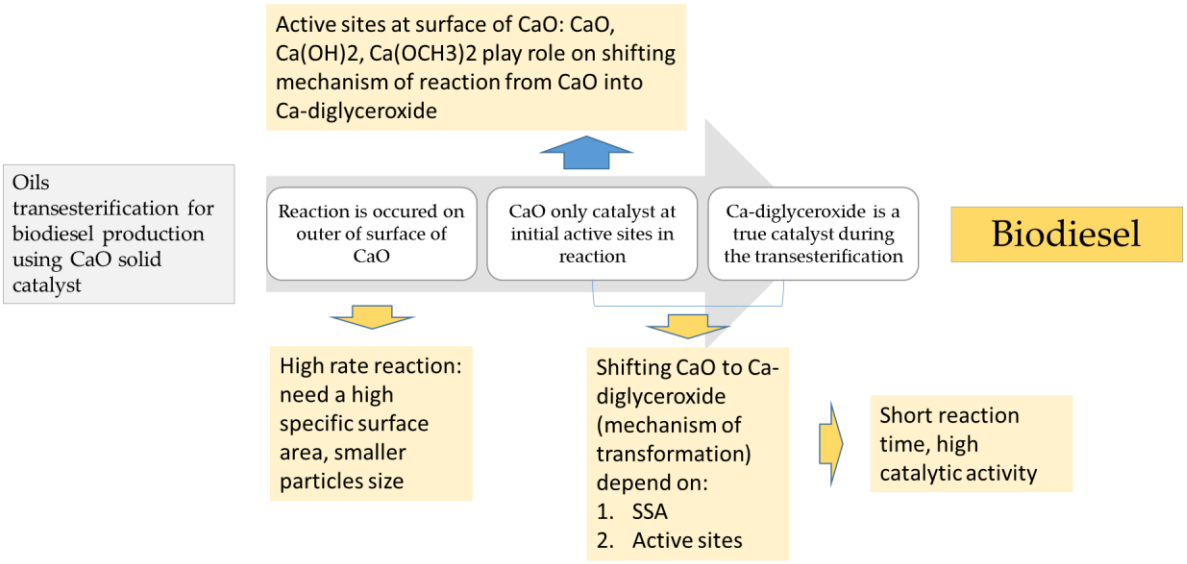

Scheme 2 Approaching the variables fact to design considerations of the thesis experiments**.**

References

[1] T. S. Portal, Projected global energy consumption from 1990 to 2035, by energy source (in million metric tons of oil equivalent) 2016; taken and available from: (http://www.statista.com/statistics/222066/projected-global-energy-consumption-by-source/).

[2] BP Energy Outlook 2035; 2016. Taken and available from: (http://www.bp.com/en/global/corporate/energy-economics/energy-outlook2035.html).

[3] J. H. Van Gerpen, Fuel Processing Technology 86:10 (2005) 1097-1107.

[4] B. Sajjadi, A.A.A. Raman, H. Arandiyan, Renewable and Sustainable Energy Reviews 63 (2016) 62-92.

[5] T. Wright, A. Rahmanulloh, Indonesian Biofuel Annual 2016, Global Agriculture Information Network, Jakarta 2016.

[6] I. B. Bankovic-Ilic, M. R. Miladinovic, O. S. Stamenkovic, V. B. Veljkovic, , Renewable and Sustainable Energy Reviews 72 (2017) 746–760.

[7] M. R. Avhad, J. M. Marchetti, Renewable and Sustainable Energy Reviews 50 (2015) 696-718.

[8] Narasimharao, K., D. R. Brown, A. F. Lee, A. D. Newman, P. F. Siril, S. J. Tavener, K. Wilson, J. Catal., **248**, 226-234 (2007).

[9] A. N. R. Reddy, A. A. Saleh, Md. S. Islam, S. Hamdan, Md. A. Maleque, Energy Fuels 30 (2016) 334-343.

[10] D. M. Marinkovic, M.V. Stankovic, A.V. Velickovic, J.M. Avramovic, M.R. Miladinovic, *et al*., Renewable and Sustainable Energy Reviews 56 (2016) 1387-1408.

[11] M. D. Serio, R. Tesser, L. Pengmei, E. Santacesaria, Energy & Fuels 22 (2008)

207–217.

[12] H. Masood, R. Yunus, T. S. Y. Choong, U. Rashida, Y. H. Taufiq-Yap, Applied Catalysis A: General 425– 426 (2012) 184– 190.

[13] L. Bournay, D. Casanave, B. Delfort, G. Hillion, J. A. Chodorge, Catal. Today 106 (2005) 190-192.

[14] A. A. Refaat, Int. J. of Environ. Sci & Technol. 8 (2011) 203-221.

[15] L. Lin, X. Li, F. Cui, H. Zhou, X. Shen, M. Dong, Bioenerg. Res. 5 (2012) 949-957.

[16] L. Zhao, Z. Qiu, S.M. Stagg-Williams, Fuel Processing Technology 114 (2014) 154-162.

[17] L. Jan, B. Ondrusschka, Chem. Eng. Technol. 27 (2004) 1156-1159.

[18] D. M. Alonso, F. Vila, R. Mariscal, M. Ojeda, M. Lopez Granados, J. Santamaria-Gonzalez, Catalysis Today 158 (2010) 114-120.

[19] S. H. Teo, U. Tashid, Y. H. Taufiq-Yap, Energy Conversion and Management 87 (2014) 618–627.

[20] A. Islam, Y. H. Taufiq-Yap, C-M Chua, E-S Chan, P. Ravindra, Process Safety and Environmental Protection 91 (2013) 131-144.

[21] M. Kouzu, T. Kasuno, M. Tajika, S. Yamanaka, J. Hidaka, Applied Catalysis A: General 334 (2008) 357-365.

[22] M. Kouzu, J. Hidaka, K. Wakabayashi, M. Tsunomori, Applied Catalysis A: General 390 (2010) 11-18.

[23] M. Kouzu, J. Hidaka, Fuel 93 (2012) 1-12.

[24] M. Kouzu, T. Kasuno, M. Tajika, Y. Sugimoto, S. Yamanaka, J. Hidaka, Fuel 87 (2008) 2798-2806.

[25] M. Kouzu, M. Tsunomori, S. Yamanaka, J. Hidaka, Advanced Powder

Technology 21 (2010) 488-494.

[26] L. Leon-Reina, A. Cabeza, J. Rius, P. Maireles-Torres, A. C. Alba-Rubio, M. L. Granados, Journal of Catalysis 300 (2013) 30-36.

[27] A. Buasri, N. Chaiyut, V. Loryuenyong, P. Worawanitchaphong, S. Trongyong, Sci. World J. 2013 (2013) 1-7.

[28] Y. Tan, H., M. O. Abdullah, Y. H. Taufiq-Yap, Appl. Energy, **160**, 58-70 (2015)

[29] A. Kawashima, K. Matsubara, K. Honda, Bioresour. Technol. 99 (2008) 3439-3443.

[30] A.Esipovich, A. Belousov, A. Rogozhin, Journal of Molecular Catalysis A: Chemical, **33**, 225-33 (20149.

[31] H. Cornu, H. Petitjean, G. Costentin, H. Guesmi, J. M. Krafft, H. Lauron-Pernot, Phys. Chem. Chem. Phys., **17**, 19870-19878 (2013).

[32] Refaat, A. A., Int. J. of Environ. Sci & Technol. 203-211.

[33] Lukic, I., Z. Kesic, M. Zdujic, D. Skala, Fuel, **165**, 159-165 (2016).

[34] B. Yoosuk, P. Udomsap, B. Puttasawat, P. Krasae, Chem Eng J 162 (2010) 135-141.

[35] M. Kaur, A. Ali, Renew Energy 36 (2011) 2866-2871.

[36] M. Kaur, A. Ali, Fuel Process Technol 119 (2014) 173-184.

[37] M. Kaur, A. Ali, Biomass- Bioenergy 46 (2012) 459-468.

[38] M. Kaur, A. Ali, Eur J Lipid Sci. Technol, 116 (2014) 80–88.

[39] A. Kawashima, K. Matsubara, K. Honda, Bioresour. Technol. 99 (2008) 3439-3443.

[40] F.S. Lisboa, F.R. Silva, C.S. Cordeiro, L.P. Ramos, F. Wypych, J. Braz. Chem. Soc. 25 (2014) 1592-1600.

[41]. X. Liu, X. Piao, Y. Wang, S. Zhu, Energy & Fuels 22 (2008) 1313-1317.

[42] Y. Wang, S. Hu, Y. Guan, L. Wen, H. Han, Catal Lett 131 (2009) 574-578.

[43] C. Xu, S. De, A.M. Balu, M. Ojeda, R. Luque, Chem. Commun. 51 (2015) 6698-6713.

[44] I. A. Tumanov, A.F. Achkasov, E.V. Boldyreva, V.V. Boldyrev. CrystEngComm 13 (2011) 2213-2216.

[45] S.L. James, C.J. Adams, C. Bolm, D. Braga, P. Collier, T. Friscic, *et al*., Chem. Soc. Rev. 41 (2012) 413-447.

[46] Z. Kesic, I. Lukic, D. Brkic, J. Rogan, M. Zdujic, H. Liu, D. Skala, Applied Catalysis A: General 427-428 (2012) 58-65.

[47] R. J. Bell, G. J. Millar, J. Drennan, Solid State Ionics 131 (2000) 211-220.

[48] L.-C Wang, Y.-M. Liu, M. Chen, Y. Cao, H.-Y. He, G.-S Wu, W.-L. Dai, K.-N. Fan, Journal of Catalysis 246 (2007) 193-204.

[49] Q. Zhang, J. Lu, F. Saito, Powder Technology 122 (2002) 145-149.

[50] A.A. Firsova, O.S. Morozova, A.V. Leonov, A.N. Streletskii, V.N. Korchak, Kinetics and Catalysis, 55 (2014) 777-785.

[51] V. Berbenni, A. Marini, Journal of Materials Science 39 (2004) 5279-5282.

[52] A. Rougier, S. Soiron, I. Hailal, L. Aymard, B. Taouk, J.-M. Tarascon, Powder Technology 128 (2002) 139-147.

[53] A. Tang, L. Su, C. Li, Powder Technology 218 (2012) 86-89.

[54] H. Moriyasu, K. Kentaro, A. Sato, M. Kouzu, Journal of the Japan Institute of Energy 91 (2012) 495-502.

[55] V.V. Molchanov, R.A. Buyanov, S.V. Tsybulya, G.N. Kryukova, A.N. Shmakov, A.I. Boronin, A.M. Volodin, Kinetics and Catalysis 45 (2004) 684-693.

Chapter 2

Clarifying True Catalytic Active Site on CaO Catalyzed Transesterification Reaction to Biodiesel

2-1 Introduction

Calcium oxide (CaO) is the most widely used and well-researched catalyst material for the heterogeneous methanolysis of oils to biodiesel. The suitability of CaO to this application arises from its high basicity, low solubility in organic solvents, and its effectiveness under mild reaction conditions. Moreover, CaO feedstocks are plentiful with sources including natural carbonate-rich minerals such as dolomite, calcite, limestone, and shells from marine life [**1, 2**]. Since the reaction occurs on the surface of the catalyst, the major factors governing the performance of CaO are: the specific surface area (SSA) which largely determines the number of molecules which are able to adsorb to the material; high basicity of the active sites of reaction (*or active phases on the surface of the catalyst*); and catalyst particle size [**2–8**]. Many investigations have confirmed that CaO catalysts with a high SSA, strong basicity of surface reaction sites, and lower particle size accelerate the conversion rate, particularly in terms of facilitating the access of reactant molecules to basic sites on the catalyst surface. Reddy *et al.* [**4**] synthesized nano-sized CaO (nano-CaO) from *Polymedosa erosa* with a diameter and SSA of 66 ± 3 nm and 90.61 m^2g^{-1}, respectively, using a calcination–hydration–dehydration technique, and reported a 98.54% biodiesel yield. Kouzu *et al.* [**9**] derived CaO from natural limestone (SSA = 13 m^2g^{-1}) by calcination of pulverized limestone at 900 °C in a He gas flow, obtaining a 93% biodiesel yield. Wilson *et al.* [**10**] derived CaO from natural dolomitic rock by calcination at 900 °C, yielding particulates with SSA = 8 m^2g^{-1}, and reporting a 100% conversion of triglyceride in a transesterification reaction after 3 h. Buasri *et al.* [**11**] utilized CaO synthesized from mussel shells (SSA = 89.91 m^2g^{-1}), cockle shells (SSA= 59.87 m^2g^{-1}), and scallop shells (SSA= 74.96 m^2g^{-1}) for biodiesel production from palm oil. Lastly, Moriyasu *et al.* [**12**] reported a SSA of 13.6 m^2g^{-1} and particle diameter 0.5 μm for CaO particles synthesized

from calcined limestone by wet mechanical grinding.

Furthermore, the presence of active phases on the surface of the CaO catalyst has also been identified as an influence on the catalytic process: methanolysis reactions proceed via surface OH^- groups which have been found to be present at basic sites on the catalyst surface [**13, 14**]. Thus, the catalytic behavior in the transesterification reaction is also determined as a function of the adsorbate coverage of the catalyst surface [**8**]. Kouzu *et al.* [**15**] and Refaat [**16**] have stated that the order of reactivity for active phases is $CaCO_3 < Ca(OH)_2 < CaO < Ca(OCH_3)_2$. Mass transfer resistance is a strong factor in determining the overall rate of the heterogeneous methanolysis reaction due to the immiscibility between the nonpolar triglyceride phase and the polar methanol phase. Ivana *et al.* [**17**] reported that calcium diglyceroxide (CaDg) acts as an emulsifier and suppresses the mass transfer resistance by increasing the interfacial area between methanol and oil: in this study, the CaO catalyst was transformed into CaDg by interaction with glycerol during the early stages of the methanolysis reaction [**18**].

Nano-grinding is a simple comminution process, which can produce ultra-fine particles (< 10 μm) with high SSA [**19, 20**]. The nano-grinding process can alter the size, structure, composition, and morphological characteristics of materials by carefully choosing the appropriate parameters [**21, 22**]. To date, little research has been reported on the use of mechanical activation to improve the catalytic properties of solid CaO with a view to biodiesel production [**17, 23**]. As such, in this study, a methanol assisted, dry nano-grinding process was employed to enhance the catalytic properties of CaO derived from scallop shell (CaO-ss). We report a comparison between two methods of nano-grinding, batchwise and stepwise addition of methanol, which produce catalytic powders with differing SSAs and differing degrees of active phases on the material surface.

Reducing mass transfer limitation during the initial stages of the heterogeneous methanolysis reaction contributes substantially to the overall rate of reaction. In detail, mass transfer limitations occur on the surface of the catalyst because the reaction proceeds *via* a liquid–liquid–solid stage [**2, 24**]. Therefore, by creating a CaO surface that is easily accessible to both methanol and oil, reductions in mass transfer limitation could be achieved [**2, 6, 8, 17**]. In addition, as mentioned previously, a combination of SSA increase with an increase in the basicity of the catalyst would also serve to improve the rate of methanolysis.

As the derivation of a CaO catalyst from scallop shell and subsequent activation by a methanol-assisted dry nano-grinding process has not been previously reported. In this study, the use of CaO-ss as a catalyst for the methanolysis of soybean oil was examined, and the effects of active phase surface composition on the initial rate of reaction were reported, as well as the effects of the oxide's SSA.

2-2 Experimental Section

2-2-1 Materials

Scallop shell powder was purchased from Tokoro-cho Industry (Kitami, Japan) which composed of calcite crystals and a small quantity of organic matter. Soybean oil (reagent grade), methanol (>99,8%), dichloromethane (solvent grade), HCl (p.a.) were purchased from Kanto Chemical (Japan). Hexane (HPLC grade), 2-propanol (>99,5%) 1-Oleoyl-rac-glycerol (monoolein, ≥99%), dioleoylglycerol (diolein, ≥99%), glyceryltrioleate (triolein, ≥99%), pyridine (HPLC grade) as buffer in sample analysis preparation were purchased as standard from Sigma Aldrich (St. Luis, USA). Tetrahydrofuran (reagent grade) and KOH standard solution (8 mol/L) were purchased from Wako Pure Chemical Industries Ltd. (Japan). Heptane (anhydrous 99%) as solvent,

N-Methyl-N-(trimethylsilyl)-trifluoracetamide (synthesis grade) as agent of derivatization of OH groups in sample analysis preparation were purchased from Sigma Aldrich (St. Luis, USA). Glyceryltridecanoate (≥99%) as internal standard for quantity analysis was purchased from Sigma Aldrich (St. Luis, USA).

2-2-2 Dry nano-grinding process and catalyst characterization

CaO-ss (SSA = 0.4 m^2g^{-1}) was obtained from the calcination of scallop shell powder at 1000 °C for 3 h. The methanol-assisted dry nano-grinding process was carried out using a planetary ball mill (P-7 premium line, Fritsch, Germany), which was equipped with two zirconia pots of 80 cm^3 volume, each containing 100 g of yttria-stabilized zirconia milling beads (3 mm diameter). To evaluate the grinding process, experiments involving batchwise and stepwise addition of methanol were carried out in a closed system. The batchwise addition method was performed by adding the whole required volume of methanol into the pot at the start of the nano-grinding process, whereas the stepwise addition method involved adding smaller quantities of methanol to the pot at predetermined intervals. During batchwise addition, the nano-grinding operation was stopped for 15 min after every 1 h of grinding to prevent the inside of the milling pot from overheating. After a predetermined grinding time, the ground mixture was removed. The range of different conditions used in the nano-grinding process is shown in **Table 1**.

The SSA of the powders was determined from nitrogen gas adsorption by using the five-point BET method (Microtrac, Adsotrac DN-04). Prior to measurement, samples were degassed at 473 K for 2 h.

X-ray powder diffraction (XRD) measurements were performed by a Multi Flex-120 NP Rigaku (Japan) equipped with a Cu-Kα anode (λ = 1.5418 Å), operated at a

tension and current of 40 kV and 20 mA, respectively. Measurements were recorded at room temperature over the 2θ range 3–70°, with a 0.02° step size. Crystalline phases were identified by comparison with ICDD data files.

Fourier-transform infrared (FTIR) spectra were recorded using a JASCO FTIR-460 PlusK spectrometer, and catalyst was measured as KBR pellets. Measurements were conducted over the range 4000–400 cm^{-1} with a 4 cm^{-1} resolution.

Total basic sites (f_m) of the catalysts were evaluated by measuring the acidity conjugate acid, by titration method. In a typical experiment, 25 mg catalyst CaO ground was dissolved in 25 mL of 0.1 M HCl and resulting mixture was stirred for an hour. The catalyst would neutralize HCl equivalent to its basicity. The resulted solution was titrated against standard NaOH solution to determine the exact concentration of excess HCl. The amount of HCl neutralized by the catalyst was determined and represented as basicity of the catalyst as mmol of HCl/g of catalyst [**25**].

Table 1

Methanol assisted dry nano-grinding conditions

Entry	Catalyst preparation
1	Calcinated scallop shells at 1000 °C for 3 h.
2	Nano-grinding with 0.2 ml methanol at 400 rpm, 3 h. Batchwise addition.
3	Nano-grinding with 1 ml methanol at 1000 rpm, 30 min. Batchwise addition.
4	Nano-grinding with 3 ml methanol at 1000 rpm, 5 h. For stepwise addition, solvent added at rate of 0.6 ml/1 h.
5	Nano-grinding with 1 ml methanol at 1000 rpm, 4 h. Batchwise addition.
6	Nano-grinding with 1.8 ml methanol at 400 rpm, 6 h. For stepwise addition, solvent added at rate of 0.3 ml/1 h.
7	Nano-grinding with 0.45 ml methanol at 400 rpm, 6 h. For stepwise addition, solvent added at rate of 0.075 ml/1 h.
8	Nano-grinding with 3 ml methanol at 400 rpm, 10 h. Batchwise addition.
9	Nano-grinding with 4.5 ml methanol at 1000 rpm, 6 h. For stepwise addition, solvent added at rate of 0.75 ml/1 h.
10	Nano-grinding with 3.75 ml methanol at 900 rpm, 5 h. For stepwise addition, solvent added at rate of 0.75 ml/1 h.
11	Nano-grinding with 3 ml methanol at 1000 rpm, 5 h. For stepwise addition, solvent added at rate of 0.6 ml/1 h.
12	Nano-grinding with 3 ml methanol at 1000 rpm, 5 h. For stepwise addition, solvent added at rate of 0.6 ml/1 h.
13	Nano-grinding with 1.8 ml methanol at 600 rpm, 6 h. For stepwise addition, solvent added at rate of 0.3 ml/1 h.
14	Nano-grinding with 4.5 ml methanol at 400 rpm, 3 h. For stepwise addition, solvent added at rate of 0.5 ml/20 min.
15	Nano-grinding with 0.9 ml methanol at 600 rpm, 6 h. For stepwise addition, solvent added at rate of 0.3 ml/2 h.

2-2-3 Methanolysis of soybean oil

The effect of SSA and surface phase composition on the initial reaction rate of methanolysis reaction was tested. Methanolysis of soybean oil was performed in a 100 mL batch-type three-necked glass flask with a condenser and magnetic stirrer. The transesterification was carried out at 65±1 °C with a methanol-to-oil molar ratio of 9:1 and catalyst concentration of 4 wt% with respect to the oil mass. The stirring rate was held at 800 rpm. A series of CaO-ss samples with the following SSA: 0.4 m^2g^{-1}; 4.5 m^2g^{-1}; 10.6 m^2g^{-1}; 17.3 m^2g^{-1}; 18.6 m^2g^{-1}; 25.9 m^2g^{-1}; 27.9 m^2g^{-1}; 31.0 m^2g^{-1}; 35.6 m^2g^{-1}; 45.2 m^2g^{-1}; 45.3 m^2g^{-1}; 45.6 m^2g^{-1}; 46.3 m^2g^{-1}; 57.4 m^2g^{-1}; 62.5 m^2g^{-1} were used. Prior to analysis, samples (1 ml) were removed from the reaction mixture and immediately treated using a procedure detailed elsewhere [**26**]. The quantities of esters, monoglyceride, diglyceride, and triglyceride were analyzed using a gas chromatograph (Shimadzu GC-14B) equipped with a flame ionization detector (FID), on a DB-5HT capillary column (14 m × 0.25 mm, 0.1 μm film thickness). The analytical work was performed with the following heating regime: holding at 50 °C for 1 min, followed by three separate steps of temperature increase, firstly to 180 °C at a rate of 10 °C/min, then to 230 °C at 7 °C/min, and lastly to 380 °C at 10 °C/min, at which point the temperature was held for 10 mins. Quantitative analysis was carried out following a procedure described in detail elsewhere [**27**]. To examine the catalyst recyclability, the spent catalyst was used five separate times through recovery by filtration, washing with 2-propanol, and drying in a vacuum at room temperature.

2-3 Result and discussion

2-3-1 Bulk and surface characterization of catalysts

Table 2 presents the variations in the SSA of the ground CaO-ss samples after being processed by methanol-assisted dry nano-grinding. As can be seen, the variations of SSA (4.5–62.5 m^2g^{-1}) were determined by a number of nano-grinding parameters: batchwise or stepwise addition of solvent; rotation of milling; grinding time with the various volumes (0.2–4.5 ml) of methanol. The presence of methanol in the nano-grinding process is thought to protect the particles from agglomeration: with a sufficient concentration of methanol, the formation of terminal methoxide groups, as opposed to bridging, is promoted; terminal methoxy groups act to hinder inter-particle bonding which is known to lead to formation of hard agglomerates. Similar behavior has been observed by other authors [**28, 29**] in organic solvent-assisted dry grinding processes. Reducing both the attractive forces between particles, as well as adhesion to the grinding media have the effect of improving the 'grindability' of the oxide which, in turn, produces material with higher SSA.

The temperature of the nano-grinding pot during processing was measured to be between 60 °C and 120 °C for batchwise addition, and between 60 °C and 80 °C for stepwise addition. As these temperatures were higher than the boiling point for methanol, CaO-ss was ground in methanol vapor. Comparing the batchwise and stepwise addition methods, the latter was found to be effective for obtaining higher SSA CaO-ss (**Table 2**). This may be explained by considering the high volatility of methanol in the vapor phase: in batchwise addition, the volatility of methanol leads to insufficient adsorption to the catalyst surface to produce the protective effect. While quantifying the effects of methanol volatility and adsorption to CaO-ss is beyond the scope of this study, the results suggest that stepwise addition can maintain the methanol vapor

concentration at a sufficient level to shield the particle surface, as evidenced by the improvements in grindability and SSA.

Table 2

CaO-ss prepared samples: SSA, XRD and Basicity Characterization

Entry	SSA (m^2g^{-1})	Crystalline phases*	Basicity (mmoles of HCl/g of catalyst)	Ester yields (%)	
				20 min	60 min
1	0.4	**CaO**	0.16	13.7	16.1
2	4.5	**CaO**	0.19	34.8	81.7
3	10.6	**$Ca(OH)_2$**, CaO	0.22	44.4	92.1
4	17.3	**$Ca(OCH_3)_2$** CaO, $Ca(OH)_2$	0.22	29.8	83.8
5	18.6	**CaO**, $Ca(OH)_2$	0.22	46.2	95
6	25.9	**CaO**, $Ca(OH)_2$, $Ca(OCH_3)_2$	0.26	50.8	94.7
7	27.9	CaO, **$Ca(OH)_2$**, $Ca(OCH_3)_2$	0.35	58.9	97.5
8	31	**$Ca(OCH_3)_2$** CaO, $Ca(OH)_2$	0.22	41.2	95.6
9	35.6	**$Ca(OH)_2$**, $Ca(OCH_3)_2$	0.22	57.6	95.7
10	45.2	**CaO**, $Ca(OH)_2$, $Ca(OCH_3)_2$	0.29	72.3	96.5
11	45.3	**$Ca(OH)_2$**	0.19	37.6	94
12	45.6	**$Ca(OH)_2$**	0.19	39.5	95.7
13	46.3	$Ca(OH)_2$, **$Ca(OCH_3)_2$**	0.22	45.5	93.5
14	57.4	**$Ca(OH)_2$**, $Ca(OCH_3)_2$	0.22	50	91
15	62.5	**$Ca(OH)_2$**	0.22	53.7	96.5

**Phases highlighted in bold indicate major phases observed by XRD analysis*.

In previous reports, it has been revealed that the nano-grinding process could promote chemisorption and physisorption reactions on the surfaces of solid particles. [**28, 30**]. The changes in the relative proportions of active phases on the surface of ground CaO-ss (which is associated with the adsorption of methanol vapor) were evaluated by XRD and FT-IR measurements. The XRD patterns of CaO-ss catalysts, treated as listed in **Table 1**, are shown in **Fig. 1 (a)-(c)**. The XRD results confirmed that a number of different calcium-based phases are formed during the methanol-assisted dry nano-grinding process. The crystalline phases were indexed and matched to three known materials: calcium oxide (ICDD file 04-1497), calcium hydroxide (ICDD file 04-0733), and calcium methoxide (reported in [**26**]). The presence of active sites on the ground CaO-ss catalyst modified the basicity of the catalysts as we can saw in **Table 2**.

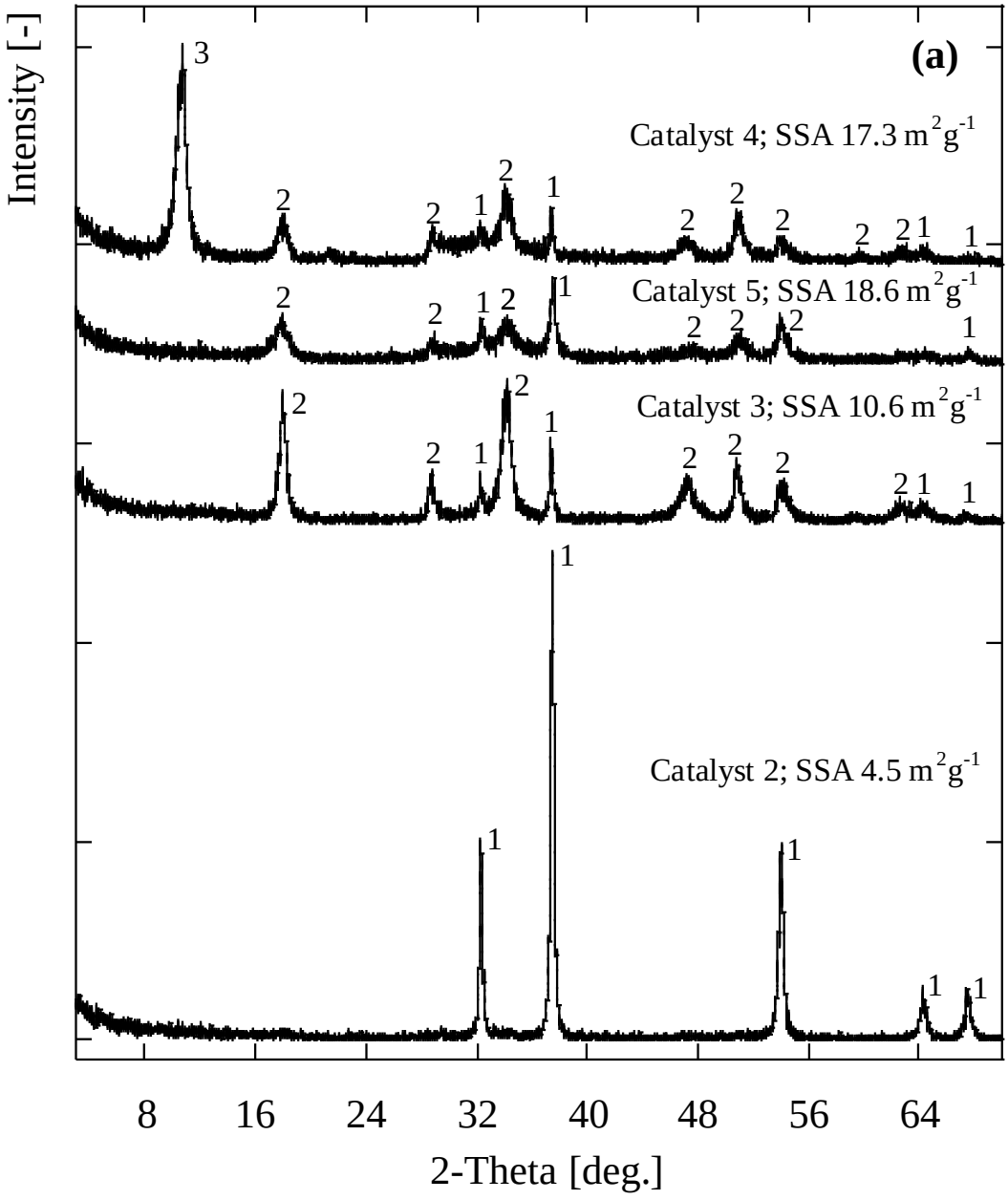

Fig. 1 (a). XRD patterns of ground CaO-ss after processing by methanol-assisted dry nano-grinding; (1) CaO, ICDD file 04-1497; (2) $Ca(OH)_2$, ICDD file 04-0733; (3) $Ca(OCH_3)_2$ refer to [**26**].

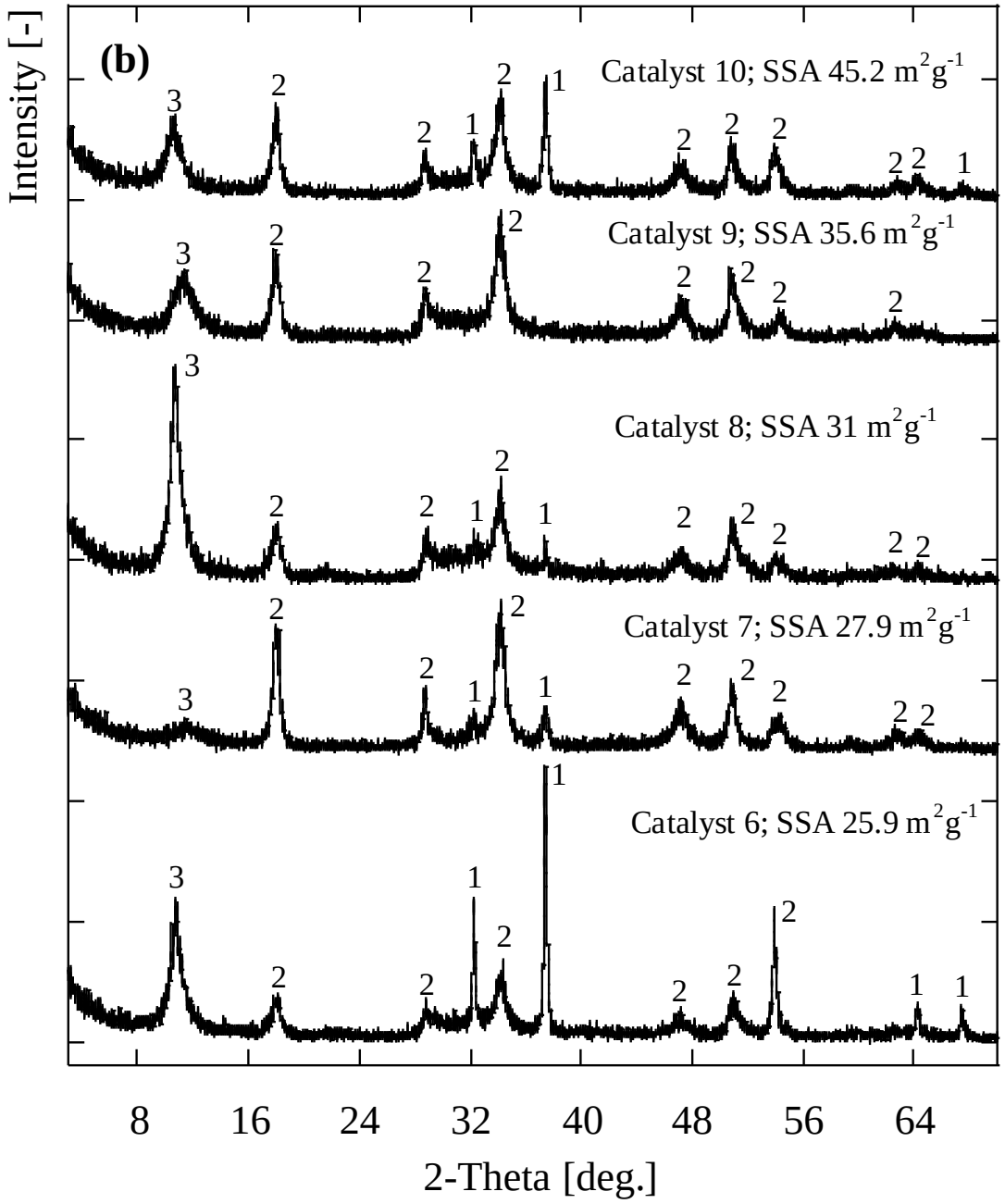

Fig. 1 (b). XRD patterns of ground CaO-ss after processing by methanol-assisted dry nano-grinding; (1) CaO, ICDD file 04-1497; (2) $Ca(OH)_2$, ICDD file 04-0733; (3) $Ca(OCH_3)_2$ refer to [**26**].

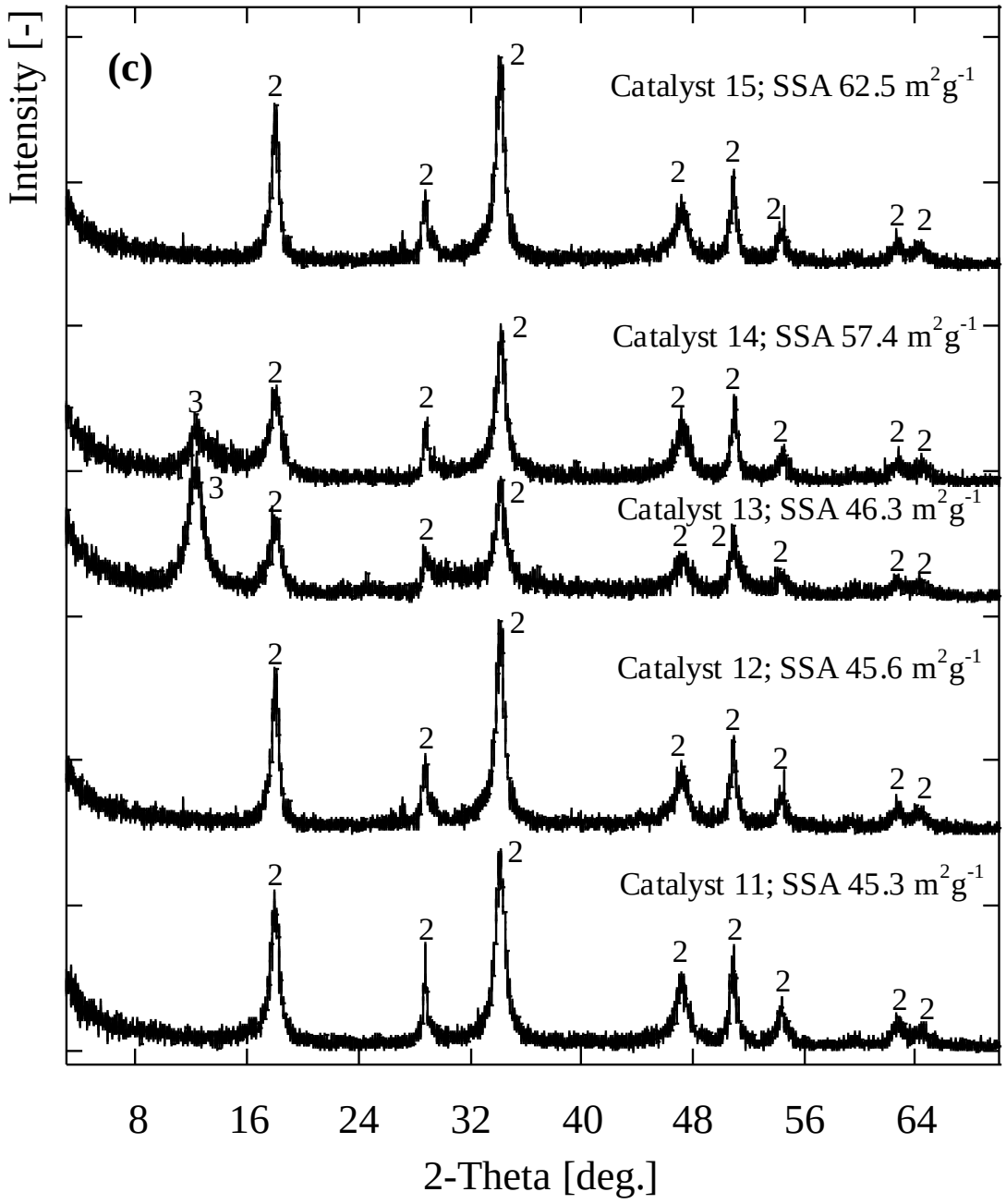

Fig. 1 (c). XRD patterns of ground CaO-ss after processing by methanol-assisted dry nano-grinding; (1) CaO, ICDD file 04-1497; (2) $Ca(OH)_2$, ICDD file 04-0733; (3) $Ca(OCH_3)_2$ refer to [**26**].

The FT-IR results (**Fig. 2**), it can be inferred that methanol vapor adsorption during the nano-grinding stage occurs *via* both chemisorption and physisorption pathways. The interaction between CaO-ss and methanol begins with the adsorption of the vapor onto the oxide surface. The adsorbed methanol can then either desorb or dissociate during the nano-grinding process. In all of the ground CaO-ss samples, sharp bands at 3643 cm^{-1} were observed in the O-H stretching vibration region *ν* (OH) of CaO-H on the ground CaO-ss surface [**31**]. This indicates that dissociation of methanol at the catalyst surface proceeds via hydrogen bonding between the methanol H and the surface O atoms of CaO-ss. These results roughly agree with results reported elsewhere, which signify that methanol vapor decomposition proceeds by O-H bond scission [**32, 33, 34**]. The methoxide groups were identified by the presence of a couple of weak bands in the C-H stretching region at 2925 cm^{-1} and 2831 cm^{-1} and in the C-H deformation region (1500–1400 cm^{-1}), attributed to the *δ*(CH) modes of methoxide. This suggests that interactions between methoxide groups and the CaO surface arises *via* the lone pair of electrons on the oxygen atom [**33**]. In the C-O stretching (primary alcohol) region, bands in the range 1148–1078 cm^{-1} were present, which correspond to CH_3O^- groups [**28, 32, 36**]. The weak peak present in the region 865–875 cm^{-1} was attributed to CO_2 adsorbed on the CaO-ss surface [**21, 31**].

A shoulder at 3229 cm^{-1} and 3300–3400 cm^{-1} was also detected and assigned to H-bonds, which form on dissociative adsorption of methanol, while the band at 3300–3500 cm^{-1} was linked to the –OH mode of water physisorption on the CaO-ss surface [**33, 35**], and the detection of a band in the region 1650–1600 cm^{-1} was assigned to the H-O-H deformation water molecules physisorbed on the catalyst surface [**31**]. In this work, the overlapping of this region band occurred for the CaO-ss samples 2–6, 8–10, 12, and 14–15. Taking FT-IR bond scission features as references, a possible reaction

mechanism for methanol adsorption during nano-grinding is proposed as follows:

$CaO \leftrightarrow Ca^{2+} + O^{2-}$ (1)

$CH_3OH_{(g)} \rightarrow (CH_3OH)_{(a)}$ (2a)

$CH_3OH_{(a)} \rightarrow CH_3O^-_{(a)} + H^+_{(a)}$ (2b)

$Ca^{2+} + 2CH_3O^-_{(a)} \rightarrow Ca(OCH_3)_{2\,(a)}$ (3a)

$Ca^{2+}\text{-}O^{2-} + H^+_{(a)} \rightarrow Ca^{2+}\text{-}O^{2-}\text{-}H^-_{(a)}$ (3b)

$O^{2-} + 2H^-_{(a)} \rightarrow H_2O_{(a)}$ (3c)

$Ca\text{-}O + H_2O_{(a)} \rightarrow Ca(OH)_{2\,(a)}$ (3d)

$Ca^{2+}\text{-}O^{2-}\text{-}H^- + H^-\text{-}O^{2-}\text{-}Ca^{2+} \rightarrow Ca\text{-}O\text{-}Ca + H_2O$ (4)

* (a) = *adsorbed*."

As mentioned previously, the stepwise addition method was found to be more effective for obtaining high SSA CaO-ss. Grinding-induced activation of CaO produced surface ions (Ca^{2+} and O^{2-}) but the overall crystal is neutral (1) [**28**]. Interactions between methanol vapor and these surface ions occurred via chemisorption and physisorption (**Fig. 2**) during the nano-grinding process. Therefore, several calcium-based phases were generated at the catalyst surface, namely calcium oxide, calcium hydroxide, and calcium methoxide. The calcium methoxide phases also act to protect the particulates from agglomeration: the lower the agglomeration energy, the smaller the agglomerated particles which form during the process, thereby yielding a higher SSA product [**37**]. Because the methanol vapor adsorbed weakly at the temperatures produced by the nano-grinding process (60–120 °C), the stepwise addition method is more effective in maintaining a sufficient concentration of methanol vapor during grinding, and therefore this variation of the process yielded higher SSA CaO-ss.

Water physisorption on the ground CaO-ss surface was also identified, as shown in **Fig. 2**, probably arising due to non-bridging hydroxyl groups tend to interact strongly on the ground CaO-ss surface, which liberates water (4). Consequently, hard agglomerates formed, which reduced the SSA of the products. Summarizing the FT-IR results, it can be concluded that methanol-assisted dry nano-grinding with stepwise solvent addition is very effective in increasing the SSA of CaO-ss catalysts, and the addition of methanol to the nano-grinding process also serves to generate several active phases on the surface of the catalysts.

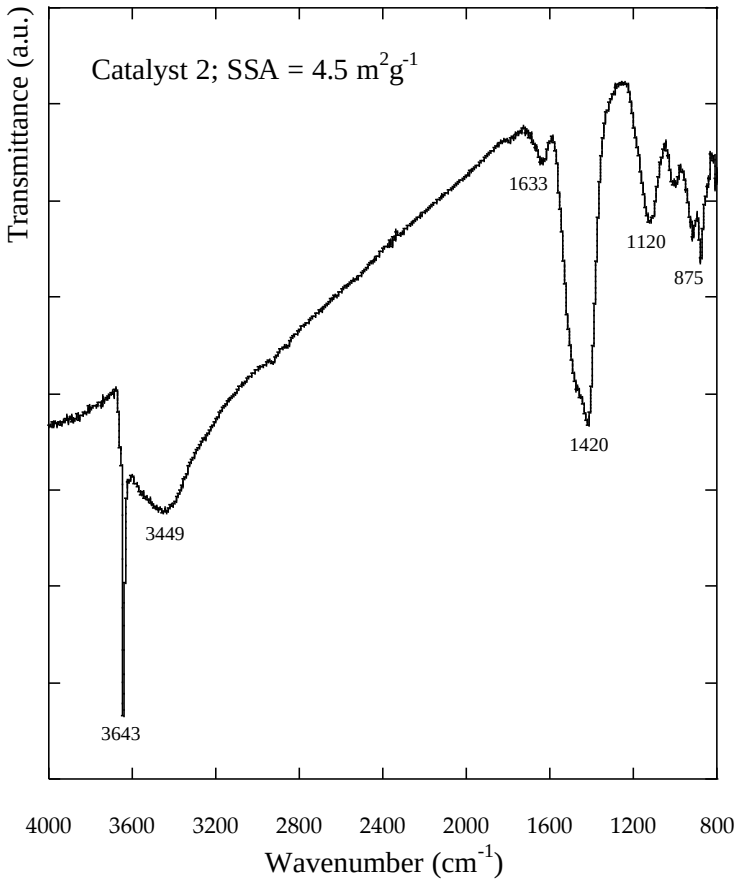

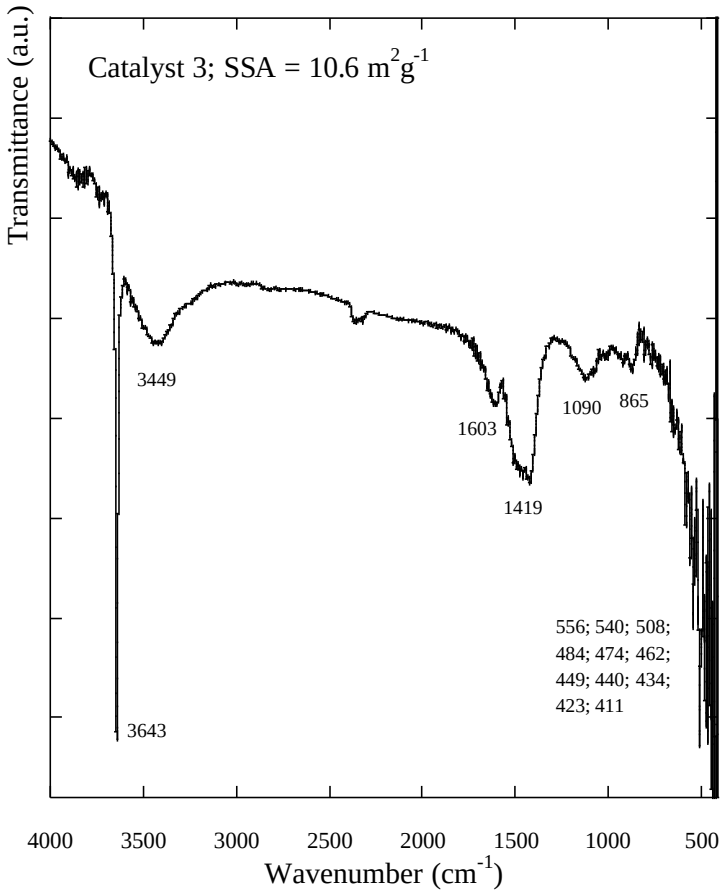
Catalyst 3; SSA = 10.6 m2g-1
Transmittance (a.u.)
3449
1603
1090
865
1419
556; 540; 508;
484; 474; 462;
449; 440; 434;
423; 411
3643
4000
3500
3000
2500
2000
1500
1000
500
Wavenumber (cm-1)

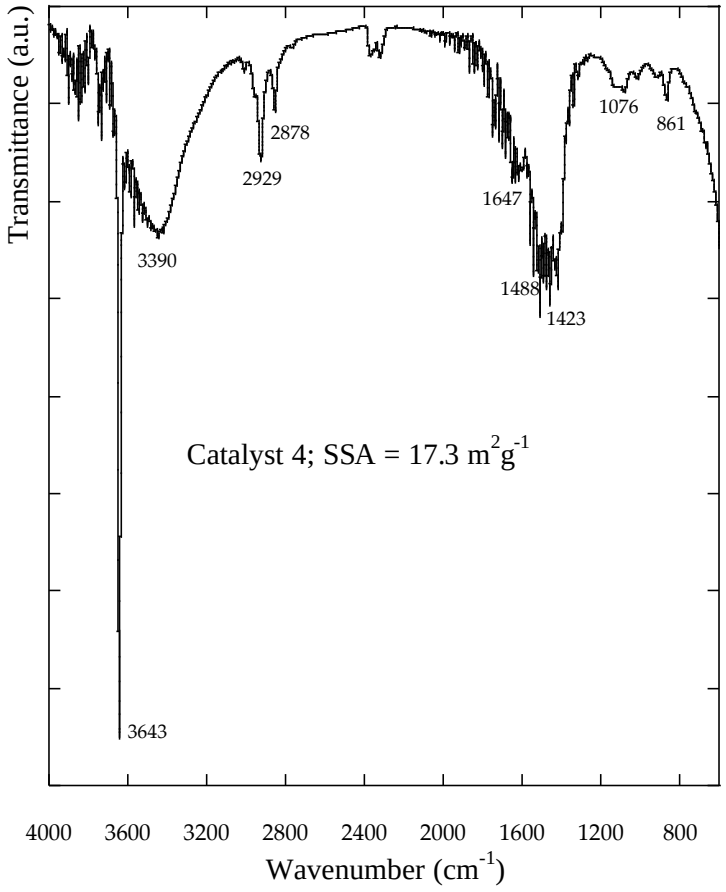
Transmittance (a.u.)
2878
2929
1076
861
1647
3390
1488
1423
Catalyst 4; SSA = 17.3 m2g-1
3643
4000
3600
3200
2800
2400
2000
1600
1200
800
Wavenumber (cm-1)

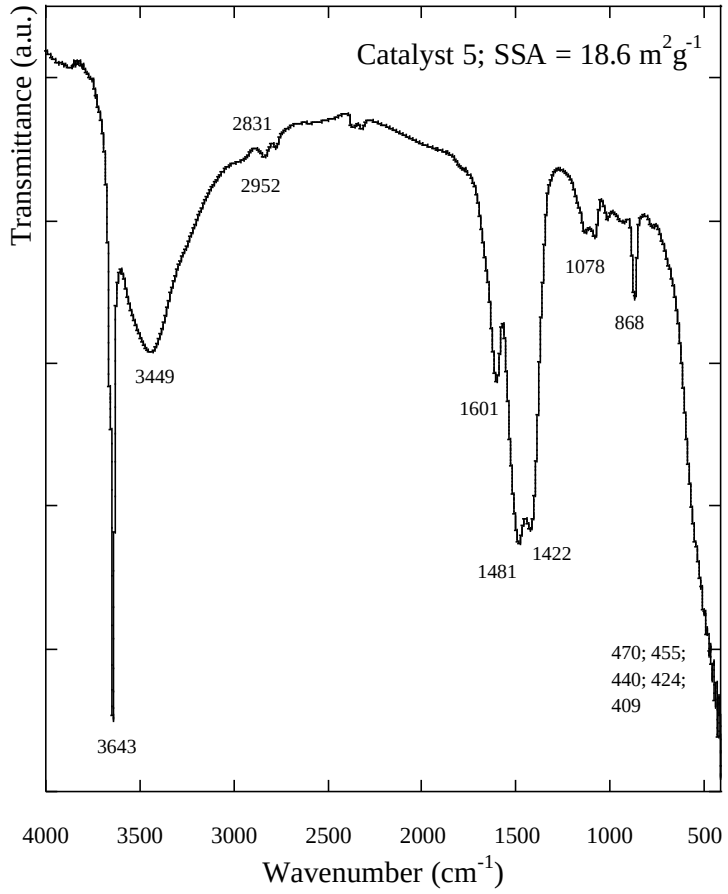
Catalyst 5; SSA = 18.6 m2g-1
Transmittance (a.u.)
2831
2952
1078
868
3449
1601
1422
1481
470; 455;
440; 424;
409
3643
4000
3500
3000
2500
2000
1500
1000
500
Wavenumber (cm-1)

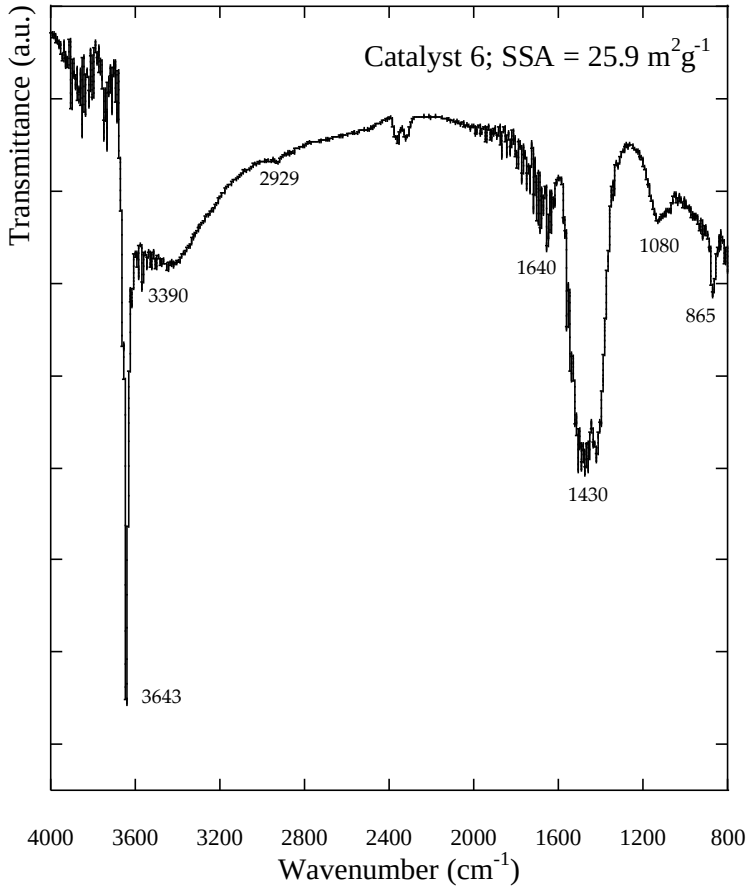
Catalyst 6; SSA = 25.9 m2g-1
Transmittance (a.u.)
2929
1080
1640
3390
865
1430
3643
4000
3600
3200
2800
2400
2000
1600
1200
800
Wavenumber (cm-1)

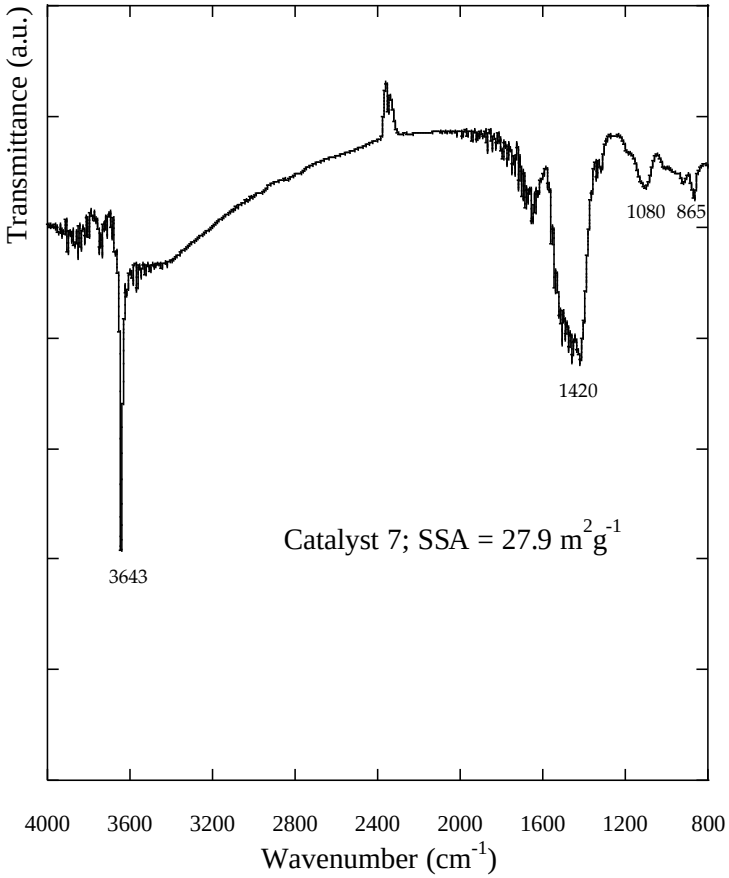
Transmittance (a.u.)
1080
865
1420
Catalyst 7; SSA = 27.9 m2g-1
3643
4000
3600
3200
2800
2400
2000
1600
1200
800
Wavenumber (cm-1)

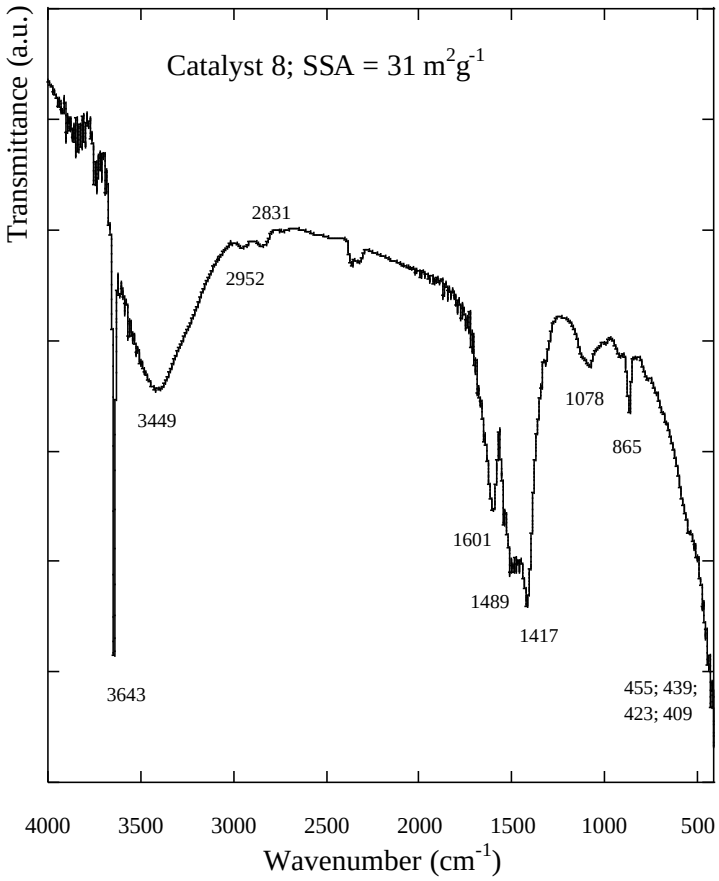
Transmittance (a.u.)
Catalyst 8; SSA = 31 m2g-1
2831
2952
3449
1078
865
1601
1489
1417
3643
455; 439;
423; 409
4000
3500
3000
2500
2000
1500
1000
500
Wavenumber (cm-1)

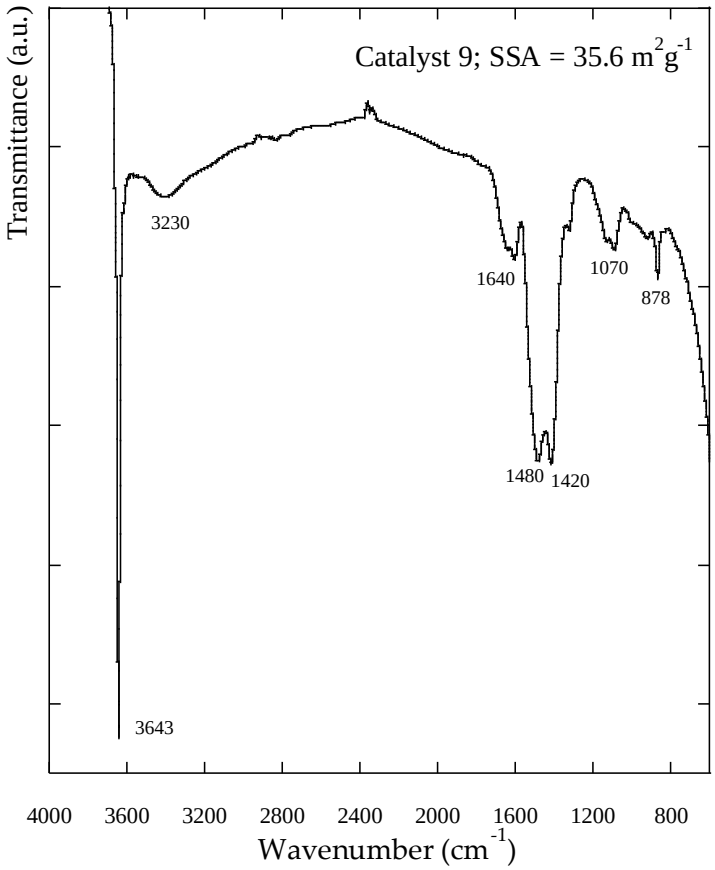
Catalyst 9; SSA = 35.6 m2g-1
Transmittance (a.u.)
3230
1640
1070
878
1480
1420
3643
4000
3600
3200
2800
2400
2000
1600
1200
800
Wavenumber (cm-1)

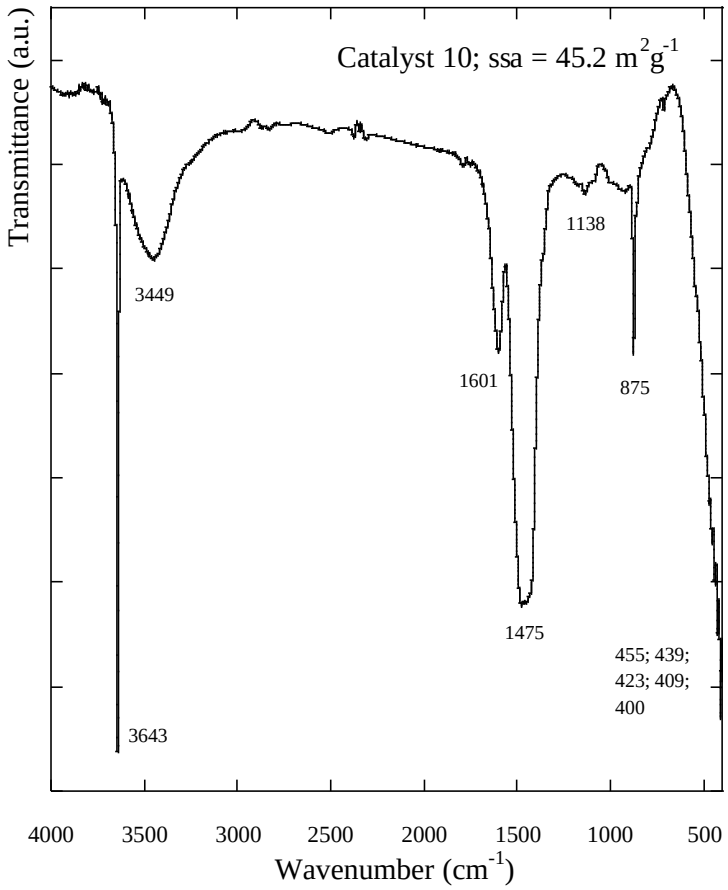
Catalyst 10; ssa = 45.2 m2g-1
Transmittance (a.u.)
3449
1138
1601
875
1475
455; 439;
423; 409;
400
3643
4000
3500
3000
2500
2000
1500
1000
500
Wavenumber (cm-1)

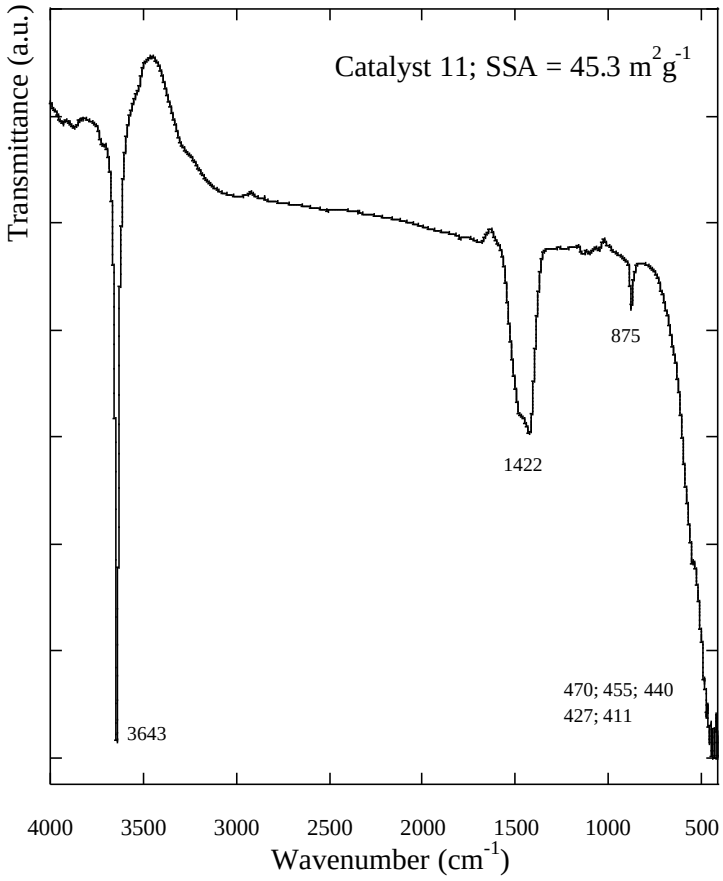
Transmittance (a.u.)
Catalyst 11; SSA = 45.3 m2g-1
875
1422
470; 455; 440
427; 411
3643
4000
3500
3000
2500
2000
1500
1000
500
Wavenumber (cm-1)

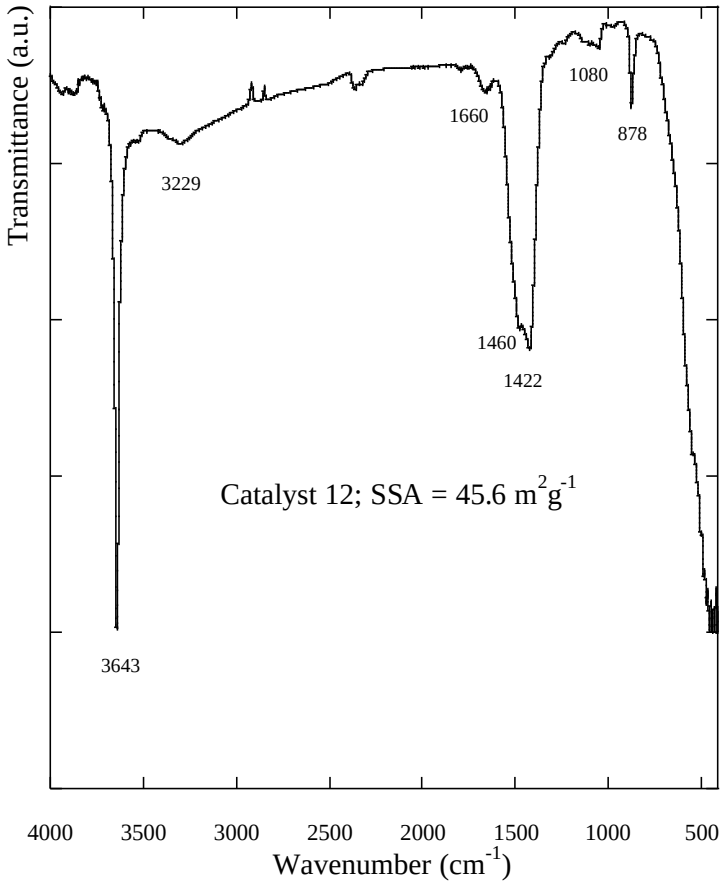
Transmittance (a.u.)
1080
1660
878
3229
1460
1422
Catalyst 12; SSA = 45.6 m2g-1
3643
4000
3500
3000
2500
2000
1500
1000
500
Wavenumber (cm-1)

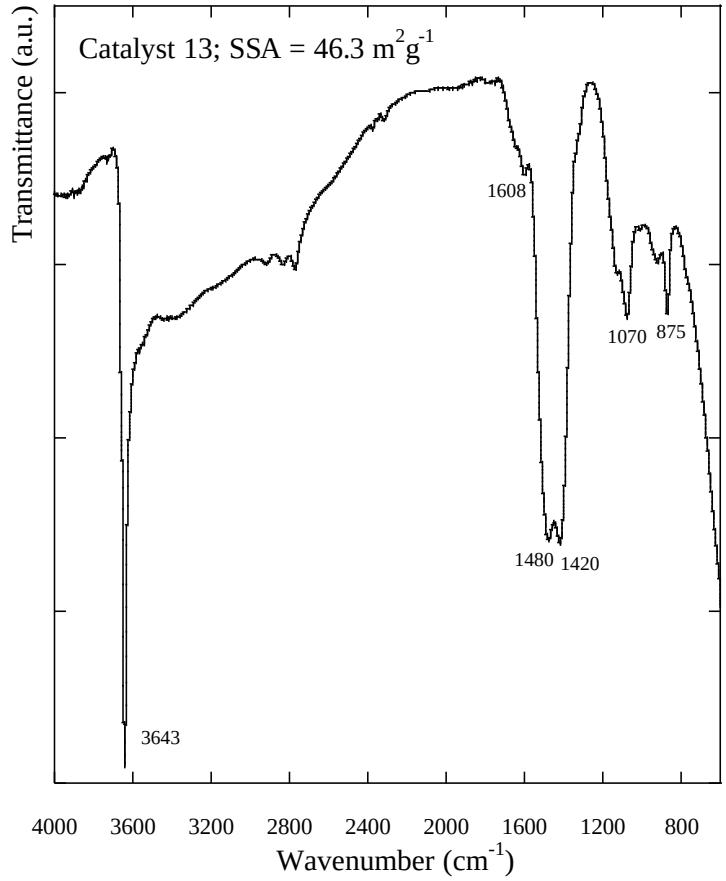
Catalyst 13; SSA = 46.3 m2g-1
Transmittance (a.u.)
1608
1070
875
1480
1420
3643
4000
3600
3200
2800
2400
2000
1600
1200
800
Wavenumber (cm-1)

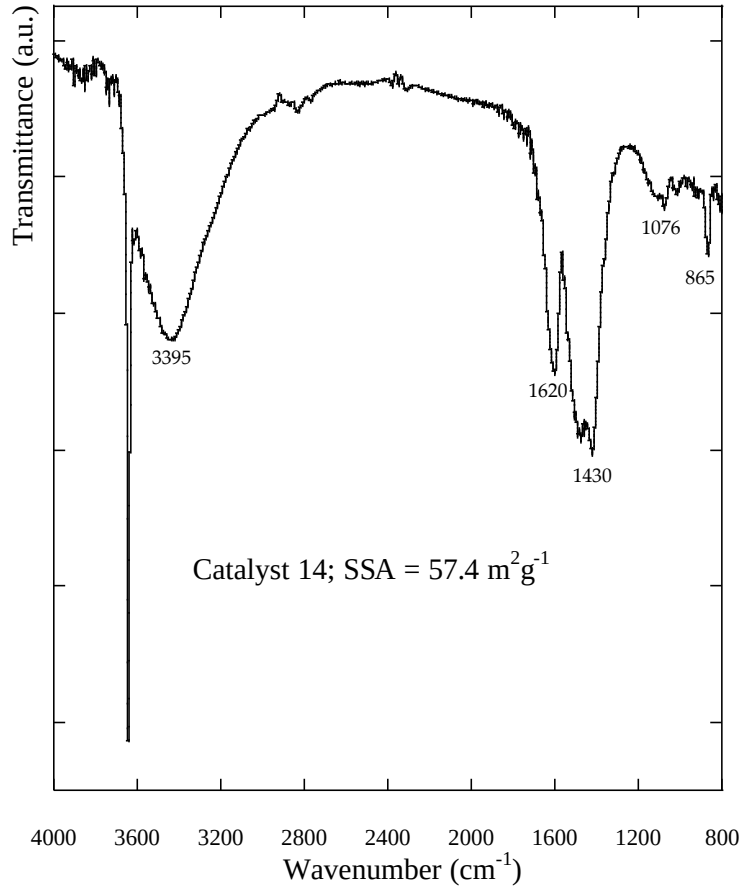
Transmittance (a.u.)
1076
865
3395
1620
1430
Catalyst 14; SSA = 57.4 m2g-1
4000
3600
3200
2800
2400
2000
1600
1200
800
Wavenumber (cm-1)

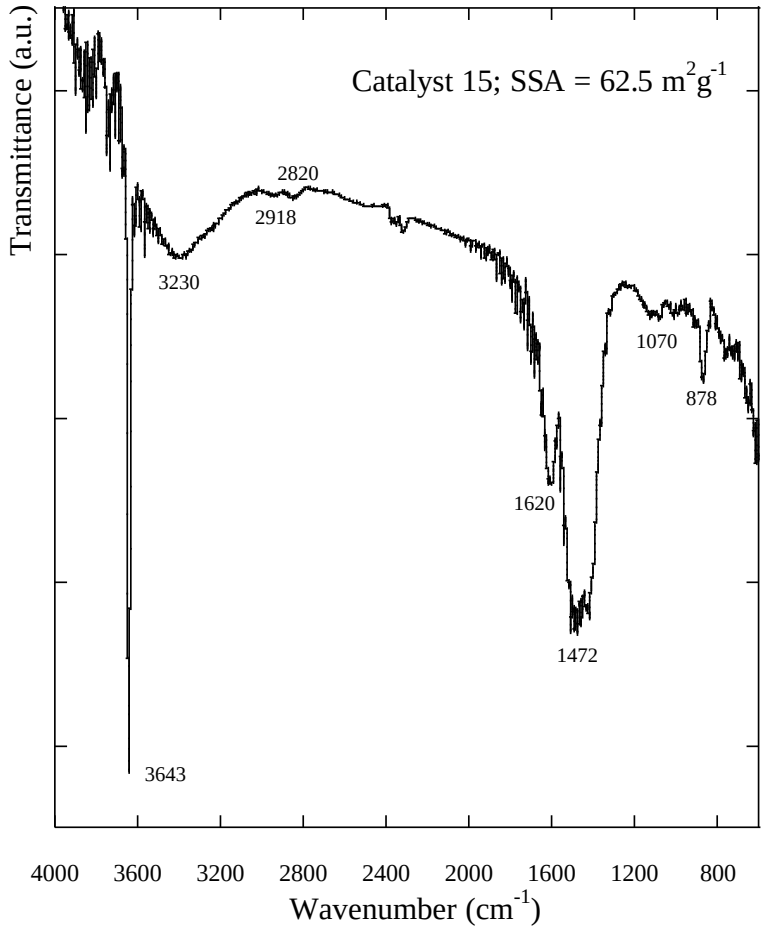

Fig. 2 FTIR spectra of ground CaO-ss after processing by methanol-assisted dry nano-grinding.

2-3-2 Methanolysis of soybean oil

As many studies have reported, the reaction rate of heterogeneous methanolysis reaction rate is predominantly determined by both mass transfer and the surface reaction, but the limitations of mass transfer limitations are slightly more significant than those of the reaction [**2, 36, 38**]. Therefore, in order to improve the overall rate, the mass transfer limitations present in the initial stages of the methanol–oil–solid catalyst system needs to be reduced first. The results of methanolysis reactions using the CaO-ss catalysts are presented in **Fig. 3 (a)** and **(b)**, showing that the catalytic activity of the ground CaO-ss is much higher compared to untreated CaO. Under the reaction conditions detailed in the Methods section, ester yields in the range of 29.8–72.3% were obtained. On increasing the catalyst SSA from the lowest value of 0.4 m^2g^{-1}, the rate of methanolysis was observed to increase drastically (**Table 2**). These faster reaction rates can be ascribed to the improved access of reactant molecules to basic sites at surface of the ground CaO-ss catalyst, which arises from the increase in surface area. Additionally, the high SSA values associated with nanoscale crystallite sizes provide shorter paths for reactant to surface of the catalyst, which also reduces the mass transfer limitations [**2**]. On decreasing the mass transfer limitations, the surface reaction rate subsequently increased, leading to a distinctly increased overall rate of reaction and decreased reaction time.

The Koras-Nowak criterion test was conducted to assess whether the measured CaO catalyst ground catalytic activity was independent of the influence of transport phenomena [**39**]. Similar to previous report in [**25**], the reaction was conducted on two catalysts, Catalyst 12 and Catalyst 15 with different SSA and active phases. In a typical test, with similar fractional exposures of basic sites but having different SSA. In present study, 2 wt.% of Catalyst 12 and or 4 wt.% of Catalyst 15 catalyst dosages was applied

at 65±1 °C with a methanol-to-oil molar ratio of 12:1 or methanol-to-oil molar ratio of 9:1. Samples were taken every 5 min, then analyzed by GC. When the conversion of the soybean oil was the same, the reaction recorded. The results exhibited in **Fig.4** showed that the TOFs on the two catalysts were nearly the same with the same conversion, thus indicated that the reaction obeyed the Koras-Nowak criterion.

Figure 3 (a) and **(b)** also show that the reaction rate did not increase directly proportionally to the SSA, as was expected. For example, in the case of catalysts 6 and 12 (**Table 1**), the former produced an ester yield of 50.8% with a SSA of 25.9 m^2g^{-1}, whereas the latter only produced an ester yield of 39.5%, despite possessing an SSA of 45.6 m^2g^{-1}. The XRD pattern of the lower SSA catalyst 6 indicated that calcium oxide was present as the major phase along with significant quantities of calcium methoxide, whereas the diffraction peak arising from calcium hydroxide was small. In contrast, catalyst 12 (higher SSA) was observed by XRD to contain only calcium hydroxide. This implies that the active phases on the catalyst surface played a crucial role in determining catalytic activity of the ground CaO-ss during the methanolysis reaction. Since the reaction occurs on the surface of the catalyst, the number of accessible basic sites, the basicity of those sites, and the rate of mass transfer to them determine the reaction rate (**Table 2**). Analogous results have been published by Kouzu *et al.*, who reported that calcium hydroxide was much less active in the methanolysis of soybean oil than calcium oxide. The authors ascribed the lower catalytic activity to the differing basicity of the catalysts [**18**].

Surprisingly, catalysts 3, 5–7, 10, 13, and 14 exhibited higher ester production: yields between 44% and 72% were achieved at 20 min, while yields of 92–97% were achieved at 1 h for all samples (**Table 2**). From the XRD patterns (**Fig 1 (a)-(c)**) and FT-IR spectra (IR bands at 3643 cm^{-1} and 3300–3500 cm^{-1}, **Fig. 2**), all of these ground

CaO-ss catalysts were found to contain calcium hydroxide on their surfaces, which would be expected to hinder the methanolysis. We attribute their high performance to a faster rate of methoxide anion generation via surface OH^- which initiates the methanolysis reaction [**14, 40, 41**]. These results are in good agreement with previous reports, which assert that neighboring hydroxyl groups (formed by methanol-assisted dry nano-grinding) modify the basic strength of the Ca^{2+}–O^{2-} pair, which methanol adsorbs onto directly prior to methoxide anion generation. The methoxide anion then forms a tetrahedral intermediate, and thus is a key component in the initiation of the transesterification reaction. Although physisorbed water molecules were detected on the surface of catalysts 3, 5–7, 10, 13, 14 (IR bands at 1650–1600 cm^{-1}), these seemingly acted as Bronsted basic sites for methanol activation [40]. On the other hand, the activities of catalysts 11, 12, and 15 showed a low rate of methanolysis—ester yield of 37–54% achieved after 20 min—most likely owing to their complete conversion to calcium hydroxide (**Fig. 1 (c)**): these results agree with the previously published reports [**15, 16**]. From these results, we can conclude that the catalytic activity of ground CaO-ss is determined not only by SSA but also by its basicity, and that the presence of high quantities of calcium hydroxide hinders the performance of the catalysts. **Fig.5** shows a possible mechanism for transesterification catalyzed by the ground CaO-ss with its active phases. Methanol and triglyceride are adsorbed on several neighboring free of CaO-ss catalytic sites (O^-, OH^-, Ca^{2+}). Surface O^- and OH^-, extracts an H^+ and Ca^{2+} adsorbs CH_3O^- from CH_3OH to form CH_3O^- and H^+ on the surface. The adsorbed triglyceride forms a surface intermediate. The two neighboring adsorbed species react to result in the formation of fatty acid methyl ester and diglyceride. The diglyceride reacts with methanol along the similar processes on the surface of catalyst to form glycerol and esters.

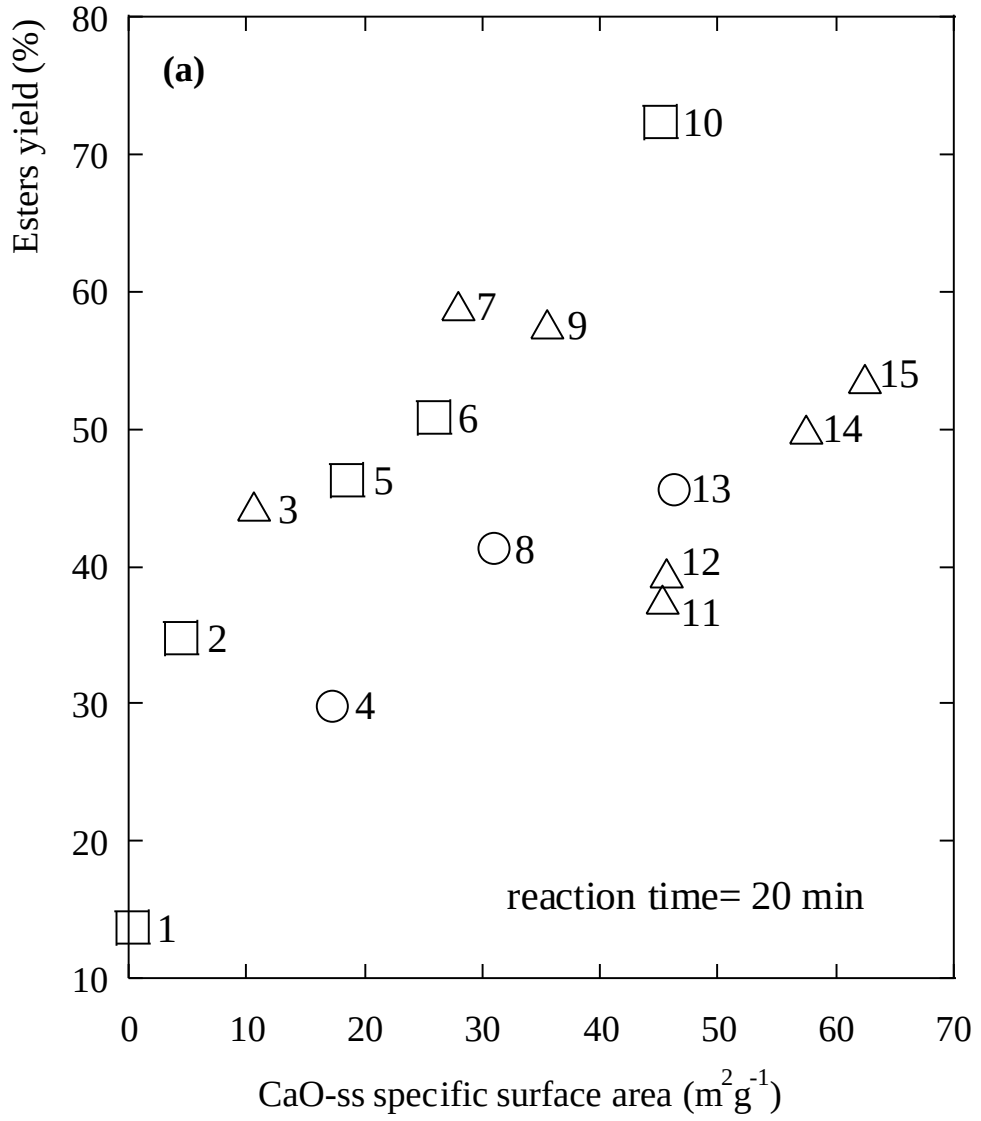

Fig. 3 (a) Ester yields after 20 min of reaction. Plot correlating the ester yield of heterogeneous methanolysis with the specific surface area and active phases of the ground CaO-ss catalyst. Square denotes that calcium oxide active phase is present; triangle denotes that calcium hydroxide active phase is present; circle denotes calcium methoxide active phase is present. Numbers indicate catalysts number (see **Table 2**).

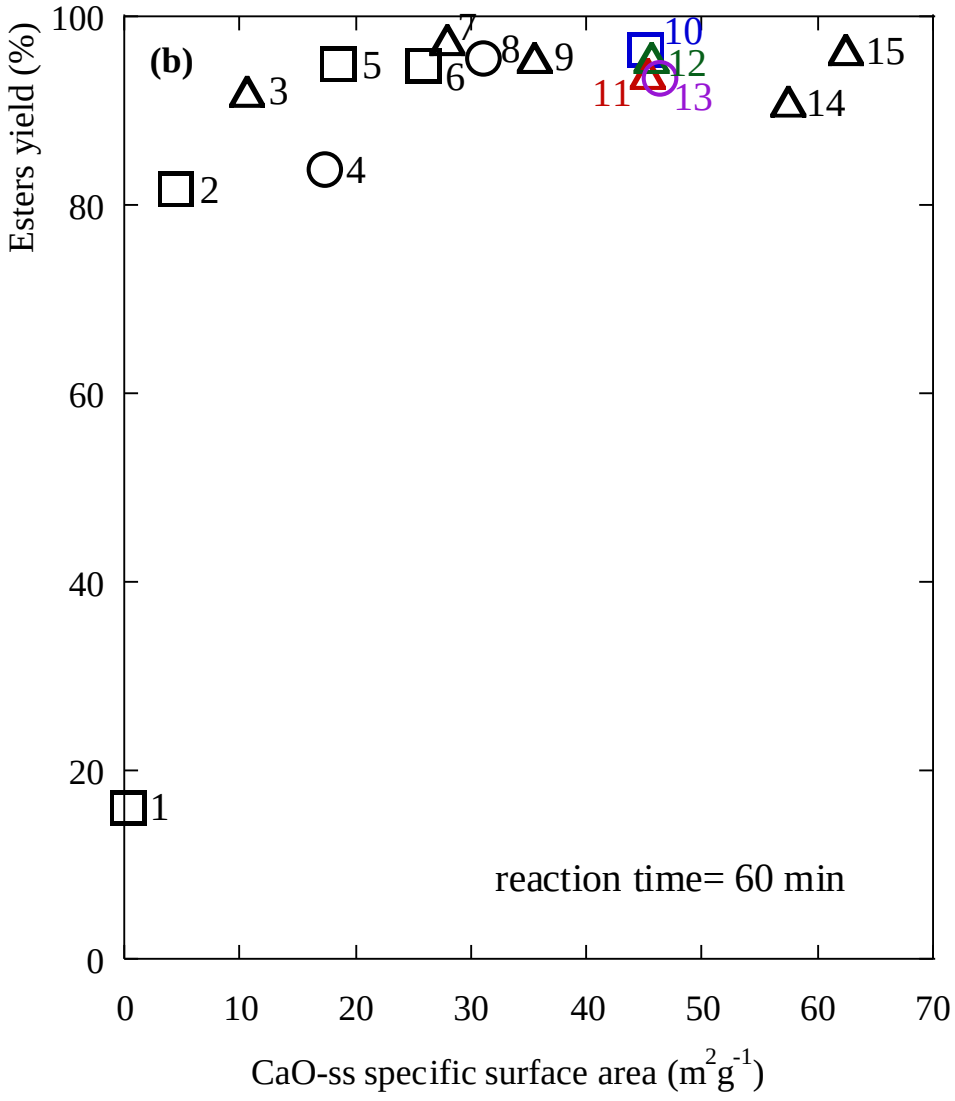

Fig. 3 (b) Ester yields after 60 min of reaction. Plot correlating the ester yield of heterogeneous methanolysis with the specific surface area and active phases of the ground CaO-ss catalyst. Square denotes that calcium oxide active phase is present; triangle denotes that calcium hydroxide active phase is present; circle denotes calcium methoxide active phase is present. Numbers indicate catalysts number (see **Table 2**).

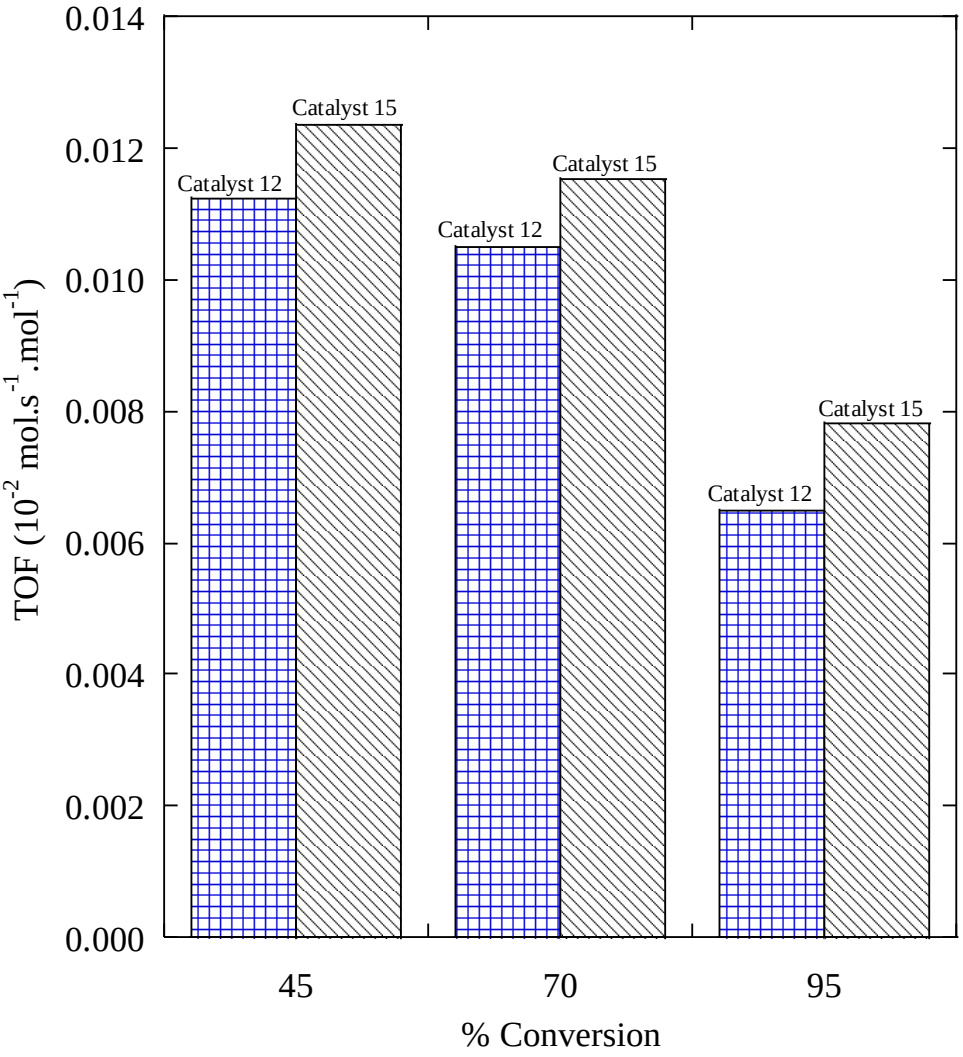

Fig.4. TOF of 2 wt.% of Catalyst 12 and or 4 wt.% of Catalyst 15 catalyst dosages was applied at 65±1 °C with a methanol-to-oil molar ratio of 12:1 or methanol-to-oil molar ratio of 9:1.

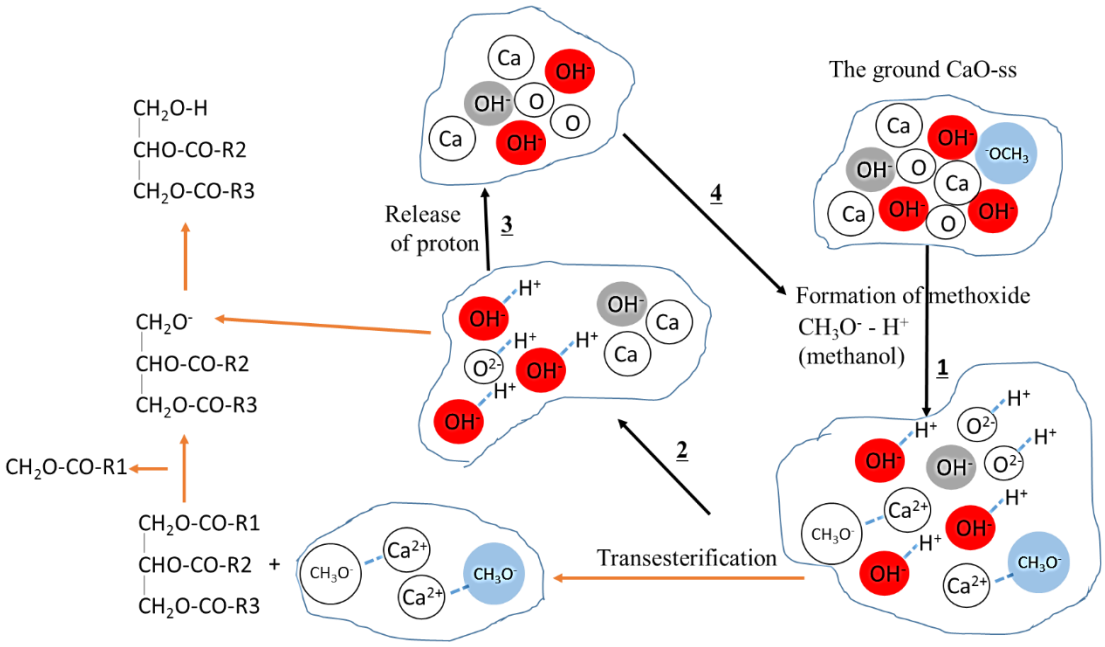

Fig.5 A proposed mechanism for transesterification catalyzed by the ground CaO-ss with its active phases. (OH^-) in red is hydroxyls from partially transformed to $Ca(OH)_2$, (OH^-) in grey is hydroxyls from totally transformed to $Ca(OH)_2$, CH_3O^- in blue is methoxide from partially transformed to Ca-methoxide on the ground CaO-ss surface.

It has been previously reported that calcium methoxide has a higher basic strength and higher catalytic activity during methanolysis compared to CaO and $Ca(OH)_2$ [**5, 24, 26, 36**]. The results in this work do not show this trend; catalysts 4 and 8 (calcium methoxide as the major active phase) displayed a lesser degree of activity compared to catalysts 5 and 6 (calcium oxide being the dominant phase) (**Table 2**). A plausible explanation for this relates to the strong bonding between the calcium methoxide phase and the bulk catalyst. This behavior would result in slower nucleophilic attack on the triglyceride carbonyl carbon to yield a tetrahedral intermediate, which starts the methanolysis reaction. As mentioned above, the rate of CaDg formation is an indication of the degree of mass transfer limitation in the system. In an attempt to assess the structural strength of the calcium methoxide active phase bonded to the bulk catalyst, XRD was used to identify the point at which the catalyst structure converts to CaDg. **Figure 6 (a)** and **(b)** shows the XRD patterns of Catalysts 4 and 8 prior to reaction and at 10 min, 20 min, and 60 min of reaction. The patterns were fingerprinted using the calcium oxide phase (ICDD file 04-1497), calcium hydroxide phase (ICDD file 04-0733), calcium methoxide reported in [**26**], and CaDg reported in [**42**]. The SSA of catalysts 4 and 8 were measured to be 17.3 m^2g^{-1} and 31 m^2g^{-1}, respectively. According to Esipovich *et al.*, CaDg can form through interaction with $Ca^{\delta+}$ and $CH_3O^{\delta+}$ groups: the surface $CH_3O^{\delta+}$ extracts H from glycerol and $Ca^{\delta+}$ adsorbs glyceroxide [**7**]. From the XRD patterns of used catalyst 4, the active calcium methoxide phase was shown to be present, even after 60 mins of reaction. The enhancement in SSA of the catalyst from 17.3 m^2g^{-1} to 31 m^2g^{-1} in catalyst 8 with reference to the XRD patterns in **Figure 6 (a) and (b)** identifying which features indicate that calcium methoxide to CaDg conversion occurs more rapidly. Hence, the higher SSA of the catalyst contributed to lowering mass transfer limitations during the initial stages of the reaction.

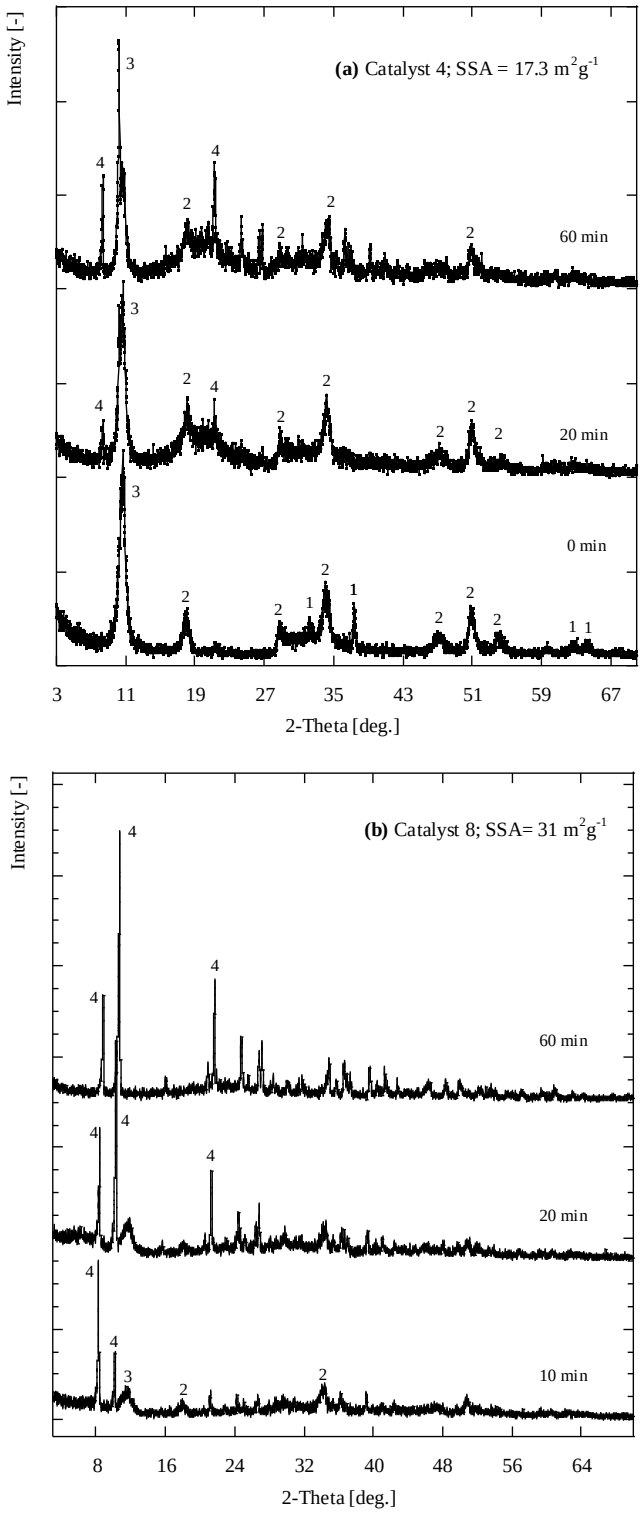

Fig. 6 XRD patterns of used catalysts collected after taking part in the heterogeneous methanolysis reaction: (a) catalyst 4, and (b) catalyst 8. (1) CaO, ICDD file 04-1497; (2) $Ca(OH)_2$, ICDD file 04-0733; (3) $Ca(OCH_3)_2$ was taken from [**26**]; (4) CaDg was taken from [**42**].

To study the role of SSA and active phases (**Fig. 2**) in reducing mass transfer limitations in the methanolysis of soybean oil, we also investigated chemical changes in the catalysts during the reaction. It has previously been reported that the presence of CaDg predominantly affects the initial stage of the methanolysis reaction [**17**]: CaDg promotes the mutual miscibility of triglycerides and methanol, increasing the area of the liquid–solid interface (the liquid component consisting of triglycerides in the methanol phase), which, in turn, increases the overall methanolysis rate. Additionally, another study concluded that CaO only acts as an active phase at the beginning of the reaction, while CaDg is believed to be the 'true' active phase in CaO-catalyzed methanolysis [**18**].

The results of this investigation show that the presence of active phases at the surface of high SSA CaO-ss catalysts play a determining role in reducing mass transfer limitations during the initial stages of reaction. From this, it is evident that active phases can modify the basicity of the catalysts to either stronger or weaker degrees, which mostly occurs in the case of calcium hydroxide.

Taking the case of catalyst 10 and Entry 12 (**Table 2**), we can investigate the effects of the presence of the active calcium hydroxide phase. The SSA of catalyst 10 was 45.2 m^2g^{-1}, and 45.6 m^2g^{-1} for catalyst 12, producing ester yields of 72.3% and 39.5%, respectively. Although measurement of catalyst basicity was not conducted in this work, it can be inferred from the results that the active calcium hydroxide phase on the surface of catalyst 10 was able to modify and enhance the surface basicity, whereas the calcium hydroxide phase on the surface of catalyst 12 did not show the same behavior. The XRD patterns (**Fig. 1 (b)** and **(c)**) showed that a $Ca(OH)_2$ peak was visible in catalyst 10, but the bulk had not been fully transformed to $Ca(OH)_2$; on the other hand, catalyst 12 was observed to have undergone a full transformation to $Ca(OH)_2$. The activity of these two

catalysts can be evaluated by comparing the time of CaDg formation in the methanolysis reaction. **Figure 7 (a)** and **(b)** show rapid formation of CaDg formation on catalyst 10 during the first 10 min of the reaction; in contrast, CaDg was only observed to form on catalyst 12 after 60 mins. This reiterates that CaDg is important not only for improving the miscibility between methanol and oil, but also, as previous authors have reported, as a highly active phase during the heterogeneous methanolysis reaction [**17, 42**].

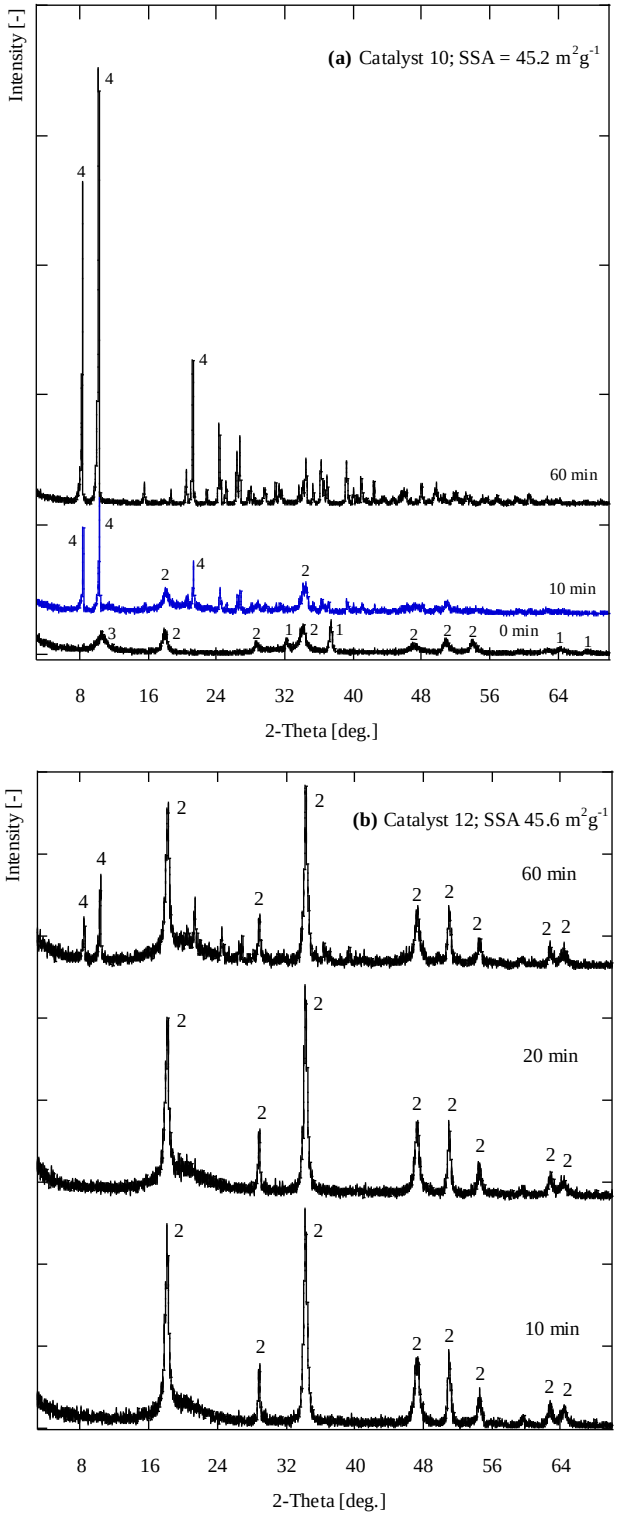

Fig. 7. XRD patterns of the used catalysts collected from the heterogeneous methanolysis reaction for (a) used catalyst 10, and (b) used catalyst Entry 12. (1) CaO, ICDD file 04-1497; (2) $Ca(OH)_2$, ICDD file 04-0733; (3) $Ca(OCH_3)_2$ refer to [26]; (4) CaDg refer to [**42**].

2-3-3 Reusability Study

The ability to be recycled of catalyst is an important aspect for practical application in industry. The reusability of the ground ground CaO-ss was examined at 65 °C for 5 cycles. The catalyst with SSA 45.2 m^2g^{-1} was chosen for stability test under conditions that mentioned in *Experimental section*. Once the batch reaction was ended, the reaction mixture was centrifuged and the spent catalyst was separated. The spent catalyst later was washed with 2-propanol in 2 times, wet spent catalyst then feed to next batch reaction. **Fig. 8** shows results of reusability experiments for ground CaO-ss catalyst with SSA 45.2 m^2g^{-1}. The results exhibited the catalyst had good stability for the 5 cycles.

A slight yield decrease was observed after 4 cycles with the yield, descending to 96.6 % at the 5^{th} cycle. To clarify this decreased yield, XRD and SEM analyses were conducted. The diffractogram of the 5^{th} spent catalyst show lower intensity of the 5^{th} cycle (CaDg peak) as shown in **Fig. 9** compared to the fresh spent catalyst. The wide peak between 2θ = 18-23^o can be ascribed to overlapping of patterns of CaDg and Ca-hydroxide. The morphology of the fresh Ca-DG and spent of the 5^{th} cycle showed the changing in crystallites shape [**Fig. 10** and **Fig. 11**]. The CaDg can be identified with a rectangular shape [**18**]. It can be noticed that true active sites of CaDg catalyst activity start to deactivate by existence of $Ca(OH)_2$. Referring to Kouzu et al. [**9**], the leaching of CaDg only in presence of H_2O: $Ca(C_3H_7O_3)_2 + 2H_2O \leftrightarrow Ca^{2+} + 2OH^- + 2C_3H_8O_3$. Possibly, a small portion water contain in alcohol used to wash the spent catalyst, and wet application induced the leaching reaction.

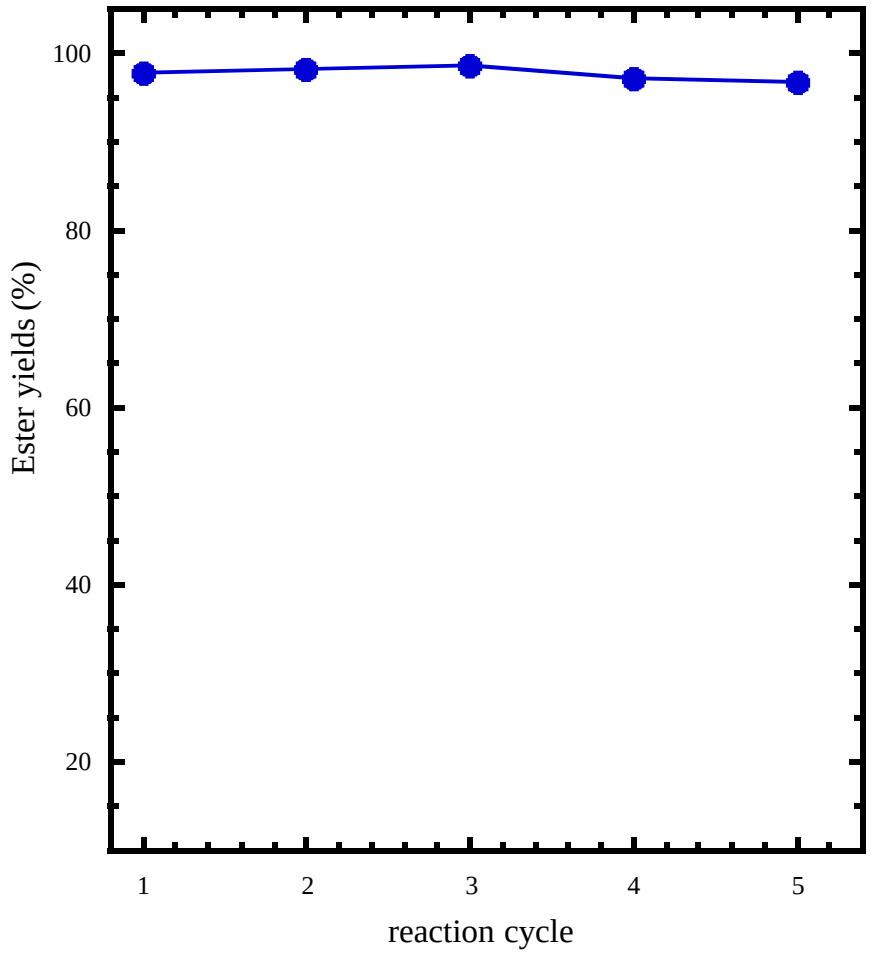

Fig. 8 Effect of reusability on biodiesel yield of ground CaO-ss catalyst with SSA 45.2 m^2g^{-1}; at 65±1 °C with a methanol-to-oil molar ratio of 9:1 and catalyst concentration of 4 wt% with respect to the oil mass.

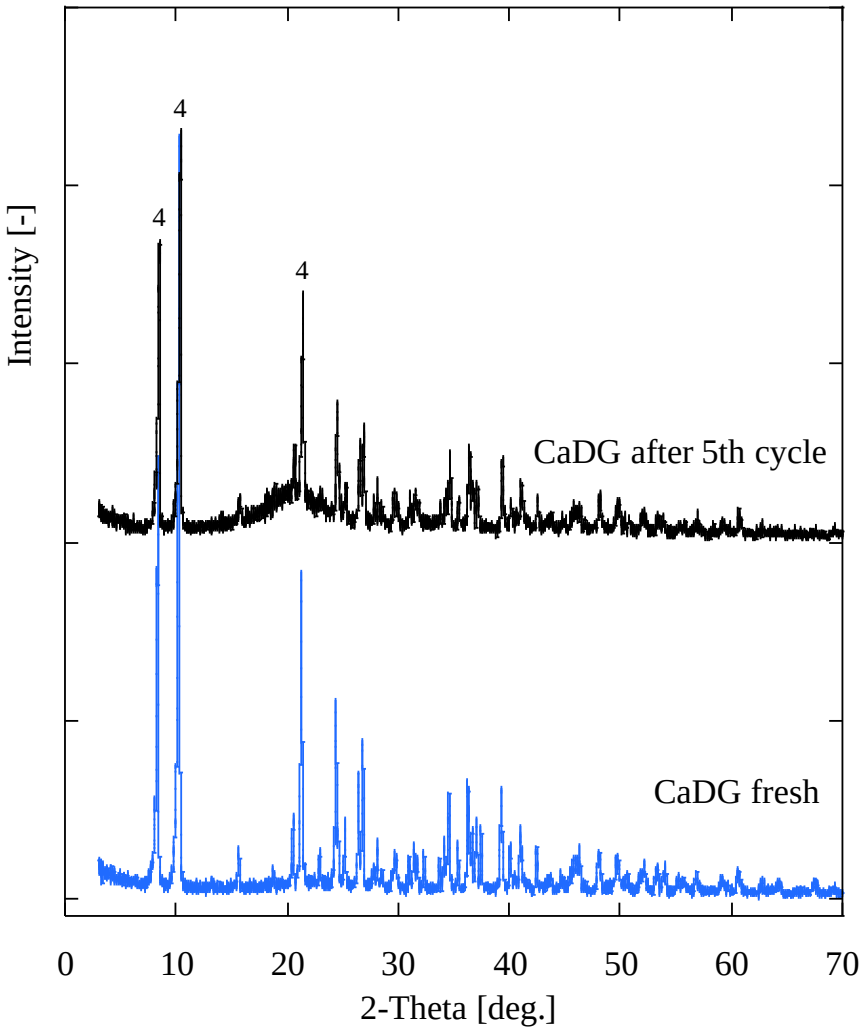

Fig. 9 XRD patterns of post reaction of ground CaO-ss catalyst with SSA 45.2 m^2g^{-1}; at 65±1 °C with a methanol-to-oil molar ratio of 9:1 and catalyst concentration of 4 wt% with respect to the oil mass; (4) CaDg refer to [**42**].

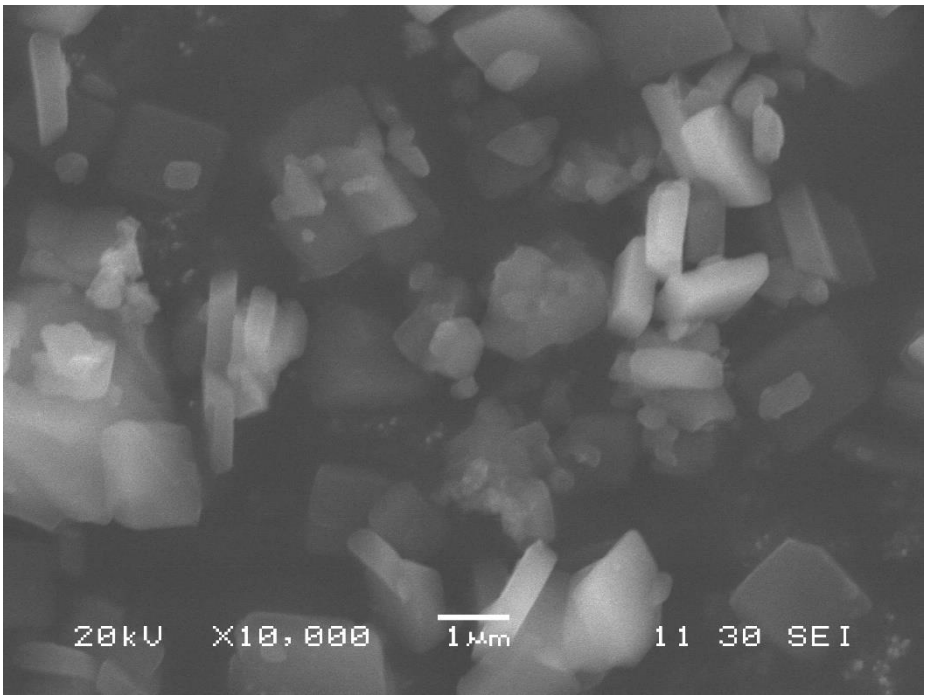

Fig. 10 SEM micrograph of CaDg fresh

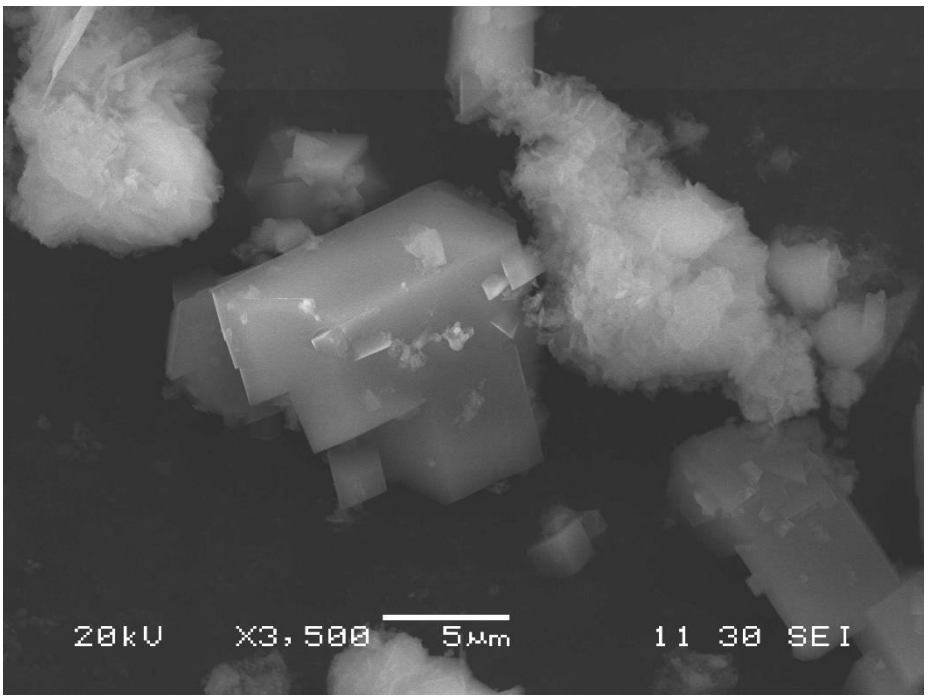

Fig. 11 SEM micrograph of CaDg after 5 cycles.

2-4. Conclusions

The SSA of CaO-ss was successfully enhanced by methanol-assisted dry nano-grinding. Characterization of CaO-ss after nano-grinding showed that this process could generate three different calcium-based phases on the oxide surface: calcium oxide, calcium methoxide, and calcium hydroxide. These active phases behave differently during methanolysis, and they were observed to modify the basicity of the catalyst surface, which can affect the overall reaction rate. The highest catalytic activity in a heterogeneous methanolysis reaction was observed for CaO-ss samples that had undergone partial surface conversion to $Ca(OH)_2$.

These results show that the combination of a high SSA and an optimal active phase surface composition of the catalyst can be highly effective in suppressing the mass transfer limitations during the initial stage of the methanolysis reaction. High SSA, nanosized particles provide a large number of accessible reaction sites and shorter paths for reactant to surface of the ground CaO-ss, while specific active phases simultaneously enhanced the basic strength of the catalysts. This behavior has an important role at the beginning of the methanolysis reaction as it strongly affects the formation of CaDg, which not only improves miscibility of oil and methanol, which reduces mass transfer limitations, but also actively catalyzes the heterogeneous methanolysis reaction. The reduction in CaDg formation time during the early stages of the reaction was an important effect arising from the combination of high SSA and effective active phase composition on the catalyst surface. Reusability of catalyst was employed for 5 successive catalytic cycles under the same experimental without loss the catalytic activity.

References

[1] R. Wang, H. Li, F. Chang, J. Luo, M.A. Hanna, et al, Catal. Sci. Technol. 3 (2013) 2244-2251.

[2] L. Zhao, Z. Qiu, S.M. Stagg-Williams, Fuel Processing Technology 114 (2014) 154-162.

[3] S. H. Teo, Y. H. Taufiq-Yap, U. Rashid, A. Islam, RSC Adv. 5 (2015) 4266-4276.

[4] A. N. R. Reddy, A. A. Saleh, Md. S. Islam, S. Hamdan, Md. A. Maleque, Energy Fuels 30 (2016) 334-343.

[5] D. Cornu, H. Guesmi, G. Laugel, J. M. Krafft, H. Lauron-Pernot, Phys. Chem. Chem. Phys. 17 (2015) 14168-14176.

[6] C. R. V. Reddy, R. Oshel, J. G. Verkade, Energy & Fuels 20 (2006) 1310-1314.

[7] A. Esipovich, S. Danov, A. Belousov, A. Rogozhin, J. of Molecular Catalysis: Chemical 395 (2014) 225-233.

[8] D. Cornu, H. Petitjean, G. Costentin, H. Guesmi, J. M. Krafft, H. Lauron-Pernot, Phys. Chem. Chem. Phys. 17 (2013) 19870-19878.

[9] M. Kouzu, S. Yamanaka, J. Hidaka, M. Tsunomori, Applied Catalysis A: General 355 (2009) 94-99.

[10] K. Wilson, C. Hardacre, A. F. Lee, J. M. Montero, L. Shellard, Green Chem. 10 (2008) 654-659.

[11] A. Buasri, N. Chaiyut, V. Loryuenyong, P. Worawanitchaphong, S. Trongyong, Sci. World J. 2013 (2013) 1-7.

[12] H. Moriyasu, K. Koshi, A. Sato, T. Suzuki, A. Nakagaito, M. Kouzu, J. of Japan Institute of Energy 91 (2012) 495-502.

[13] M. L. Granados, A. C. Alba-Rubio, F. Vila, D. Martin Alonso, R. Mariscal, Journal of Catalysis; 276 (2010) 2 229-236.

[14] Y. Xi, R. J. Davis, J. Catal. 254 (2008) 190-197.

[15] M. Kouzu, M. Tsunomori, S. Yamanaka, J. Hidaka, Adv. Powder Technol. 21 (2010) 488-494.

[16] A. A. Refaat, Int. J. of Environ. Sci & Technol. 8 (2011) 203-221.

[17] I. Lukic, Z. Kesic, M. Zdujic, D. Skala, Fuel 165 (2016) 159-165.

[18] M. Kouzu, T. Kasuno, M. Tajika, S. Yamanaka, J. Hidaka, Applied Catalysis A: General 334 (2008) 357-365.

[19] S. Yamanaka, A. Suzuma, T. Fujimoto, Y. Kuga, J. Nanopart. Res. 15 (2013) 1573-1581.

[20] M. Hasegawa, M. Kimata, M. Shimane, T. Shoji, M. Tsurata, Powder Technology 114 (2001) 145-151.

[21] A. M. Kalinkin, E. V. Kalinkina, O. A. Zalkind, T. I. Makarova, Inorganic Material 41 (10) (2005) 1073-1079.

[22] P. L. Guzzo, J. B. Santos, R. C. David, Int. J. of Mineral Proc. 126 (2014) 41-48.

[23] Z. Kesic, I. Lukic, D. Brkic, M. Zdujic, H. Liu, et al., Appl Catal Gen 427-428 (2012)58-65.

[24] A. Kawashima, K. Matsubara, K. Honda, Bioresour. Technol. 99 (2008) 3439-3443.

[25] N. Kaur, A. Ali, Fuel Processing Technology 119 (2014) 173-184.

[26] A. Kawashima, K. Matsubara, K. Honda, Bioresour. Technol. 100 (2009) 696-700.

[27] C. Plank, E. Lorbeer, J. of Chromatography A 697 (1995) 461-468.

[28] T. Watanabe, J. Liao, M. Senna, J. of Solid State Chemistry 115 (1995) 390-394.

[29] M. S. Kaliszewski, A. H. Heuer, J. Am. Ceram. Soc. 73 (6) (1990) 1504-1509.

[30] M. Senna, Advanced Powder Technol. 13 (2) (2002) 115-138.

[31] M. L. Granados, M. D. Zafra Poves, D. Martin Alonso, R. Mariscal, F. Cabello Galisteo, et al, Applied Catalysis B: Environmental 73 (2007) 317-326.

[32] J. Kondo, Y. Sakata, K. Maruya, K. Tamaru, T. Onishi, Applied Surface Science 28 (1987) 475-478.

[33] C. T. Vo, L. K. Huynh, J. –Y. Hung, J. Chaing Jiang, Applied Surface Science 280 (2013) 219-224.

[34] H. Jeziorowski, H. Knozinger, W. Meye, H. D. Muller, J. Chem., Faraday Trans, 1, 69 (1973) 1744-1758.

[35] Y. Tang, L. Li, S. Wang, Q. Cheng, J. Zhang, Environmental Progress & Sustainable Energy 35 (1) (2016) 257-262.

[36] X. Liu, X. Piao, Y. Wang, S. Zhu, H. He, Fuel 87 (2008) 1076-1082.

[37] M. Weibel, R. K. Mishra, ZKG 6 (2014) 29-39.

[38] X. Liu, X. Piao, Y. Wang, S. Zhu, J. Phys. Chem. A. 114 (2010) 3750-3755.

[39] R. Song, D. Tong, J. Tang, C. Hu, Energy Fuels 25 (2011) 2679-2686.

[40] M. Sanchez-Chantu, L. M. Perez-Diaz, I. Pala-Rosas, E. Cadena-Torres, L. Juarez-Amador, et al., Fuel 110 (2013) 54-62.

[41] H. Petitjean, H. Guesmi, H. Lauron-Pernot, G. Costentin, D. Loffreda, et al., ACS Catal. 4 (2014) 4004-4014.

[42] M. Kouzu, J. Hidaka, K. Wakabayashi, M. Tsunomori, Applied Catalysis A: General 390 (2010) 11-18.

APPENDIX

Characters of calcined scallop shell

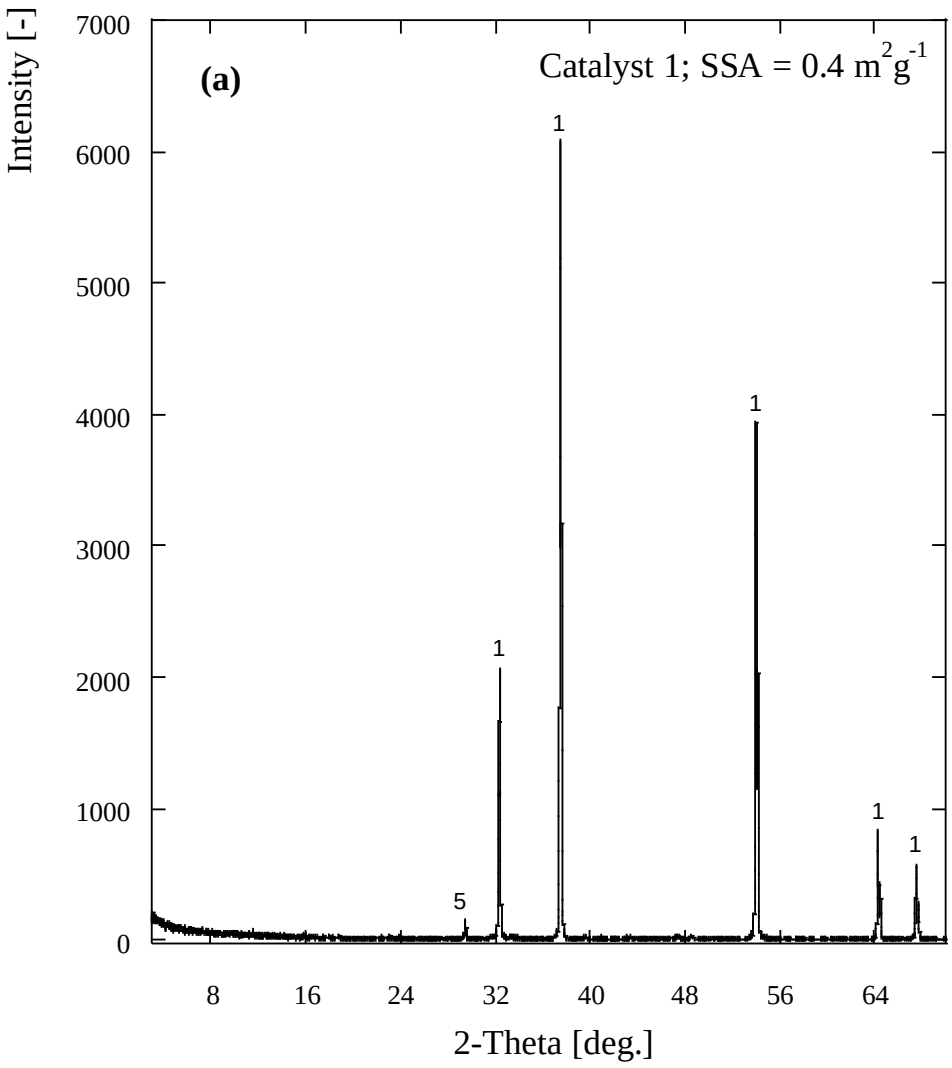

Fig. A.1 XRD patterns of scallop shells thermally calcined at 1000 °C for 3 h.

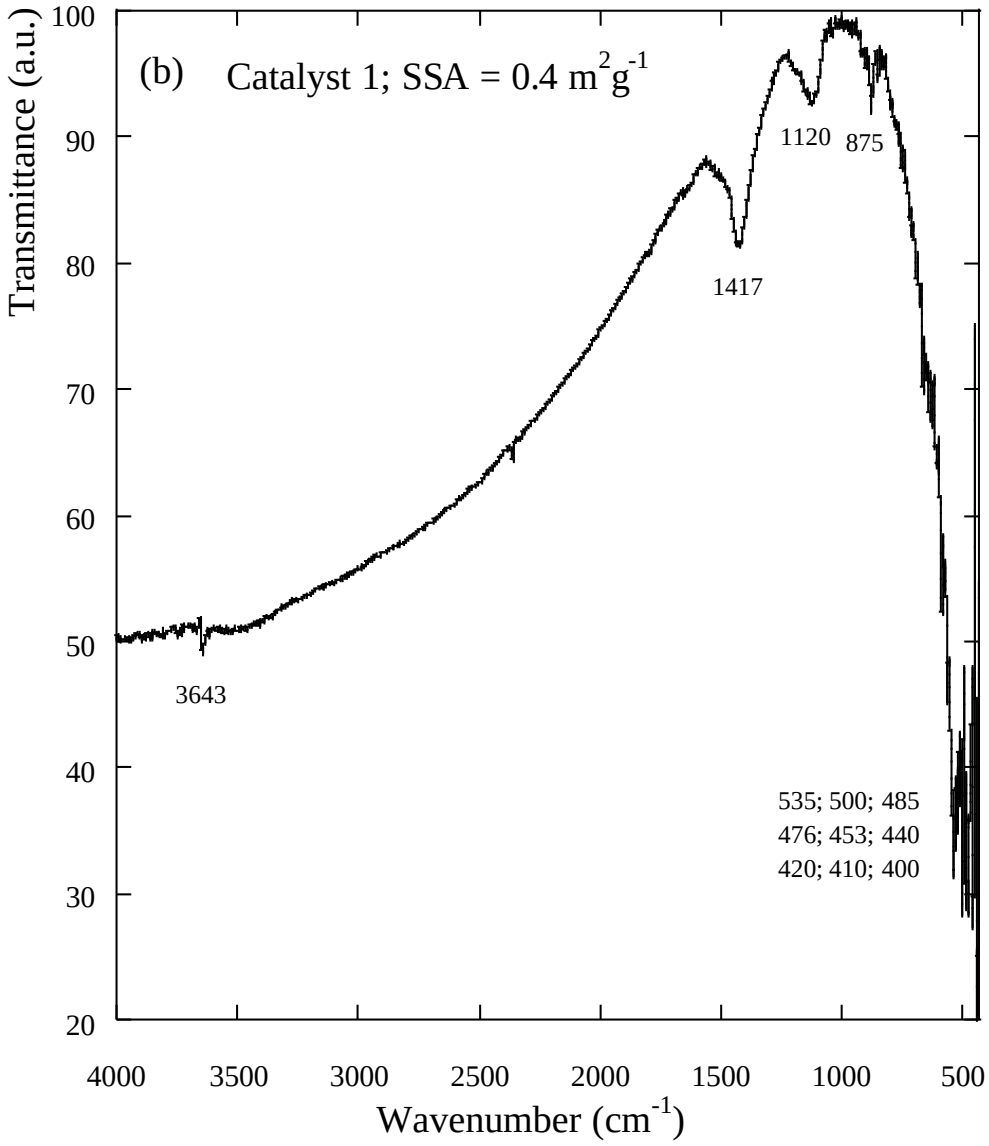

Fig. A.2 FTIR spectra of scallop shells thermally calcined at 1000 °C for 3 h.

Chapter 3

Enhancing scallop shell-derived CaO catalyst activity on biodiesel producing from waste cooking oil by alcohol-assisted nano-grinding

3-1 Introduction

CaO is a solid base catalyst extensively investigated in the transesterification to produce methyl ester (ME). ME is an alternative to fossil fuels that can be used alone or blended with fossil-diesel because its combustion characteristics are nearly similar with fossil-diesel [**1, 2**]. CaO is widely studied due to its high basicity, low solubility in organic solvents, available in a wide variety of sources, long service lifetime, and its effectiveness under mild reaction conditions [**3**]. However, the conversion rate is lower in comparison to homogeneous catalyst system which caused by mass transfer limitation in the initial heterogeneous regime and the specific surface area (SSA) of CaO catalyst is not sufficient to serve the reaction. Its raises some drawbacks in its industrial application, such low reaction rate, requires long time to achieve the maximal ME production, and requirement of high methanol to oil ratio [**2, 4-6**]. According to Liu *et al*. [**7**] the reaction rate of heterogeneous transesterification reaction rate is mainly determined by mass transfer and the surface reaction, but the limitations of mass transfer in the initial stage of reaction are slightly more significant than those of the reaction. This fact was as the prime drawback of reactivity of CaO catalysis in transesterification reaction [**4-6, 8, 9**].

In transesterification catalysis, the reaction is believed to take place at active sites on the catalyst surface. Hence, the catalytic constituents of CaO – such as SSA and active sites on catalyst surface *viz*. calcium hydroxide (Ca-hydroxide), calcium monoglyceroxide, calcium diglyceroxide and calcium alkoxide (Ca-alkoxide) – have important effects on activity of CaO catalyst on transesterification reaction in producing ME [**4, 10-15**]. In recent years, nanosized CaO catalyst with high SSA become a research topic in enhancing reaction rate of transesterification to produce biodiesel. In such previous works, have reported the activity of nanosized CaO was generally

showed to be higher than that of conventional CaO catalyst for biodiesel production. Nano-CaO with 85.0 m^2g^{-1} of SSA, a conversion as high as 94% was achieved after 2.5 h of reaction, temperature of 65 ^oC, molar ratio oil to methanol of 1:15 and catalyst weight percent of 2.5% [16]. While Zhao *et al*. [**4**] utilized a higher surface area (HSA) nano-CaO with 89.5 m^2g^{-1} of SSA, at 65 ^oC, 99.8% biodiesel yield was obtained at 2 h when 3 wt. % catalyst was used with 1:9 molar ratio oil to methanol. Meanwhile, Buasri *et al.* [**17**] utilized nano-CaO synthesized from mussel shells with SSA = 89.9 m^2g^{-1}, cockle shells with SSA= 59.9 m^2g^{-1}, and scallop shells with SSA= 74.9 m^2g^{-1} for biodiesel production from palm oil at 3 h reaction time, 1:9 molar ratio oil to methanol, at 65 ^oC, catalyst loading 10 wt. % and the reported at these conditions were 95.5%, 94.1% and 95.4%, respectively. Reddy *et al.* [**18**] synthesized nano-CaO from *Polymedosa erosa* with 90.6 m^2g^{-1} and reported a 98.5% biodiesel yield.

For CaO heterogeneously-catalyzed transesterification reaction for biodiesel synthesis, active sites concentration on CaO surface was found to be important factor for CaO catalyst activity. The active sites such as calcium methoxide, calcium ethoxide, calcium hydroxide and calcium glycerolate could improve the reaction rate. The existence of several active sites on CaO surface, significantly improve the strength of CaO basic [**14, 15, 19, 20**]. Most the authors ascribed the strength basic of active sites present at the surface are partly responsible of the catalytic activity due to transesterification reaction occurs on basic sites on the surface of CaO catalyst.

Another issue related with the CaO-catalyzed biodiesel production is susceptible of CaO pure to the existence of FFA and moisture content [**21**]. Commonly, in transesterification reaction, strong base catalyst produce soap instead of biodiesel and become deactivated if moisture is > 0.3 wt% and/or free fatty acid (FFA) contents is > 0.5 wt% in raw material [**22**]. To improve the activity of CaO towards low-quality

feedstocks, CaO could be enhanced by impregnating it with La_2O_3 or CeO_2, Mo, and Zn [**21, 22, 23, 24**].

The aim of the present work was to enhance the scallop shell-derived CaO catalyst activity on biodiesel production by using a simple alcohol-assisted nano-grinding method. Increasing the SSA and basicity and decreasing the crystalline size could provide high catalytic activity of CaO-based catalyst.

It is challenging to prepare CaO-based catalyst with high SSA and created several active sites at the surface of CaO at one-step process. To overcome this challenge, we tried to prepare the CaO-based catalyst with alcohol-assisted nano-grinding in batchwise and stepwise methods. In most of the studies on CaO-based catalyst preparation *via* the nano-grinding process, the effects of alcohol-assisted on nano-grinding on physico-chemical properties have not been extensively reported. The changes of physico-chemical properties of CaO-based catalyst due to alcohol-assisted nano-grinding and elucidation of the nano-grinding mechanism and their relationship in generating high SSA were examined in detail. The activity of the ground scallop shell-derived CaO catalyst on the biodiesel production from waste cooking oil (WCO) containing 10 wt% FFA and 0.11% moisture content also studied.

3-2 Experimental Section

3-2-1 Materials

Scallop shell powder, as a source of CaO, was purchased from Tokoro-cho Industry Promotion Public Corporation (Kitami, Japan). The powder then calcined at 1000 °C for 3 h. WCO was obtained from cafeteria of Muroran Institute of Technology (Japan). Chemicals used were synthesis grade methanol (>99.8%), ethanol (99.5%), 1-butanol (99.0%), dichloromethane (95%), hexane (99%), HCl and KOH. All the

chemicals were procured from Kanto Chemical (Japan). The basic strength of the CaO-based catalysts Hammett indicators: p-Nitroaniline (97%), Thymolphthalein, and Phenolphthalein (98%) were purchased from Kanto Chemical (Japan). Pyridine (99.8%) purchased from Sigma-Aldrich (Japan).

The FFA content in waste cooking oil was estimated in terms of KOH in milligrams in order to neutralize 1 g of fatty acid according to the procedure described elsewhere [**18, 25**]. A 2 g of the WCO diluted with 50 ml of 95% ethanol and diethyl ether in a 1:1 molar ratio were thoroughly mixed in a conical flask using magnetic stirrer. The mixture was titrated against 0.1 of KOH drop wisely using phenolphthalein solution (0.05 g of phenolphthalein to 50 ml of 95% pure ethanol and diluted to a 100 ml using distilled water) until the color turned pink and lasted for 10 s. The measurement repeated two times for accuracy and the FFA content was measured at 10 wt%. Determination of the moisture content (% wet basis) of WCO was measured as described in literature [**26**]. A 2 g of the WCO were placed in aluminium can which previously dried and tared. The moisture content were measured using an oven at 105 ^{o}C. After sitting in desiccator for 1 h to cool, the sample was weighed every 6 h until the weight remained constant. The measurement also repeated two times for accuracy, first measurement 0.105% of moisture content, second measurement 0.107% of moisture content. The average of the moisture content was measured at 0.11%.

3-2-2 Alcohols-assisted nano-grinding process

Calcined scallop shell (hereafter is labelled CaO) was ground in a planetary ball mill (Fritsch Pulverisette-7 premium line, Germany). The planetary ball mill was equipped with two zirconia pots of 80 cm^3 volume, each containing 100 g of yttria-stabilized zirconia milling beads (3 mm diameter). According to the manufacturer

(Nikkato Corporation, Japan) the grinding media has a density of 5.950 kg m^{-3} and chemical composition of 95% of zirconia and 5% yttria.

Alcohols used as solvents-aid were methanol, ethanol, and 1-butanol. The nano-grinding was conducted in two kind methods: batchwise and stepwise in alcohol addition [**27**]. The batchwise addition method was performed by adding the whole required volume of alcohol into the pot at the start of the nano-grinding process, whereas the stepwise addition method involved adding smaller quantities of alcohol to the pot at predetermined intervals. During batchwise addition, the nano-grinding operation was stopped for 15 min after every 1 h of grinding to prevent the inside of the milling pot from overheating. After a predetermined grinding time, the ground mixture was removed. The samples obtained from batchwise addition method are designated as M-CaO for methanol-assisted, E-CaO for ethanol-assisted, and B-CaO for 1-butanol-assisted. For comparison, the nano-grinding also conducted with bare grinding-assisted, thus the sample obtained labelled as N-CaO. The samples obtained from stepwise addition method are labelled as Ms-CaO for methanol-assisted and Bs-CaO for 1-butanol-assisted. We measured the temperature inside the pot-milling after 6 h grinding process in attempt to obtain the approximately temperature during the course of nano-grinding. The measurement conducted by direct contact of mercury thermometer (scale of 200 ^{o}C) with the ground CaO directly after the grinding process stop. To suspend the heat out after the pot opened, a rubber cover apply directly to the pot. The measurement repeated two times. The temperature of the nano-grinding pot of batchwise addition after 6 h processing was measured (as average): 90 °C for methanol-assisted, 140 °C for ethanol-assisted, 140 °C for 1-butanol-assisted, and 145 °C for bare grinding-assisted. The temperature of stepwise addition was 70 °C for methanol-assisted and 120 °C for 1-butanol-assisted. The conditions used in the nano-grinding

process are listed in **Table 1**.

Table 1

Alcohol-assisted nano-grinding conditions

Dry nano-grinding process conditions	
Zirconia pot volume, V	80 cm^3
Mass of milling beads, W_B	100 g
Bead-filling ratio relative to the pot volume, J[a] [**28**]	0.35
Bead diameter	3 mm
CaO weight charge in the pot, W_S	10 g
Sample loading ratio to void fraction of the beads, U[b] [**28**]	0.27
Revolution speed	900 rpm
Grinding time	6 h
Grinding method	1. Bare grinding-assisted 2. Batchwise with 1.25 g alcohol. 3. Stepwise with 0.66 g/h of methanol-assisted. 4. Stepwise with 0.66 g/h of 1-butanol-assisted.

[a] $J = [W_B/\{\rho_{ball} \times (1\text{-}0.4)\}]/V$
[b] $U = (W_S/\rho_p)/(0.4 \times J \times V)$

3-2-3 Catalysts characterization

The SSA of the powders was determined from nitrogen gas adsorption by using BET method (Microtrac, Adsotrac DN-04). Prior to measurement, samples were degassed at 473 K for 2 h.

X-ray powder diffraction (XRD) measurements were performed by a Multi Flex-120 NP Rigaku (Japan) equipped with a Cu-Kα anode (λ = 1.5418 Å), operated at a tension and current of 40 kV and 20 mA, respectively. Measurements were recorded at

room temperature over the 2θ range 3–70°, with a 0.02° step size. Crystalline phases were identified by comparison with ICDD data files.

Fourier-transform infrared (FTIR) spectra were recorded using a JASCO FTIR-460 PlusK spectrometer. A standard KBr pellet technique was applied for the sample preparation. Measurements were conducted over the range 4000 to 400 cm^{-1} with a 4 cm^{-1} resolution.

Hammett indicator investigations was conducted to determine the basic strength of the CaO-based catalysts. The following Hammett indicator were used: phenolphthalein (H_ = 9.3), thymolphthalein (H_ = 10.0), and 4-nitroaniline (H_ = 18.4). The total basicity (f_m) of the samples was measured by the method of Hammett indicator-benzene carboxylic acid (0.1 M anhydrous methanol solution) titration [**29**]. To quantify the Bronsted and Lewis acid sites in catalysts, pyridine adsorption method as described in literature [**30**] was employed. In typical experiment, catalyst sample was saturated with pyridine at room temperature and vacuum condition. The sample was then dried under vacuum at 50 ^oC for 2 h, further heated for 10 min at 300 ^oC to desorb the pyridine, and finally their FTIR spectra was measured.

A scanning electron microscope (SEM) analysis was carried out in JEOL JSM-6380A with an acceleration voltage of 20 keV. Prior to analysis, the sample was covered a carbon film.

Thermogravimetric (TAG) was performed with SII Exstar 6200 N thermogravimetric analyzer from 25 ^oC to 800 ^oC at a heating rate of 20 ^oC/min under nitrogen atmosphere.

Optical microscopy for catalyst dispersion on WCO-methanol system was performed through a 4x or 10x objective on an Olympus BX-51 inverted microscope, equipped with an Olympus DP72 digital camera (Olympus, Center Valley, PA).

3-2-4 Transesterification

The transesterification reaction of WCO with methanol was carried out in a glassware setup. The SSA used are 48.2 m^2g^{-1} M-CaO, 43.0 m^2g^{-1} E-CaO, and 51.4 m^2g^{-1} B-CaO. The transesterification was carried out at 65±1 °C with a methanol-to-oil molar ratio of 9:1 and catalyst concentration of 2 wt% with respect to the oil mass. The stirring rate was held at 800 rpm. For comparison, transesterification WCO with methanol under the same conditions also performed with SSA 1.6 m^2g^{-1} CaO reagent, 10.8 m^2g^{-1} N-CaO, and homogeneous base catalyst NaOH. Concentration used for NaOH was 1.2 wt% with respect to the oil mass.

Prior to analysis, samples (1 ml) were removed from the reaction mixture and immediately treated using a procedure detailed elsewhere [**31**]. The quantities of methyl ester, monoglyceride, diglyceride, and triglyceride were analyzed using a gas chromatograph (Shimadzu GC-14B) equipped with a flame ionization detector (FID), on a DB-5HT capillary column (14 m × 0.25 mm, 0.1 µm film thickness). The analytical work was performed with the following heating regime: holding at 50 °C for 1 min, followed by three separate steps of temperature increase, firstly to 180 °C at a rate of 10 °C/min, then to 230 °C at 7 °C/min, and lastly to 380 °C at 10 °C/min, at which point the temperature was held for 10 mins. Quantitative analysis was carried out following a procedure described in detail elsewhere [**32**].

3-3 Results and discussion

3-3-1 Changes in physico-chemical properties

3-3-1-1 XRD characterization studies

XRD patterns of CaO-based catalysts before and after alcohol-assisted nano-grinding are shown in **Fig. 1** and **Fig. 2**. Before nano-grinding, CaO, whereas starting material, the main peaks was related to CaO (ICDD file 04-1497), except peak (4) at 2θ of 29.4 indicated the existence of calcium carbonate (ICDD file 47-1743). For samples of the post alcohol-assisted nano-grinding with batchwise and stepwise method, XRD patterns suggested a number of different active sites on CaO-based catalysts surface. The crystalline active sites were indexed and matched to three known materials: Ca-oxide (ICDD file 04-1497), Ca-hydroxide (ICDD file 04-0733), and Ca-alkoxide (reported in [**15**]). The formation of Ca-hydroxide and Ca-alkoxide on surface of the ground CaO-based catalysts surface was due to adsorption of alcohol vapor which could promoted chemisorption during the nano-grinding process. As shown in **Fig. 1 (b)**, the primary active site of Ca-oxide accompanied with weak peaks Ca-alkoxide and Ca-hydroxide were existed in the ground CaO-based catalysts. A more significant occurrence of these peaks were observed when the nano-grinding conducted with stepwise method (**Fig. 2 (a)** and **(b)**). As suggested by XRD patterns, the formation of partially Ca-alkoxide can be found when methanol or ethanol assisted the nano-grinding process, while in 1-butanol assisted could not detected. As reported in [**33, 34, 35, 36**] that hydrogen atoms (H) from alcohol groups form hydrogen bonds with oxygen atoms (O) of CaO and hydroxide ions (OH). Thus, oxygen atoms (O) of alcohol groups coordinate with calcium ions (Ca) of the CaO-based catalyst to form partial crystallite of alkoxide. However, mostly adsorption of alcohol vapor is reversible. Furthermore, according to author in [**36**], generally at grinding temperature above the boiling point

of grinding aid has small binding force, therefore adsorbed molecules can desorb from the surface of ground material. Small binding force caused by poor interaction or adsorbed too weakly of alcohol vapor on the ground CaO particles which resulted poor chemisorption and unstable separating layers between the ground CaO particles. This phenomenon might be explained the differing of active sites on the surface of ground CaO-based catalysts (**Fig. 1 (b)**).

At the case stepwise addition method (**Fig. 2 (a)** and **(b)**), it is necessary to increase the amount added of alcohol assists to cover at least half of the ground CaO particles. It can be maintained the sufficient adsorption of the amount of alcohol vapor on the particles and increase the chemisorption reaction to form partially Ca-alkoxide or Ca-hydroxide on the ground CaO-based catalyst surface. According to XRD patterns (**Fig. 2 (a)** and **(b)**), the stronger of crystallite of active sites formed, during the nano-grinding with stepwise addition, resulted by the higher of addition level of alcohol. Nevertheless, sufficient of alcohol adsorption on particles surface did not lead the formation partially of Ca-alkoxide directly, as shown in (**Fig. 2 (a)** and **(b)**), decomposition of alcohol in the level of nano-grinding temperature and binding forces of decomposed material determine the reaction on particles surface to form the active site [**35**].

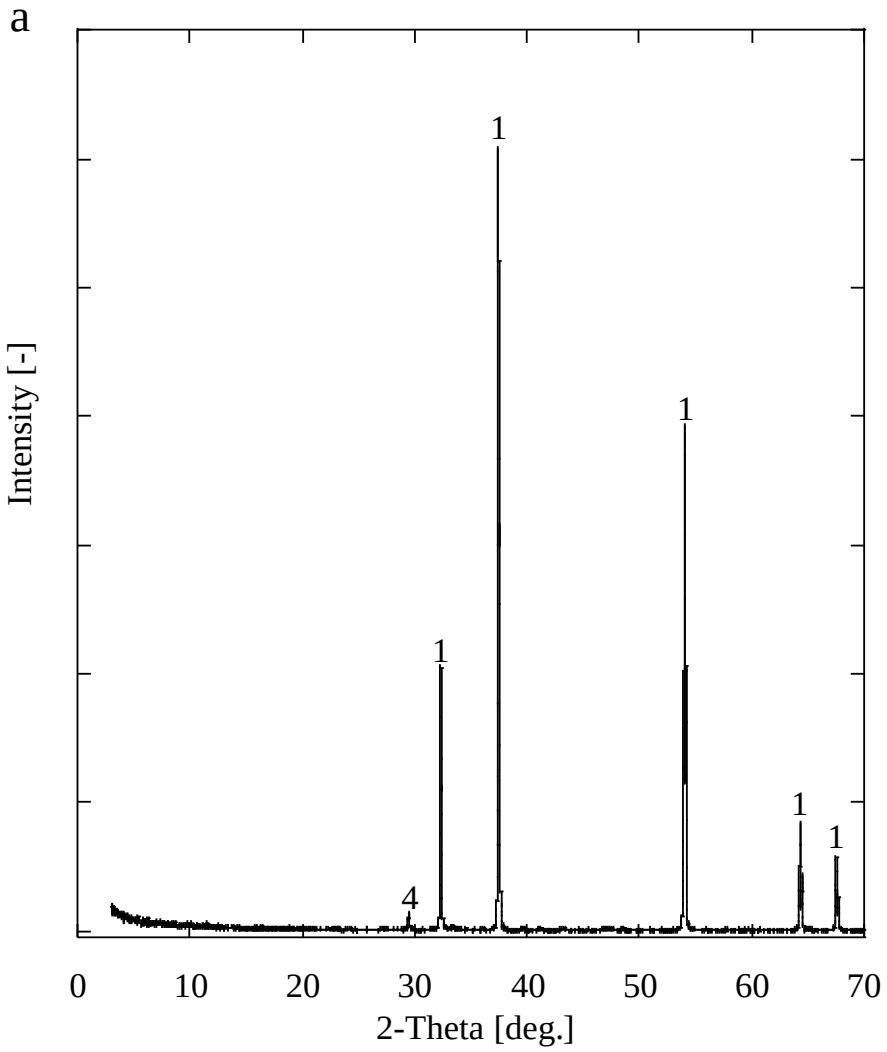

Fig. 1. **(a)** XRD patterns of the calcined scallop shells (CaO); (1) Ca-oxide, ICDD file 04-1497; (4) $CaCO_3$, ICDD file 47-1743.

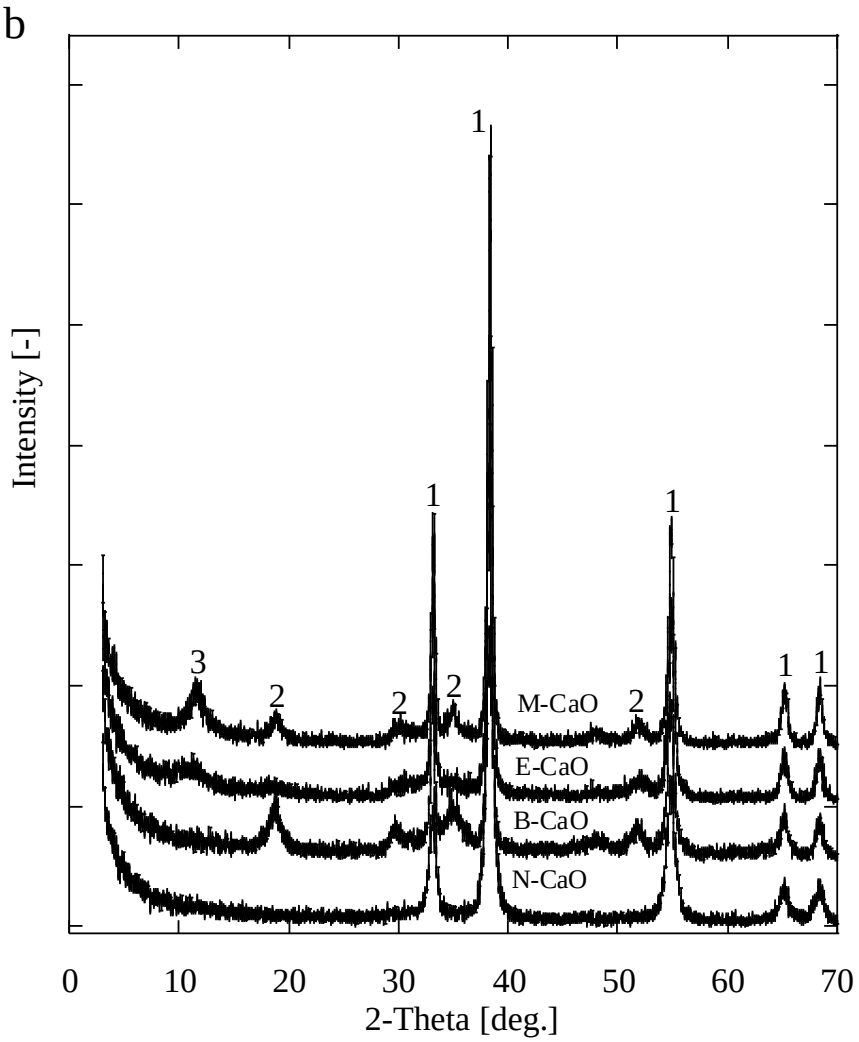

Fig. 1. **(b)** after 6 h alcohol-assisted nano-grinding with batchwise method; (1) Ca-oxide, ICDD file 04-1497; (2) Ca-hydroxide, ICDD file 04-0733; (3) Ca-alkoxide refer to [**15**].

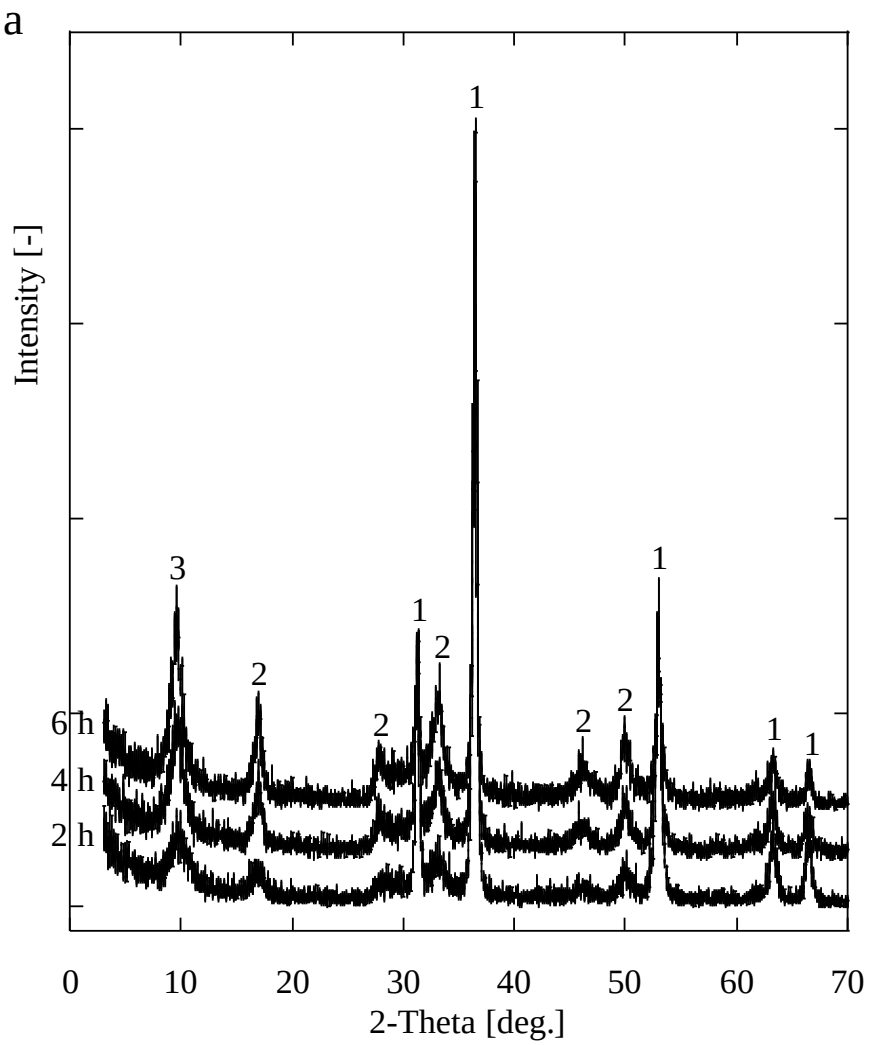

Fig. 2. **(a)** Ms-CaO; XRD patterns of the ground CaO-based catalysts after 2, 4 and 6 h alcohol-assisted nano-grinding with stepwise method; (1) Ca-oxide, ICDD file 04-1497; (2) Ca-hydroxide, ICDD file 04-0733; (3) Ca-alkoxide refer to [**15**].

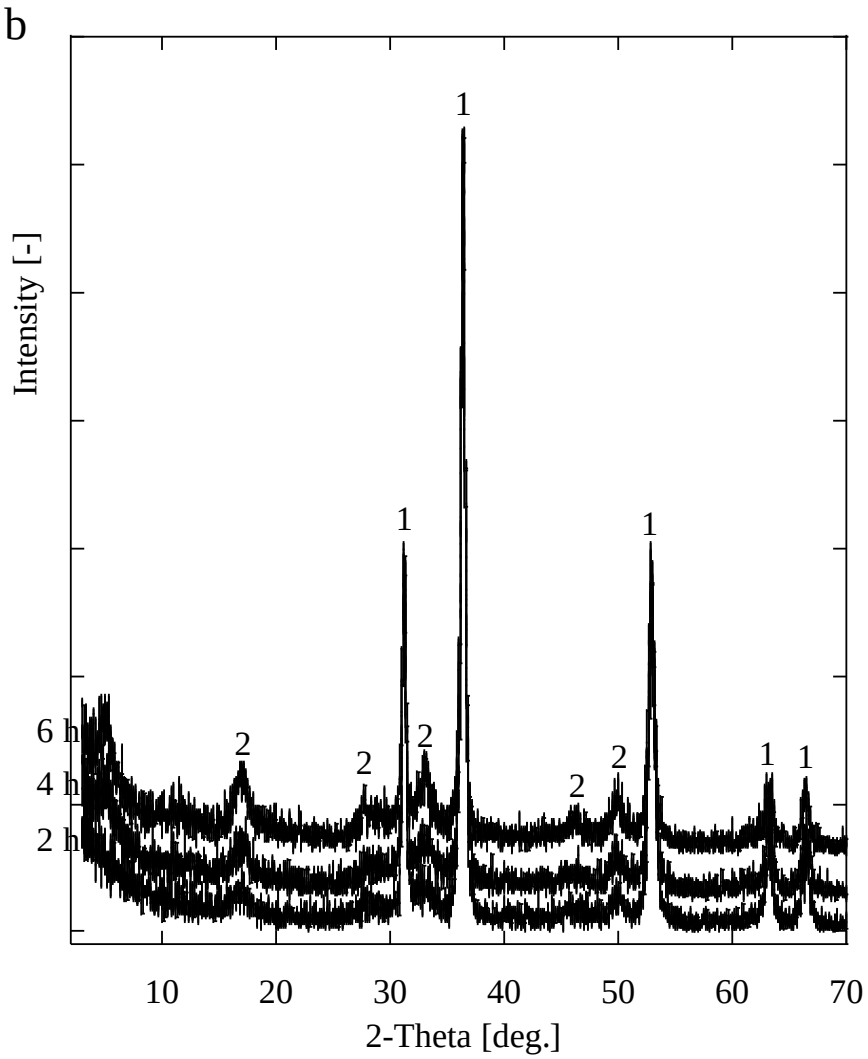

Fig. 2. **(b)** Bs-CaO; XRD patterns of the ground CaO-based catalysts after 2, 4 and 6 h alcohol-assisted nano-grinding with stepwise method; (1) Ca-oxide, ICDD file 04-1497; (2) Ca-hydroxide, ICDD file 04-0733.

3-3-1-2 FTIR characterization studies

The FTIR spectra for CaO-starting material, the gound CaO-based catalysts and post reaction the ground CaO-based catalysts were analyzed in order to characterize the surface species (surface sites). The FTIR spectra of CaO-starting material is presented in **Fig. 3 (b)**. For CaO-starting material the bands at 3642 cm^{-1} and 3400 cm^{-1} correspond to hydroxyl features of $Ca(OH)_2$ [**10, 37, 38**]. The band at 1640 cm^{-1} was assigned to the bending OH mode of water molecules physisorbed on the surface of the CaO-starting material [**10**]. Besides hydroxyl bands, FTIR spectra also showed vibrational features at 1480 cm^{-1}, 1130 cm^{-1} and 860 cm^{-1} ascribable to carbonates species [**10, 38**]. The band at 2310 and 2372 cm^{-1} can be assigned to atmospheric CO_2 [**39**]. This behavior similar with reported in [**10, 40**] that CaO surface sites can be poisoned rapidly by contact with CO_2 (carbonation) and H_2O (hydration) in room air by formed carbonates and hydroxyl species at CaO surface.

The FTIR spectra for the gound CaO-based catalysts: M-CaO, E-CaO, B-CaO, N-CaO, Ms-CaO and Bs-CaO are presented in **Fig. 3 (a)-(b)** and **Fig. 4 (a)-(b)**. The spectra of alcohol chemisorbed on the gound CaO-based catalysts after nano-grinding were observed at bands 2890 cm^{-1}, 2795 cm^{-1} (for M-CaO and Ms CaO), 2960 cm^{-1} (for E-CaO) and 2960 cm^{-1}, 2934 cm^{-1}, 2870 cm^{-1} (for B-CaO and Bs CaO) which ascribable to C-H stretching of Ca-alkoxide [**10, 34, 38, 41, 42**]. The C-H bending modes of hydrocarbon (R= alkyl: CH_3, C_2H_5, C_4H_8) can be observed at bands 1590 cm^{-1}, 1560 cm^{-1}, 1507 cm^{-1}, 1495 cm^{-1}, 1469 cm^{-1}, 1418 cm^{-1}, 1416 cm^{-1}, and 1410 cm^{-1} [**10, 38**]. Two bands at 1120 cm^{-1}, 1114 cm^{-1} can be assigned to stretching vibration of the C-O bonds of alkoxide [**43, 44**]. The bands at 3852 cm^{-1}, 3735 cm^{-1}, 3463 cm^{-1} are corresponded to the stretching vibrations of hydroxyl groups of $Ca(OH)_2$ at the surface of the gound CaO-based catalysts. The bands at 3410–3400 cm^{-1} and 1650–1620 cm^{-1}

were assigned to the stretching vibration of O–H and the H–O–H bending modes of the coordinated and adsorbed water [**10**]. A small sharp band at 860 cm^{-1} can be assigned to the symmetric deformation of carbonate groups [**39**].

In the region 1500–1400 cm^{-1}, the bands attributed to deformation of C–H modes of alkoxy groups and presence of carbonate groups mostly overlap [**10, 43**]. In order to prove the overlapping of these species, the samples evacuated under air at 300 ^{o}C. The broad band at 1500–1400 cm^{-1} and small peak at 1114 cm^{-1} disappears upon evacuation at 300 ^{o}C (**provided in Appendix A**). It can be attributed that alkoxy species were overlapped with carbonates species [**43, 44**].

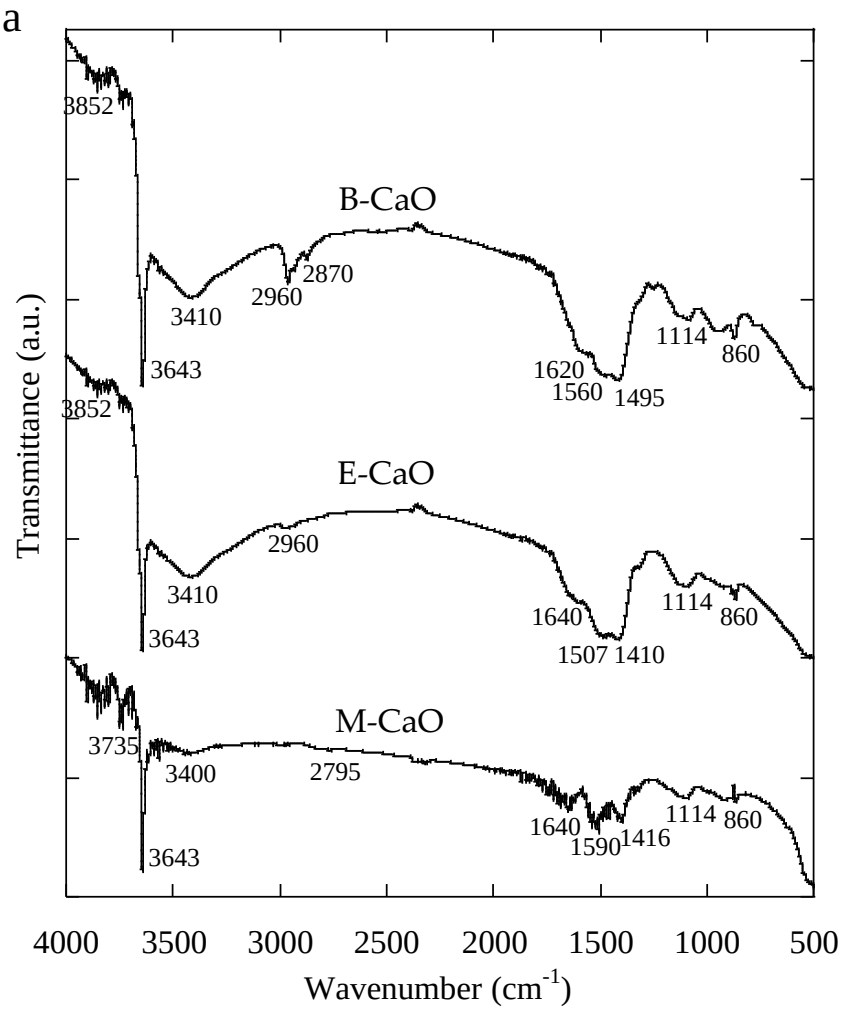

Fig. 3 (a) FTIR spectra of M-CaO, E-CaO and B-CaO after 6 h of nano-grinding in batchwise addition

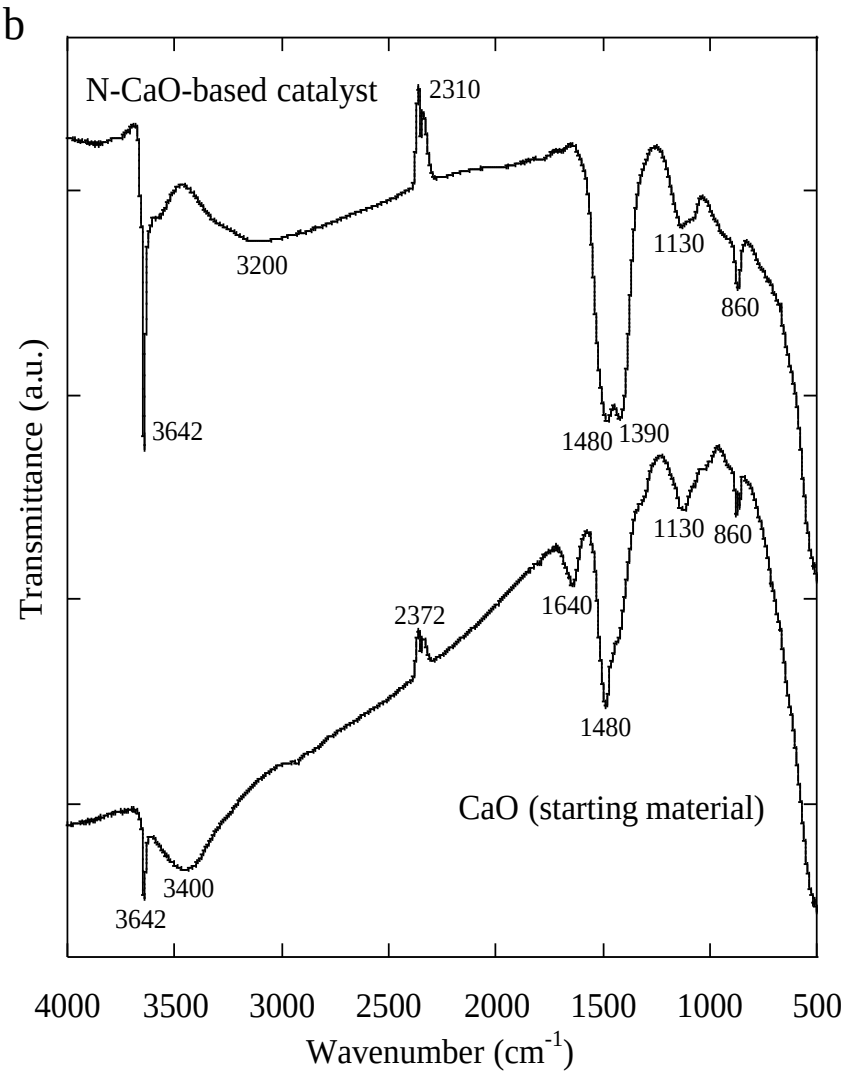

Fig. 3 (b) FTIR spectra of CaO starting material; N-CaO after 6 h of nano-grinding.

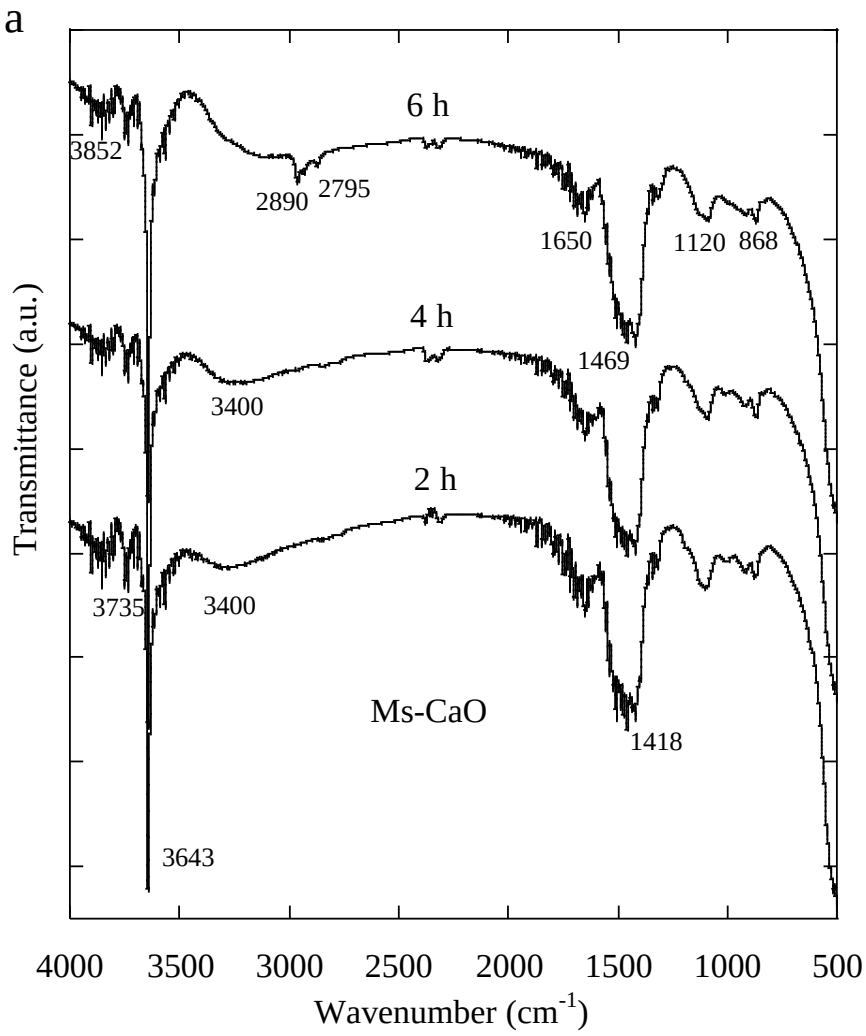

Fig. 4 (a) Ms-CaO; FTIR spectra of samples with stepwise addition method after 2h, 4h and 6 h grinding.

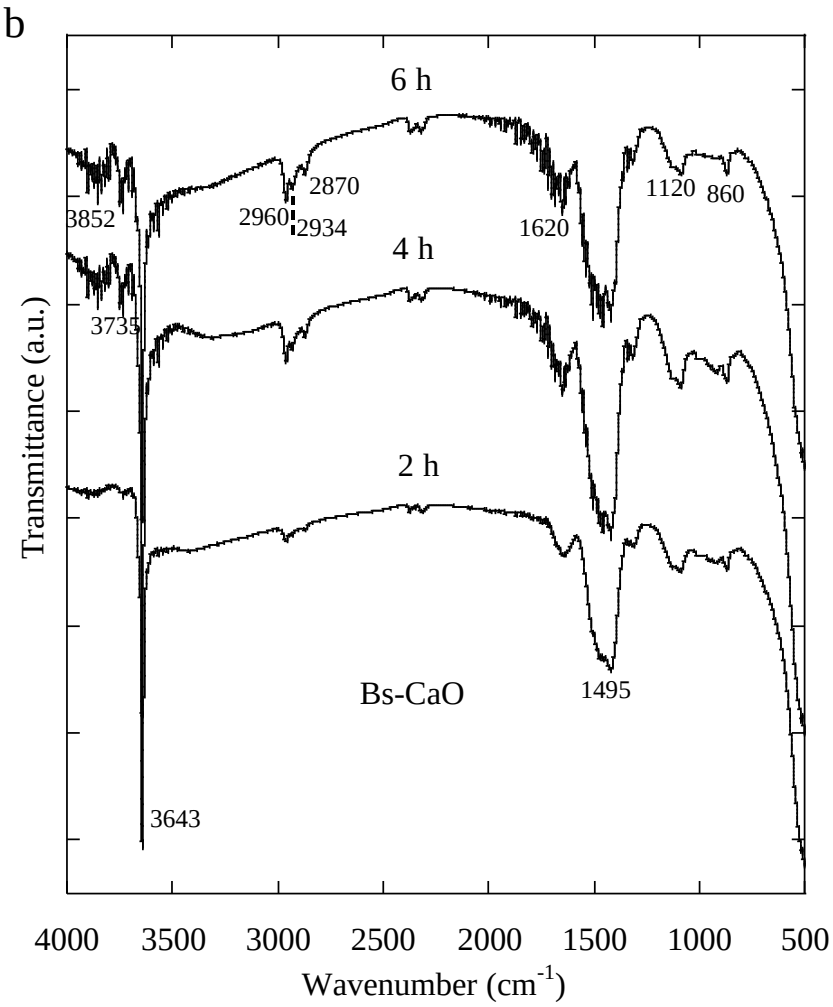

Fig. 4 (b) Bs-CaO; FTIR spectra of samples with stepwise addition method after 2h, 4h and 6 h grinding.

3-3-1-3 SEM characterization studies

The morphology of the CaO material and the post nano-grinding samples was examined by SEM (**Fig. 3 (a)-(g)**). The CaO, as the raw material for nano-grinding showed compact in shape, high crystallinity and irregular crystallites smaller than 10 µm. The micrographs for post nano-grinding samples show that, in alcohol-assisted nano-grinding, smaller CaO particles size and agglomerates formation were observed. As can be seen in **Fig. 3 (b)-(d)** and **(f)-(g)**, the size reduction underwent with attrition mechanism. Alcohol adsorbed on the surface of the CaO and reduce surface hardness which help the size reduction during the nano-grinding [**45, 46**]. The alcohol adsorption can formed surfaces covered and active sites on particles surface which can reduced the polarity or surface energy further as the nonpolar hydrocarbon parts shield the polarity. This is of utmost importance as a direct impact on the grindability to produces the CaO-based catalysts with higher SSA.

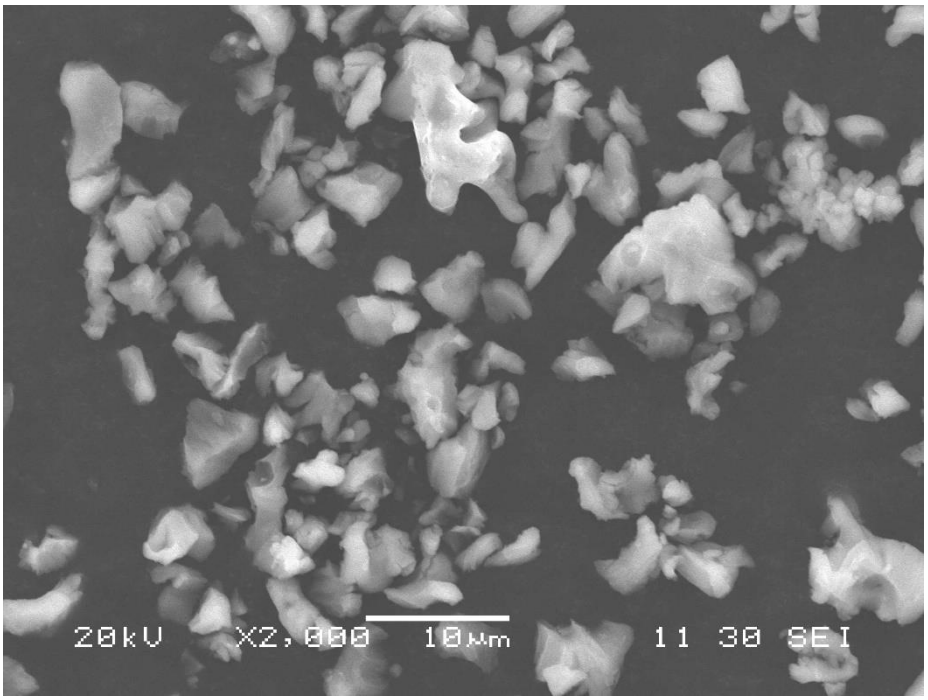

Fig. 5 (a) SEM micrograph of CaO, calcined scallop shell

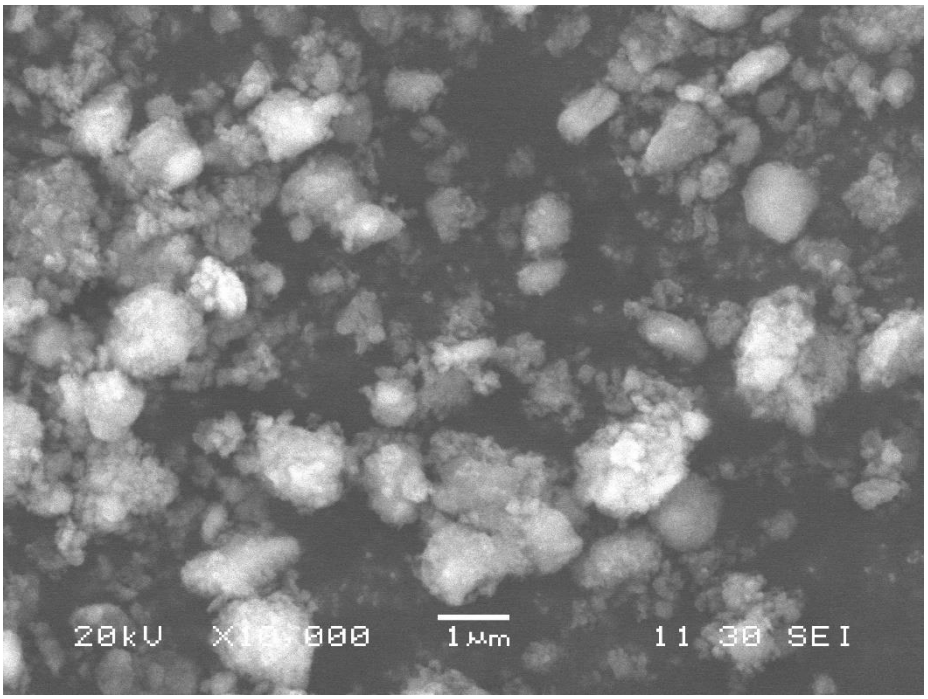

Fig. 5 (b) SEM micrograph of M-CaO

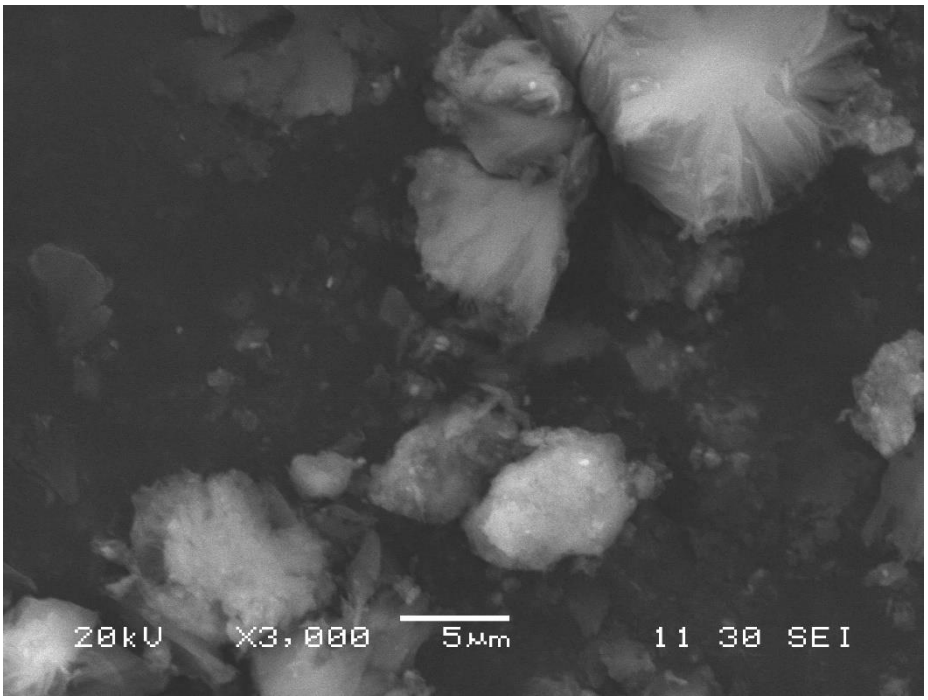

Fig. 5 (b*) SEM micrograph of M-CaO post reaction

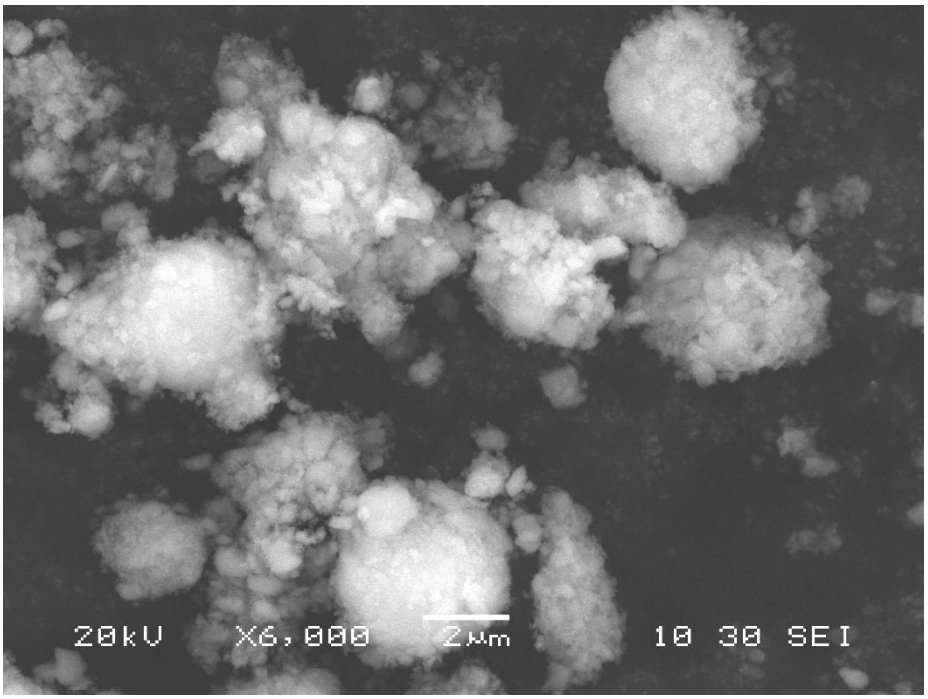

Fig. 5 (c) SEM micrograph of E-CaO

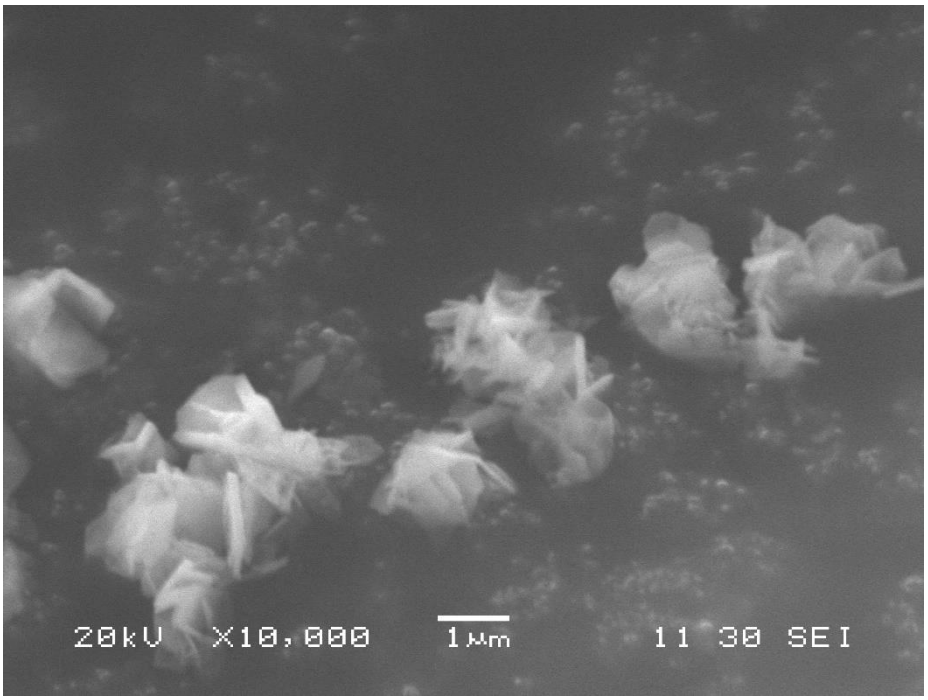

Fig. 5 (c*) SEM micrograph of E-CaO post reaction

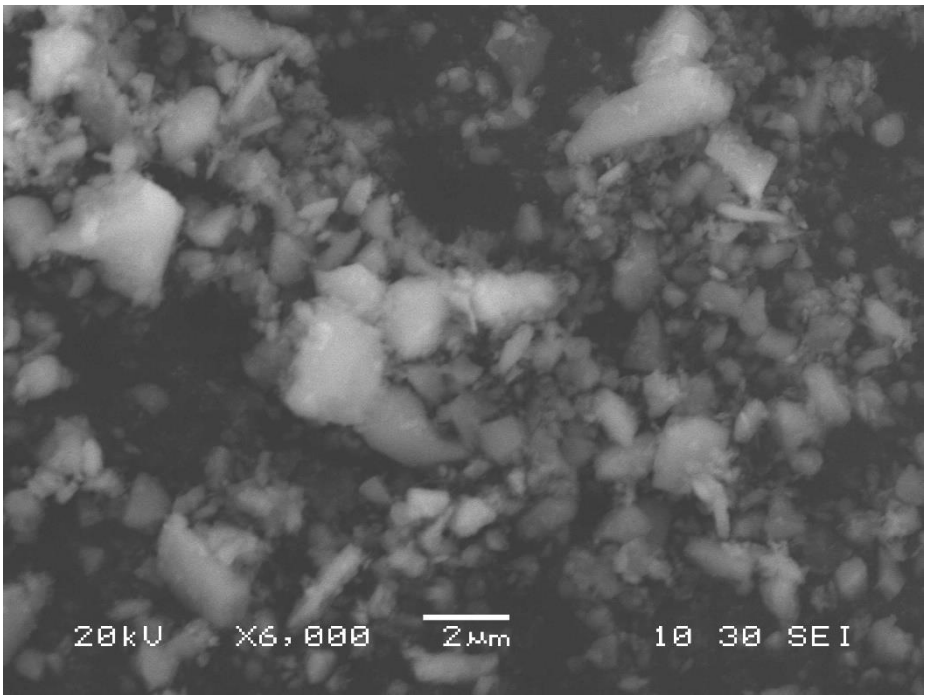

Fig. 5 (d) SEM micrograph of B-CaO

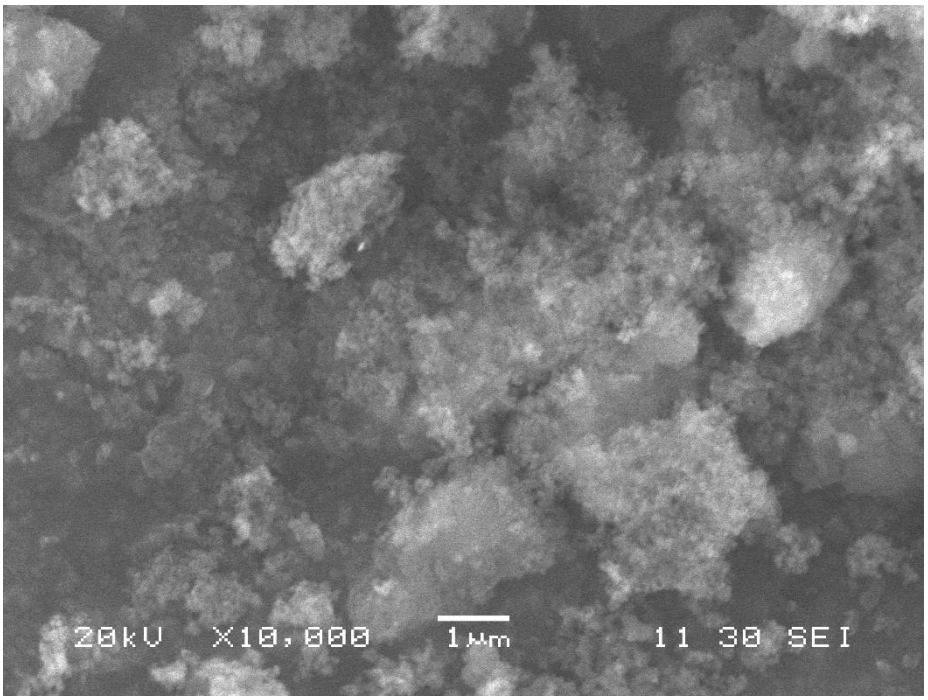

Fig. 5 (d*) SEM micrograph of B-CaO post reaction

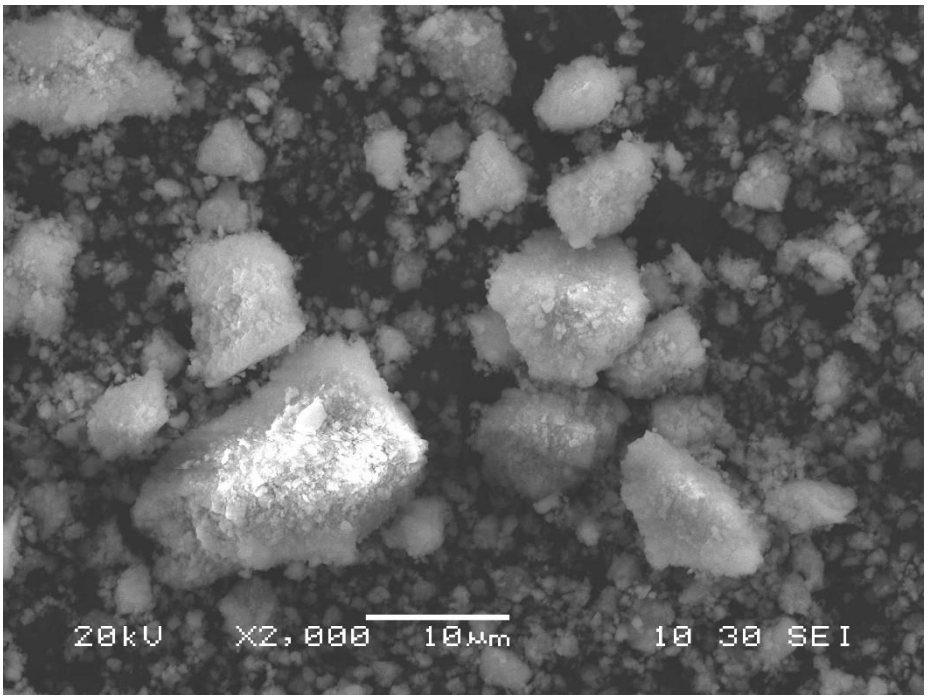

Fig. 5 (e) SEM micrograph of N-CaO

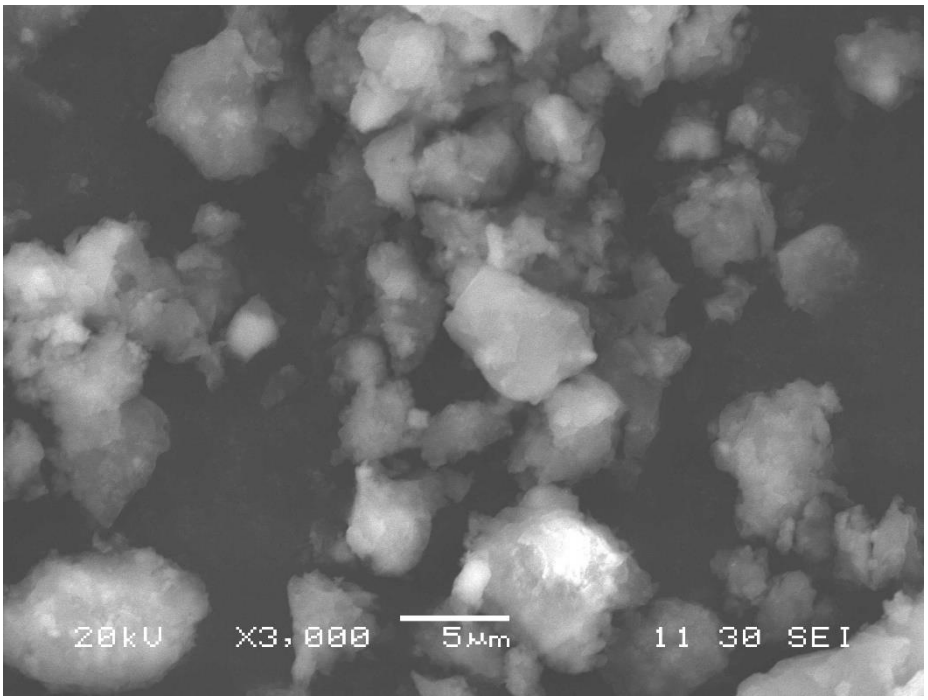

Fig. 5 (e*) SEM micrograph of N-CaO post reaction

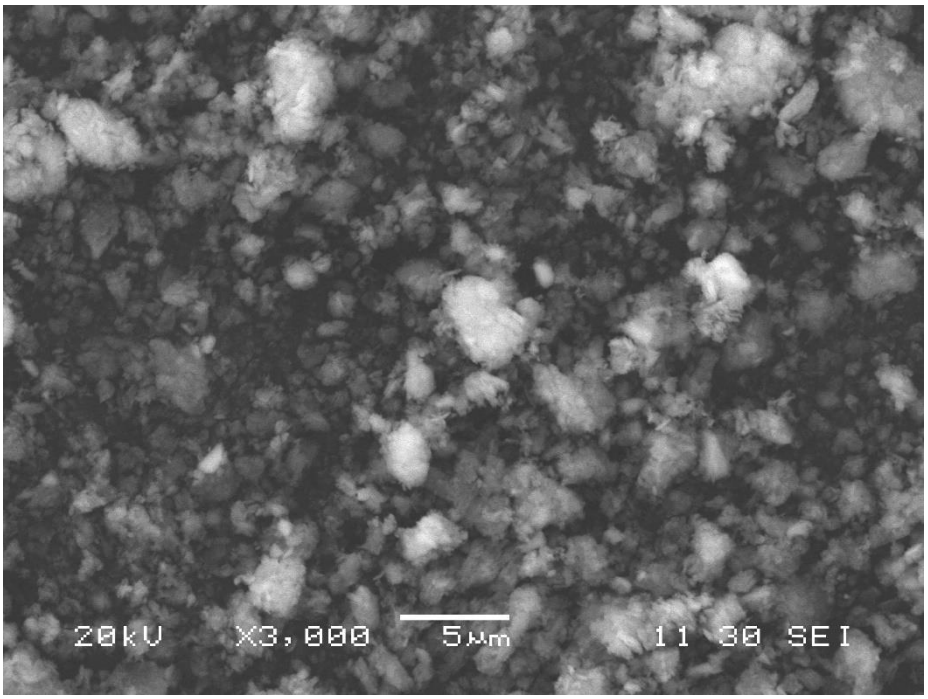

Fig. 5 (f) SEM micrograph of Ms-CaO

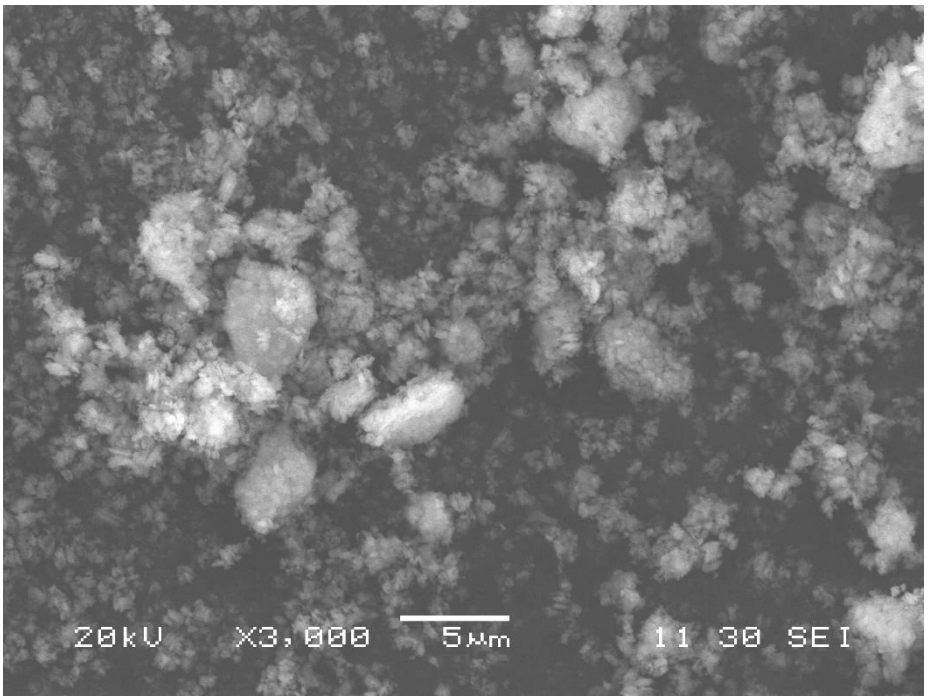

Fig. 5 (g) SEM micrograph of Bs-CaO

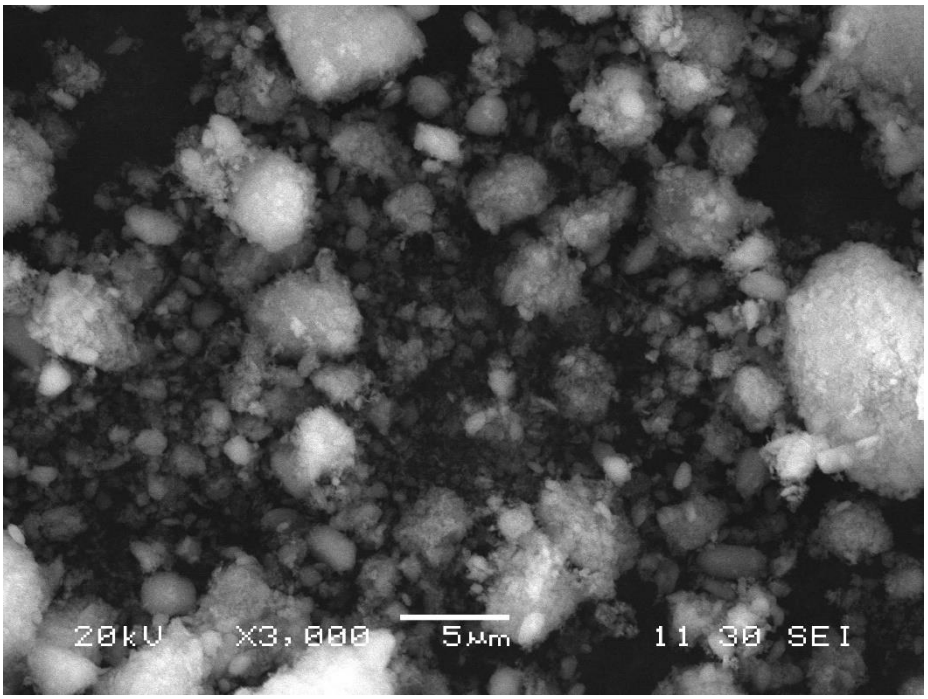

Fig. 5 (h) SEM micrograph of CaO reagent

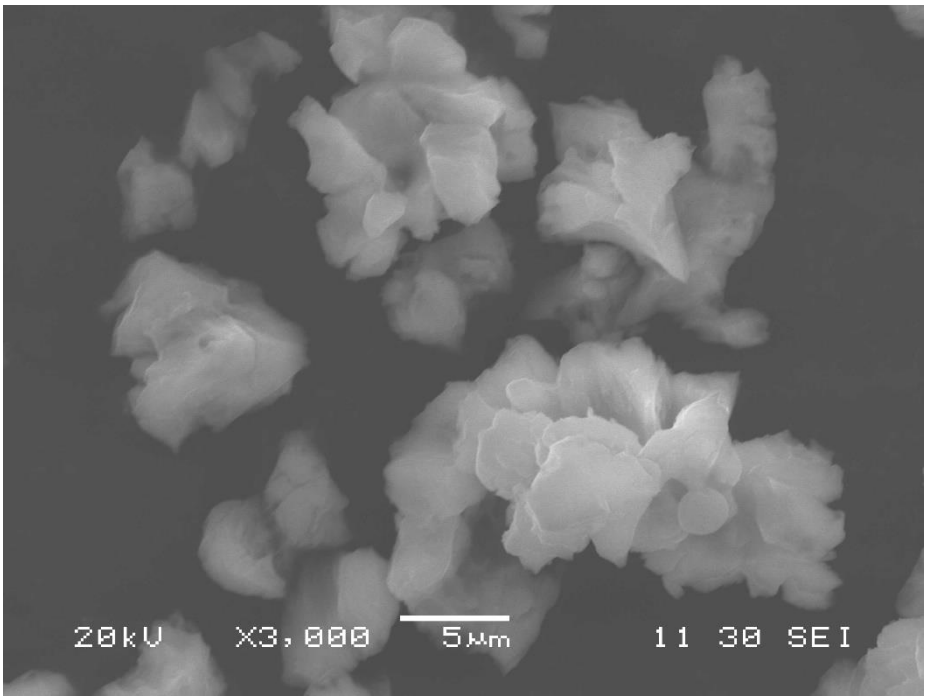

Fig. 5 (h*) SEM micrograph of CaO reagent post reaction

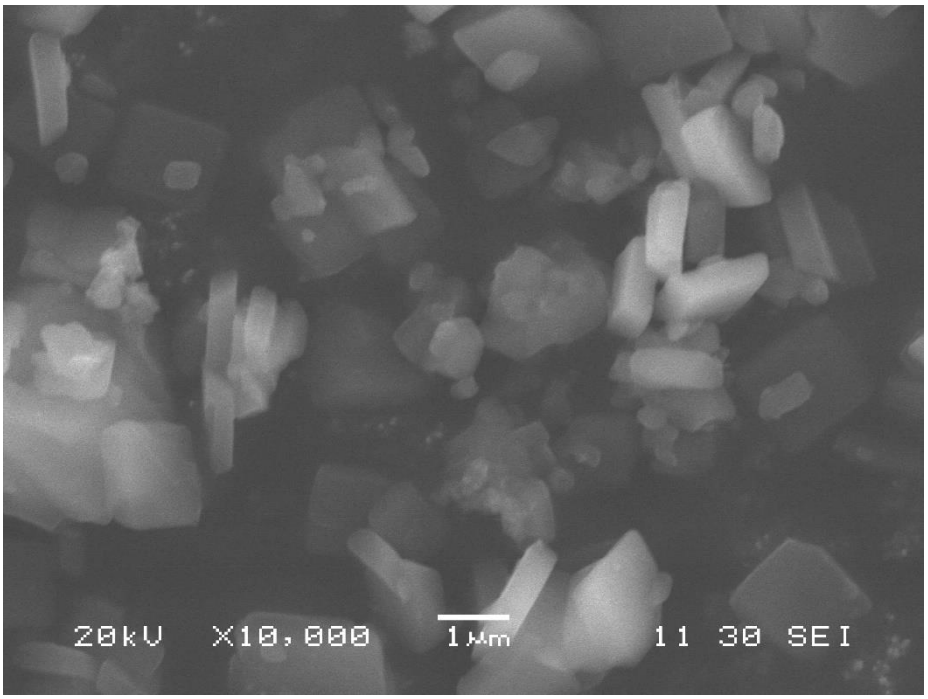

Fig. 5 (g*) SEM micrograph of M-CaO post reaction from transesterification refined SBO with methanol (180 min of reaction).

The SEM micrographs of post reaction samples showed changes in morphology plausibly because of the formation of Ca-hydroxide, Ca-methoxide and also Ca-diglyceroxide during the transesterification reaction. Ca-methoxide seems to be flower like cluster shape (**Fig. 3 (b*)** and **(c*)**), while the crystallites shape with a rectangular can be identified as Ca-diglyceroxide (**Fig. 3 (g*)**). The morphologies were similar in shape as reported in [**19, 47**].

3-3-1-4 Lewis and Bronsted acid sites characterization studies

Furthermore, according to author in [**48**], mechanical grinding causes significant changes in surface tension (Lifshitz-van der Waals component and Lewis acid-base parameters). The adsorption of grinding-aid on the ground material surfaces can greatly modify thermodynamic properties of the ground material surfaces. Although the calculation of surface tension beyond of this study, the changes in surface tension of the ground CaO-based catalysts from the original material can be identified from their hydrophobic or hydrophilic properties [**48**].

CaO is hydrophilic material, however after the nano-grinding with alcohol-assisted, the ground CaO-based catalysts became less hydrophilic to hydrophobic as can be seen in **Fig. 6 (a)-(d)**. These phenomenon can be ascribed to increase of Lewis-acid sites on the surface of particles due to nano-grinding. Accordingly, hetero bridging bond (metal atoms abridged by an oxygen atom), Ca-O-Ca, can be produced during the nano-grinding [**49**]. As Lewis acid sites are provided by Ca^{2+} cation, Lewis acid sites possibly increased after the nano-grinding process. The hydrocarbon parts (R) which coordinated with Lewis acid sites, shield the polarity of CaO. The larger R parts the lowest polarity of CaO.

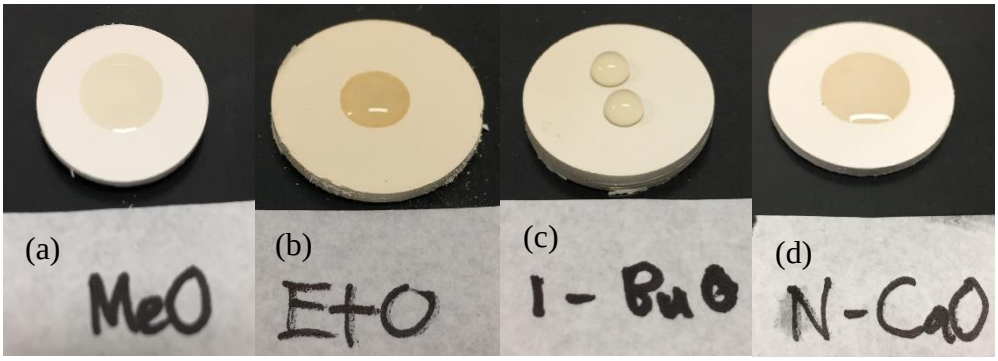

Fig. 6 (a) M-CaO; **(b)** E-CaO; **(c)** B-CaO and **(d)** N-CaO; Hydrophilic and hydrophobic properties of the ground CaO-based catalysts.

Used FTIR spectra information in **Fig. 3 (a)** and Fig. **4 (a)-(b)**, the less hydrophilic to hydrophobic mechanism is represented in **Scheme 1**, respectively.

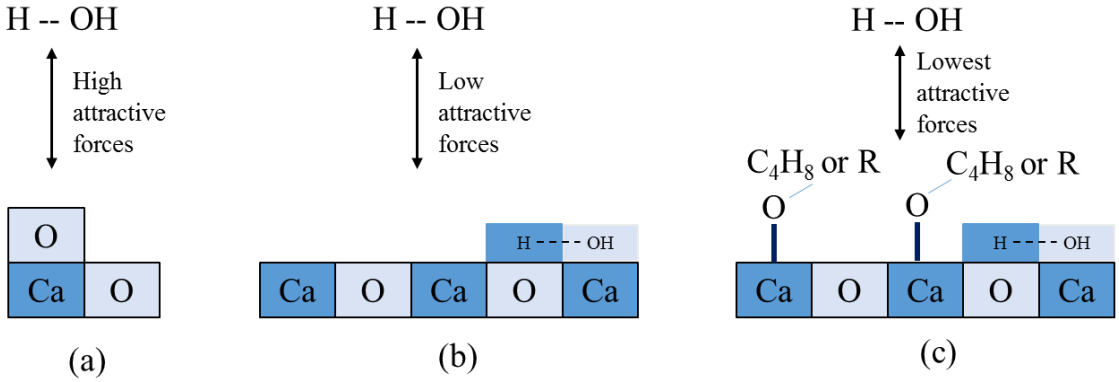

Scheme 1. (a) CaO, polar and hydrophilic; **(b)** the ground CaO with Lewis acid sites on its surface, less polar and less hydrophilic; **(c)** the ground CaO with hydrocarbon (R) shielding on its surface, less polar and hydrophobic.

In order to prove the occurrence of Lewis acid on the surface of the ground CaO-based catalysts: M-CaO, E-CaO, B-CaO and N-CaO, quantification of Bronsted and Lewis acid sites conducted with Pyridine adsorption method [**30**]. The features of pyridinium ion (Bronsted acid sites, B) and covalently bonded pyridine (Lewis acid sites, L) showed in **Fig. 7**. The bands observed at 1604 cm^{-1} and 1483 cm^{-1} are due to the presence of Lewis acid sites. The Bronsted acid sites on surface of the ground CaO-based catalysts observed at 1570 cm^{-1} and 1424 cm^{-1} [**50**]. During the nano-grinding, the ratio of finer particles and concentration of the lattice defects, increase with appearance of the free valences. Here, effect collisions and adsorption of alcohol-assisted may arise new fragments of structure of the ground CaO catalysts. Such active sites hydroxyl groups or alkoxide groups and their position on the surface of material yielded new properties of CaO-based catalyst. Agreed with author in [**51**], the position

and shape of the hydroxyl groups affected the strength of Bronsted acid sites. As reported in [**51**], ionic terminal hydroxyl groups has highest OH stretching (or Bronsted acid sites), intermediate for ionic bridging hydroxyl groups and lowest for ionic triply bridging hydroxyl groups. The presence of Lewis acid sites can be explained with this term where ionic hydroxyl groups adsorbed on the surface of Ca^{2+} cations in different coordination led the electron donor activity. Maximum Lewis acid sites were found for the CaO-based catalyst assisted by 1-butanol.

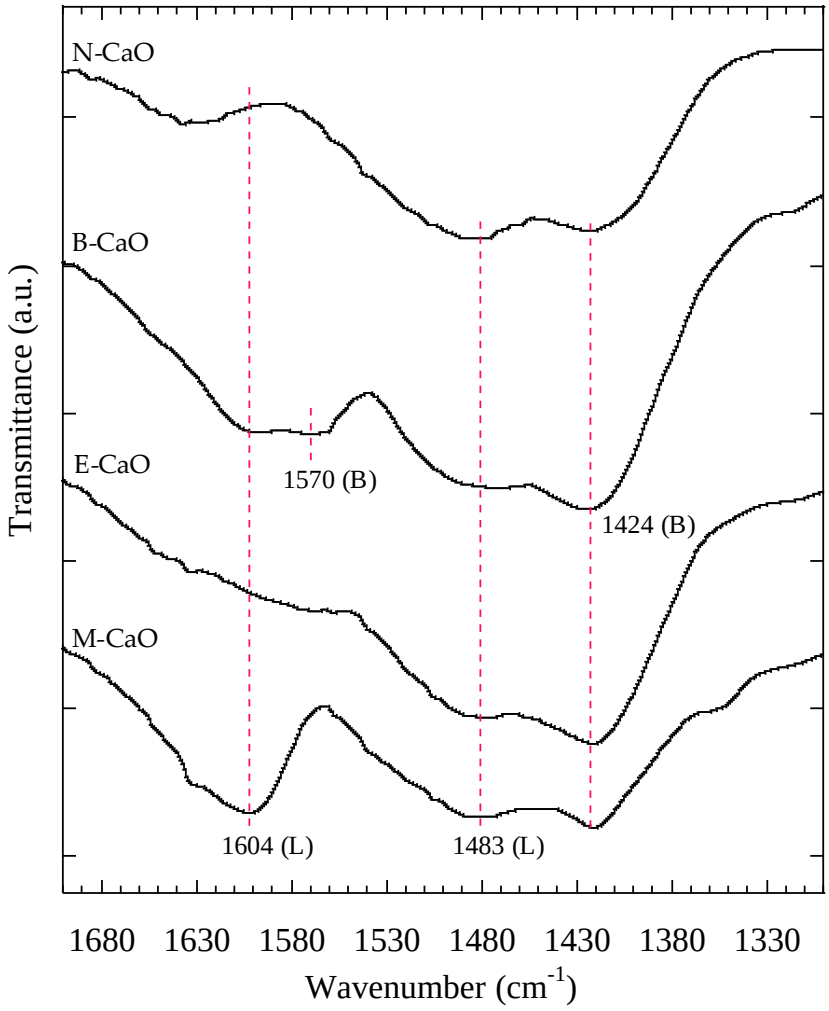

Fig. 7 FTIR spectra of pyridine adsorbed on the ground CaO-based catalysts.

3-3-1-5 Thermogravimetric characterization studies

In order to identify the active sites formed on surface of the ground CaO-based catalysts (M-CaO, E-CaO and B-CaO) during the alcohol-assisted nano-grinding, the catalysts were analyzed by TAG under nitrogen. The thermograms shown in **Fig. 8 (a)-(b)** suggested three weight-loss steps. The first weight loss, in the *T* range 100–200 ^{o}C, of (2.7–10.6%) due to desorption of alcohols physical adsorbed and dehydration of water [**52, 53**]. This was confirmed by FTIR analysis (**provided in Appendix A**), showing evacuated under air at 300 ^{o}C removed OH (mode of molecularly alcohol) and OH (mode of water) completely. The second weight loss, in the *T* range 350–450 ^{o}C, of (12.3–15.1%), corresponded to the decomposition of Ca-alkoxide into $CaCO_3$. As can be seen in TAG thermograms that Ca-alkoxide begins to decompose at about 300 ^{o}C which confirms with FTIR analysis in (**provided in Appendix A**). In addition to this analysis, this result consistent with XRD analysis in (**provided in Appendix B)** confirmed the presence of calcite phases. In addition, the presence of hydroxyl groups on partial hydroxylated of CaO on its surface, during decomposition is stable at 300 ^{o}C as can be seen in (**provided in Appendix A**) and (**provided in Appendix B)**. This hydroxyl type exhibited a higher Bronsted basicity than usual hydroxyl type. This in good agreement with literature in [**53, 54**]. The sequence of alkoxide decomposition is roughly similar with reported in [**55**]. The reactions are given as $Ca(OH)_2$ (ads) ➔ $Ca(OH)_2$ (ads) and $Ca(OR)_x + xO_2$ ➔ $CaCO_3 + CO_2 + xH_2O$.

The final weight loss, in the *T* range 600–700 ^{o}C, of (20.5–26.6%), is due to dehydroxylation of portlandite, which form $CaO + H_2O$ [**52**]. Also, an alkoxide produce $CaCO_3$ which in turn decomposes into $CaO + CO_2$ at $T > 600$ ^{o}C.

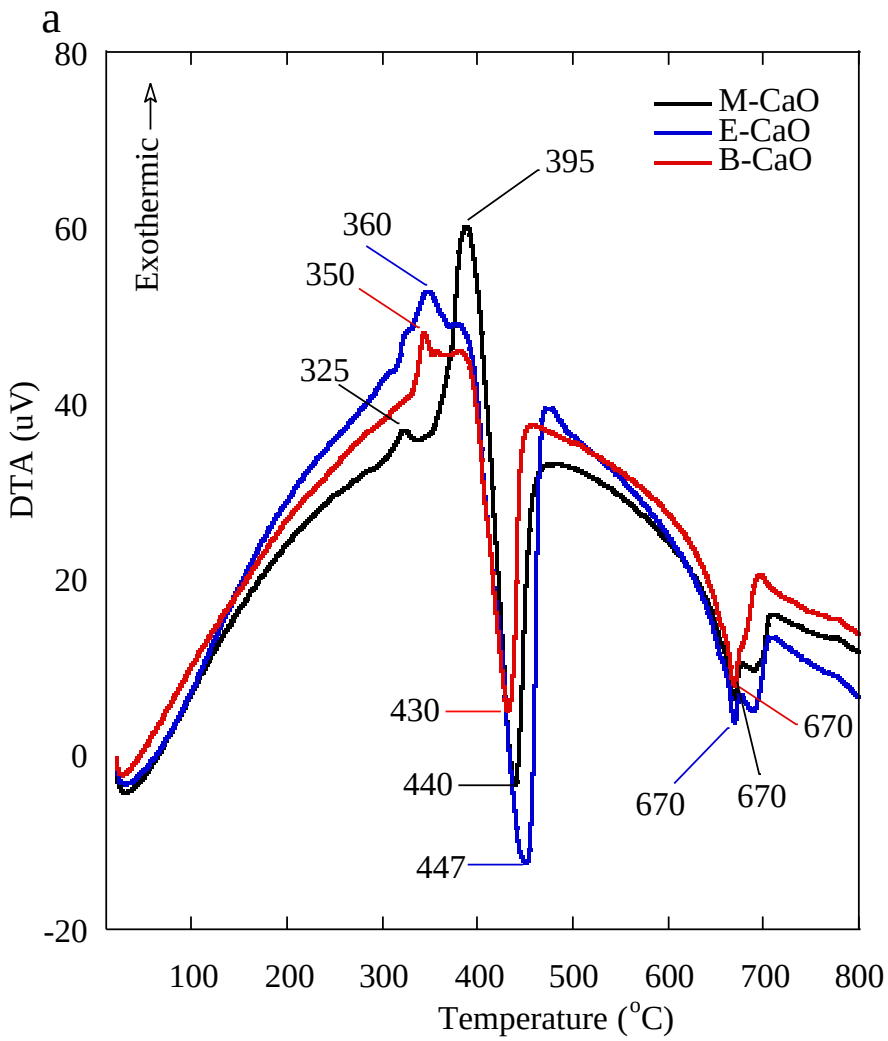

Fig. 8 (a) DTA curves of M-CaO, E-CaO and B-CaO after 6 h nano-grinding with alcohol-assisted used 1.25 g in batchwise addition system.

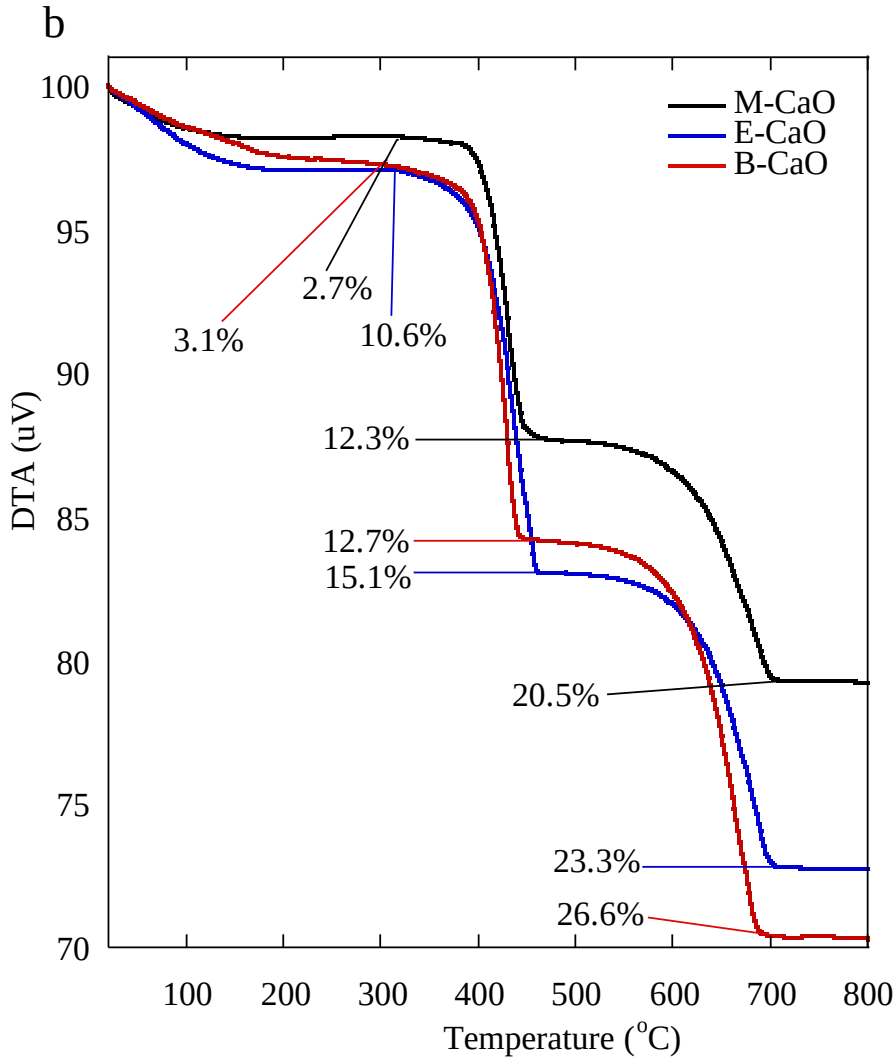

Fig. 8 (b) TGA curves of M-CaO, E-CaO and B-CaO after 6 h nano-grinding with alcohol-assisted used 1.25 g in batchwise addition system.

3-3-1-6 Basicity characterization studies

The basic strength of the catalysts (H_) was measured by Hammett indicators [**29, 56, 57**]. The following Hammett indicator were used: phenolphthalein (H_ = 9.3), thymolphthalein (H_ = 10.0), and 4-nitroaniline (H_ = 18.4). For accurate analyses due to rapidly CaO poisoned by CO_2 and H_2O at the room air, before all the measurement, 0.1 g of catalyst was dried at 200 ^oC in vacuum condition. After the sample transferred into the flask and added 2 mL of benzene, nitrogen then put to clear CO_2 and H_2O. Subsequently, a few drops of the indicator solution were added to the mixture of the catalyst in benzene. A few minute later, a color change was appeared, indicating that the larger part of indicator molecules had been deprotonated. The flask was later stored for 24 h to confirm the color change.

Table 2 displays the results of the ground CaO-based catalysts basic strength *via* Hammet indicator measurement. Overall, the basicity of the gound CaO-based catalysts increased compare to the initial basic strength. These results in good agreement with author in [**33**], the basicity increased due to mechanochemical interaction between the grinding-aid with the gound material. As expected, 1-butanol-assisted was observed to be the most basic catalyst, while without alcohol-assisted was the least basic catalyst after the nano-grinding treated. Total basicity (f_m) of the samples was measured by the method of Hammett indicator-benzene oxalic acid (0.1 M anhydrous methanol solution) titration [**29**]. The Hammett indicators study thus showed the overall basicity to follow order Bs-CaO > B-CaO > Ms-CaO > M-CaO > E-CaO > N-CaO > CaO.

Table 2 Basicity, H_ *via* Hammet indicator measurement for the ground CaO-based catalysts

Catalyst	Basicity under different indicators (H_*) (mmol g^{-1} of catalyst)			f_m (mmol g^{-1} of catalyst)
	Phenolphthalein H_ = 9.3	Thymolphtalein H_ = 10.0	4-nitroaniline H_ = 18.4	
CaO	0.8	0.01	0.004	0.81
M-CaO	2.05	2.16	0.83	5.04
E-CaO	1.68	1.50	0.91	4.09
B-CaO	2.13	1.94	1.44	5.51
N-CaO	0.93	0.04	0.05	1.02
Ms-CaO	2.34	2.20	1.08	5.62
Bs-CaO	2.62	2.52	1.48	6.62

* The H_ value refers to the strength of solid bases as the pKa range between the last indicator showing color change and the first one for which the color change could not be appreciated.

3-3-2 Effect of alcohol-assisted dry nano-grinding on SSA

As the nano-grinding produced finer particles and increased concentration of the lattice defects therefore increased the appearance of the free valences. According to author in [**36**], the free valences have high interfacial energy that could induces adhesive forces between particles which favors agglomeration and reducing the grindability and the flowability, thus lowering the SSA of the ground materials.

In order to obtain high SSA of CaO-based catalysts, prolonged the grinding time is needed. However, the grindability and the flowability need to be maintained to promote fruitful nano-grinding process. Weibel [**36**] reported that presence of grinding

aid leads to a different minimum energy state which can reduce the agglomeration energy in all cases. As showed in **Fig 9 (a)**, the SSA of the ground CaO-based catalysts was seriously high after treated with alcohol-assisted nano-grinding at 6 h in batchwise method. Higher SSA of the ground CaO-based catalysts was obtained when stepwise method was conducted (**Fig 9 (b)**). By summarizing XRD, FTIR, SEM and TAG analyses, elucidation of the nano-grinding mechanism and their relationship in generating high SSA, as described below.

1. Once the alcohol adsorbed on the surface of the CaO, the alcohol molecules compensate and reduce the polarity of CaO surface through the shielding effect. The shielding agents are alkoxide and hydroxide groups which created as active sites on surface of CaO during the nano-grinding. Alcohol molecularly covering on CaO surface also compensated the polarity.
2. As the surface polarity was reduced, in parallel there was also reduction in surface energy as resultant of combination alcohol molecularly covering and occurrence of active sites on surface of CaO, then in latter stage led to breaking or size-reduction process via attrition mechanism.
3. Reduction of agglomeration energy by efficient and stable covering of particles surface by molecularly adsorption or active sites. The lower agglomeration energy the fewer agglomerates state and improve the grindability and flowability to produce high SSA of ground material. In this case, behavior of the alcohol-assisted affected the nano-grinding performance.

As **Fig. 9 (a)-(b)** shown, the effectiveness of alcohol used to produce high SSA in nano-grinding decreased in the sequence 1-butanol > ethanol > methanol. This is in

good agreement in [**36**], the larger the hydrocarbon chain the smaller is the agglomeration energy and the better grindability and flowability during the nano-grinding, thus increasing the specific surface area. In this work, the stepwise addition method was found to be more effective for obtaining high SSA. It might be the stepwise addition method provides sufficient concentration of alcohol to cover at least half of CaO surface during the grinding process.

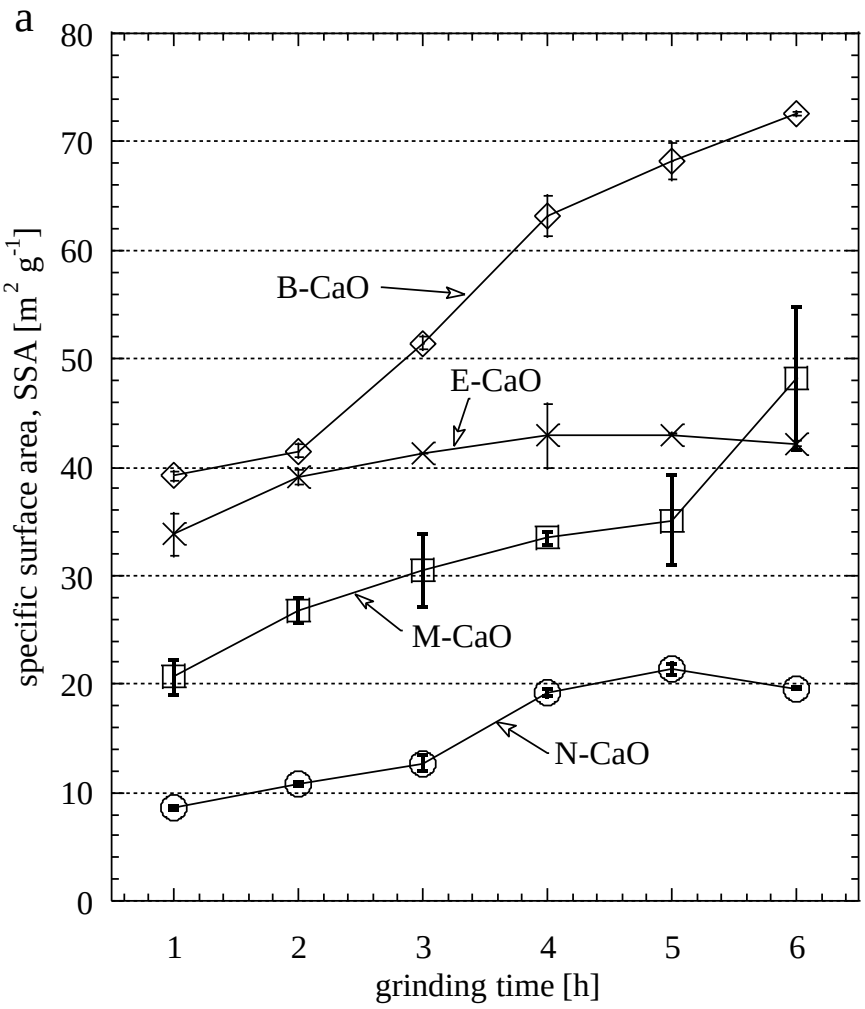

Fig. 9 (a) Relationship between the SSAs and nano-grinding time with batchwise addition method.

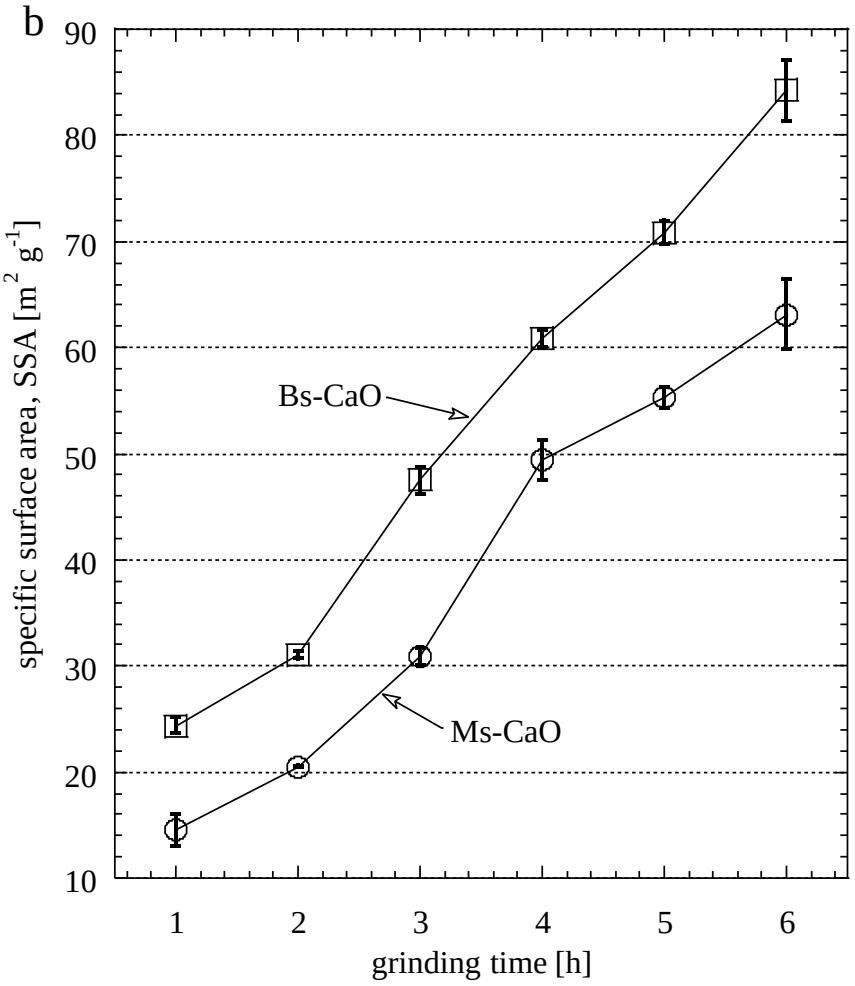

Fig. 9 (b) Relationship between the SSAs and nano-grinding time with stepwise addition method.

3-3-3 Catalytic activity for the transesterification reaction

The catalytic activity of the ground CaO-based catalysts was tested in transesterification of WCO with methanol at 65 ^{o}C. The physicochemical properties of the catalysts used are provide in **Table 3**. The activity of CaO reagent catalyst and NaOH catalyst in WCO transesterification are carried out for performance comparison.

In **Fig. 10 (a)**, relationships among the catalytic activity of the catalysts and SSA, basicity values and kind of alcohol-treated the CaO catalyst with ME yields are displayed. The catalysts: M-CaO, E-CaO and B-CaO were able to complete the transesterification of WCO having up to 10 wt% FFA and 0.11 wt% moisture content and gave ME yields 98.6 % for M-CaO catalyst, 99.9 % for E-CaO catalyst and 99.7% for B-CaO catalyst in 2 h reaction. The catalysts showed comparable activity with NaOH catalyst performance. The high performance of those catalysts could be ascribable to a synergic effect of properties changing after alcohol-assisted nano-grinding treated.

For comparison, the activity of N-CaO catalyst and CaO reagent catalyst were evaluated in comparison to that of alcohol-assisted nano-grinding treated. N-CaO catalyst and CaO reagent catalyst were found to be less activity towards transesterification of WCO, ME yields obtained only 20 % and 4.3 %, respectively.

The difference of ME yields could be due to the difference in SSA, basicity and surface properties (Lewis-Bronsted acid sites) of the CaO-based catalysts. The ground CaO-based catalysts also exhibit high tolerance with the 10 wt% of FFA during the first batch reaction [**Fig 10 (b)**]. The presence of Lewis acid sites on surface of catalyst led the catalyst also work for transforming FFA into ME [**30**]. Additionally, the changes of surface species on surface of catalysts during the nano-grinding also contributes to catalyst dispersion on reactants phase (**provided in Appendix C)**. This behavior

ascribable to lowering the polarity of surface of the ground CaO-based catalysts with the presence of alkoxy species. Seemingly, catalyst dispersion on reactants phase influences the reducing of mass transfer limitation on the initial stage of reaction by decreasing diffusion of fatty acids from the bulk liquid phase to surface of catalyst. The larger the chain of alkoxy species, the better dispersibility performance [**13**].

Table 3

The physicochemical properties of the catalysts used in transesterification.

Catalyst	Total basicity, f_m (mmol g^{-1} of catalyst)	SSA (m^2g^{-1})
CaO reagent	0.08	1.6
M-CaO	5.04	48.2
E-CaO	4.00	43.0
B-CaO	4.93	51.4
N-CaO	0.94	10.8

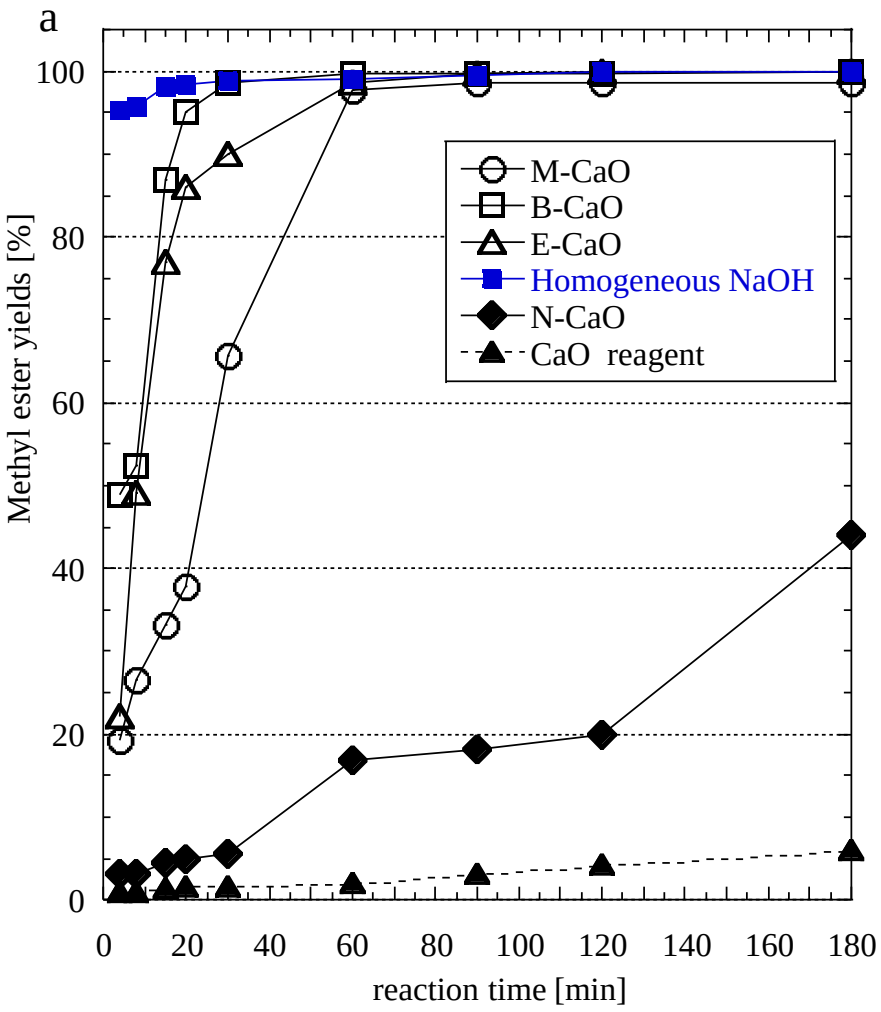

Fig. 10. **(a)** Effect of alcohol-assisted on the ground CaO-based catalysts activity towards WCO transesterification (having 10 wt% FFA and 0.11 wt% moisture content) (Reaction conditions: Methanol/WCO molar ratio = 9:1; catalyst amount = 2 wt% (except NaOH = 1.2 wt%); temperature = 65 ^{o}C)

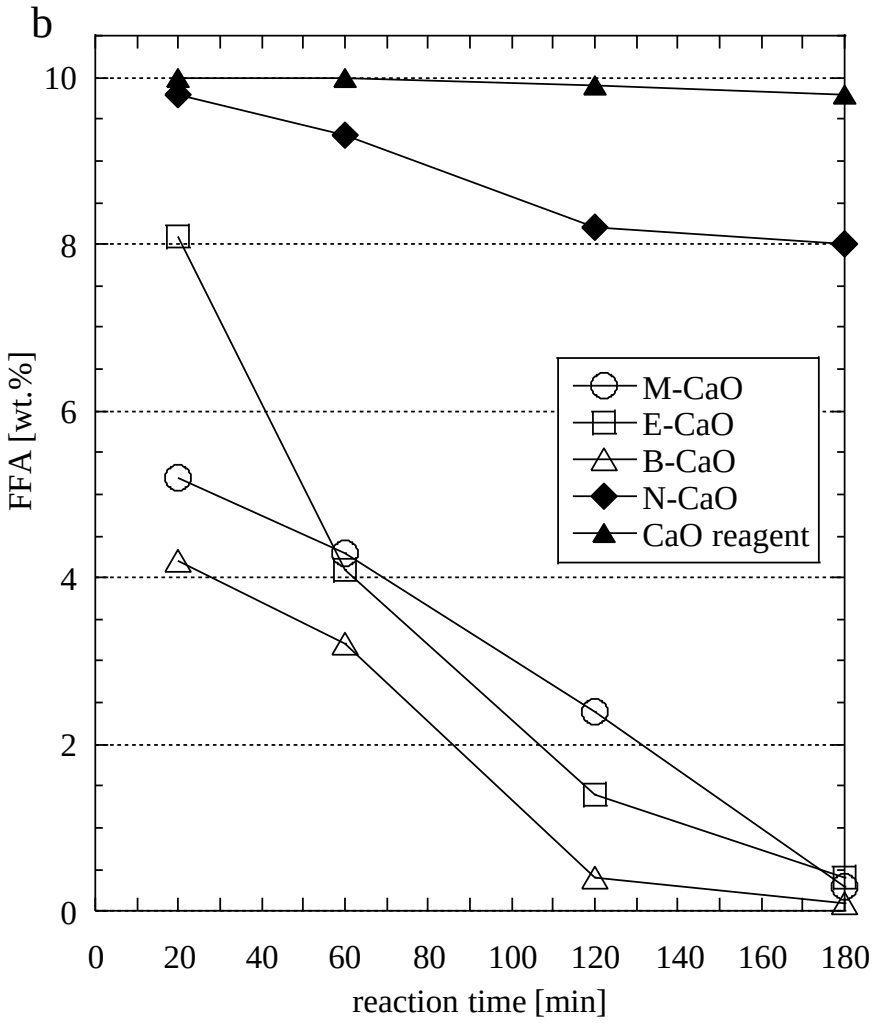

Fig. 10. **(b)** Effect of alcohol-assisted on the ground CaO-based catalysts activity towards WCO transesterification (having 10 wt% FFA and 0.11 wt% moisture content) (Reaction conditions: Methanol/WCO molar ratio = 9:1; catalyst amount = 2 wt%; temperature = 65 ^{o}C).

Accordingly, it is verified that CaO catalyst during the transesterification with methanol transformed in calcium diglyceroxide (CaDg) by combining CaO and glycerol-side product. Additionally, CaDg has been demonstrated to be an active phase (true catalyst) in transesterification to produce biodiesel [**11, 58**].

The structural changes of the catalysts in the reaction medium were evaluated in order to clarify the effect of FFA and moisture content on structural of the ground CaO-based catalysts. The XRD patterns in **Fig. 11 (a)** and **(b)** show that all the spent catalysts seriously suffer a fast decay due to low crystallinity. These behavior confirm by SEM micrographs in **Fig. 5 (b*)-(e*)** and **(h*)**. The micrographs for the post reaction samples (marking with *) show that samples loose the characteristic morphology during the WCO transesterification. The morphologies can be identified as Ca-methoxide (flower like cluster shape), some crystallites with rectangular shape that can be identified as CaDg, and some like aggregate of spheroids which can be identified as Ca-hydroxide [**19, 47**].

FTIR spectra of the spent catalysts: M-CaO, E-CaO, B-CaO, and N-CaO as shown in **Fig. 12** notice that only N-CaO has hydroxyl features (3644 cm^{-1}), this agrees with the Ca-hydroxide XRD pattern obtained in **Fig. 11 (b)**. It is possible moisture content on WCO hydrated the surface of N-CaO [**59**]. Inversely, moisture content has negative effect on the surface of the catalysts treated by alcohol-assisted nano-grinding. It can be attributed to the presence alkoxy-shielding on the surface of catalysts after the nano-grinding. Hence, the surface polarity reduced by hydrocarbon tails of alkoxy-shielding, thus the hydroxyl group was not easy adsorbed on the surface of catalysts.

For all the catalysts treated by alcohol-assisted nano-grinding yield of ME was above 98.5 % at 2 h of reaction, even in 4 min ME yield was above 19 %. The presence of the Lewis acid sites seemingly has significant contribution in FFA conversion into

ME. If the FFA was directly neutralized the surface of catalysts, the ME yields would not completed in 2 h. It was certain also that FFA were converted into ME during the transesterification WCO as the **Fig.10 (b)** suggested, FFA decreased during the reaction time. The reduction of FFA seemingly depend on kind of alcohol-treated on nano-grinding.

It should be noted, after the first batch reaction of WCO transesterification, all the catalysts neutralized by FFA. FTIR spectra in **Fig. 12** described deterioration of the catalysts on surface by FFA. The features in 2923 cm^{-1} and 2854 cm^{-1} are assigned to C-H stretching of Ca-methoxide [**15**]. The FTIR spectra of spent catalysts: M-CaO, E-CaO, B-CaO, and N-CaO and CaDg catalyst to identify the species of FFA on the surface of catalysts. According to authors in [58] the CaDg characteristic bands were: 2923 cm^{-1} and 2854 cm^{-1} assigned to ν(C-H), 1470 cm^{-1}, 1311 cm^{-1}, and 1126 cm^{-1} assigned to (C-H) and (C-O-H) bending modes (**Fig. 12**). The presence a band at 1577 cm^{-1} can be ascribed as the existence of carbonyl adsorbed species of FFA [**60**]. This was an evident to the catalyst basic site neutralization by FFA. Such a gel results from the saponification reaction between FFA and calcium observed on spent catalysts. This finding in good agreement with authors in [**38**].

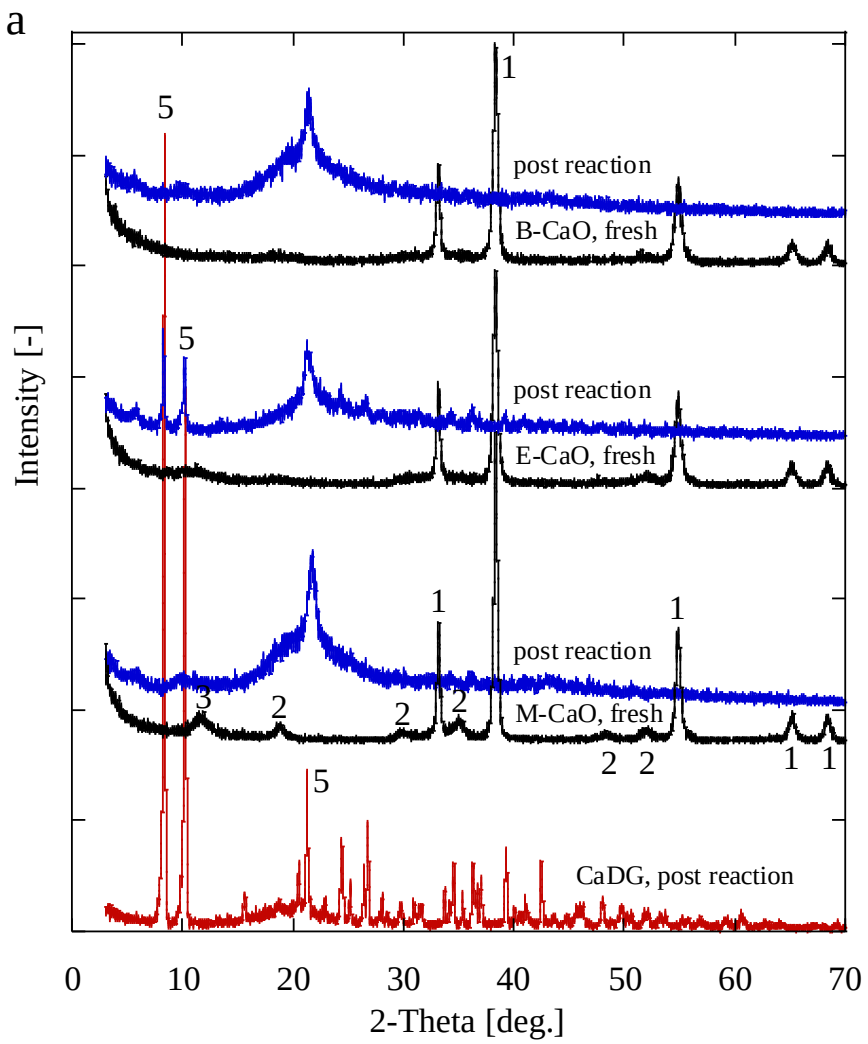

Fig. 11. **(a)** XRD patterns of CaDG from post reaction using refined SBO (see in Chapter 2, the red line), CaDG from post reaction using WCO (the blue line); (1) Ca-oxide, ICDD file 04-1497; (2) Ca-hydroxide, ICDD file 04-0733; (3) Ca-alkoxide refer to [**15**]; (5) CaDG refer to [**19**].

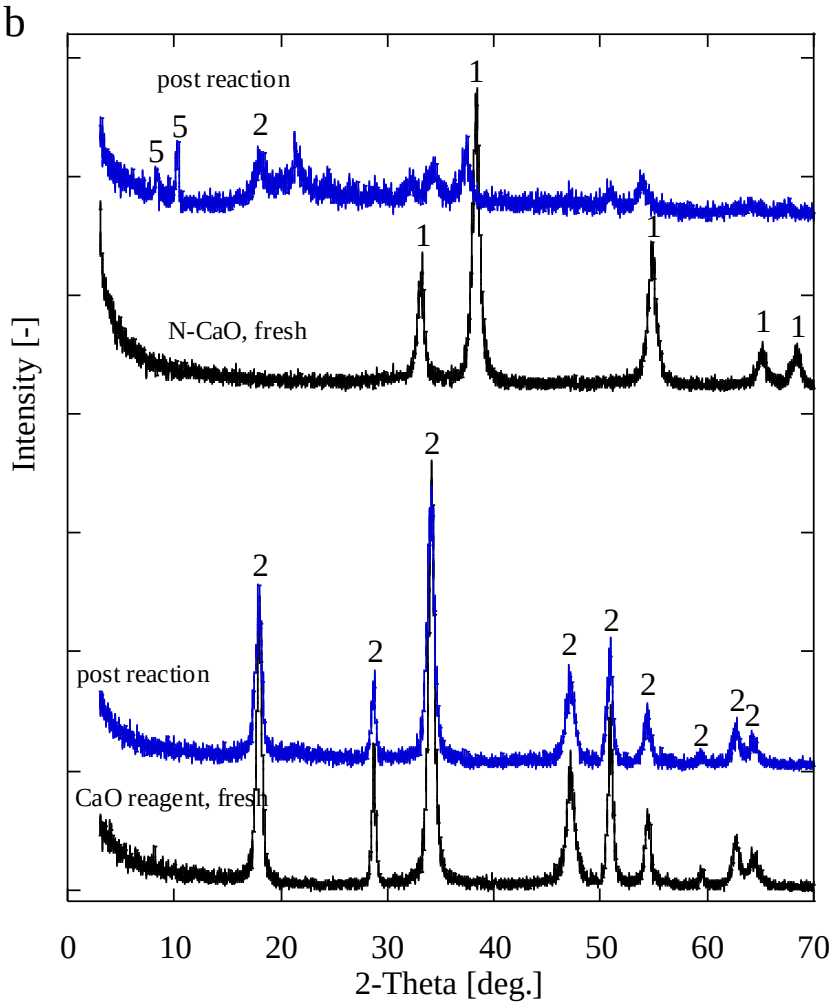

Fig. 11. **(b)** XRD patterns of CaDG from post reaction for CaO reagent catalyst and N-CaO catalyst; (1) Ca-oxide, ICDD file 04-1497; (2) Ca-hydroxide, ICDD file 04-0733; (5) CaDG refer to [**19**]

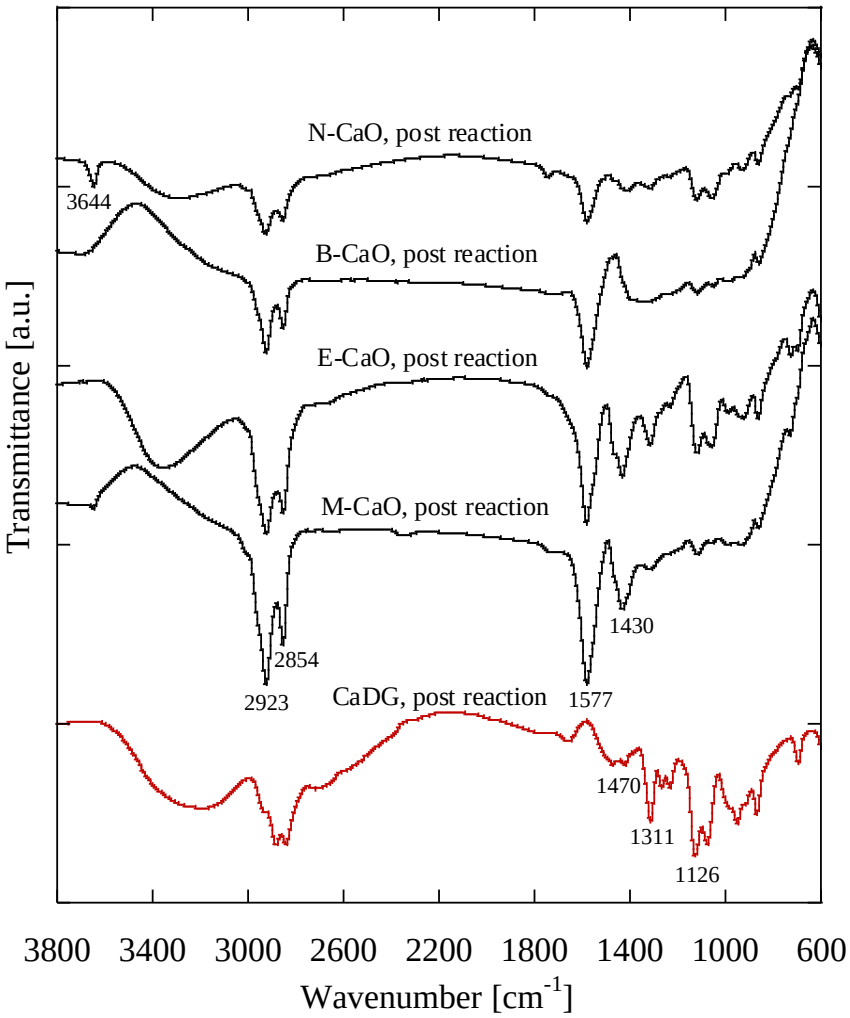

Fig. 12 FTIR spectra of CaDG from post reaction using refined SBO (the red line), CaDG from post reaction using WCO (the black line).

3-3-4 Reusabilty study

The reusability was carried out with spent B-CaO catalyst. The reaction conditions were methanol to WCO molar ratio = 9:1; catalyst amount = 2 wt%; temperature at 65 ^{o}C. Once the batch reaction was ended, the reaction mixture was centrifuged and the spent catalyst was separated. The spent catalyst later was washed with 2-propanol in 2 times, wet spent catalyst then feed to next batch reaction. As shown in **Fig. 13**, the catalyst reused seriously loss in activity, only 2.7 % of ME yield can reached after 3 h reaction. The loss of catalytic activity could be attributed to structural changes in catalyst, and also the decrease of SSA and basicity. The XRD pattern [**Fig. 14**] showed that spent catalyst of B-CaO loss its crystallinity due to neutralizing of FFA on catalyst surface.

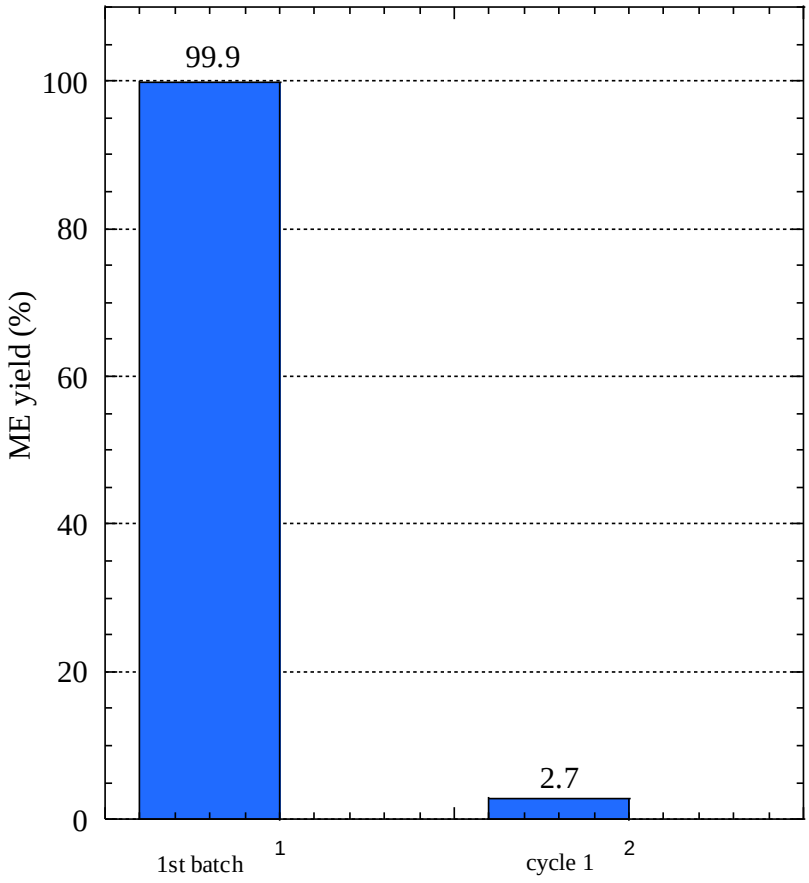

Fig. 13 Reusability of B-CaO catalyst in transesterification WCO with methanol. (Reaction conditions: Methanol/WCO molar ratio = 9:1; catalyst amount = 2 wt%; temperature = 65 ^{o}C).

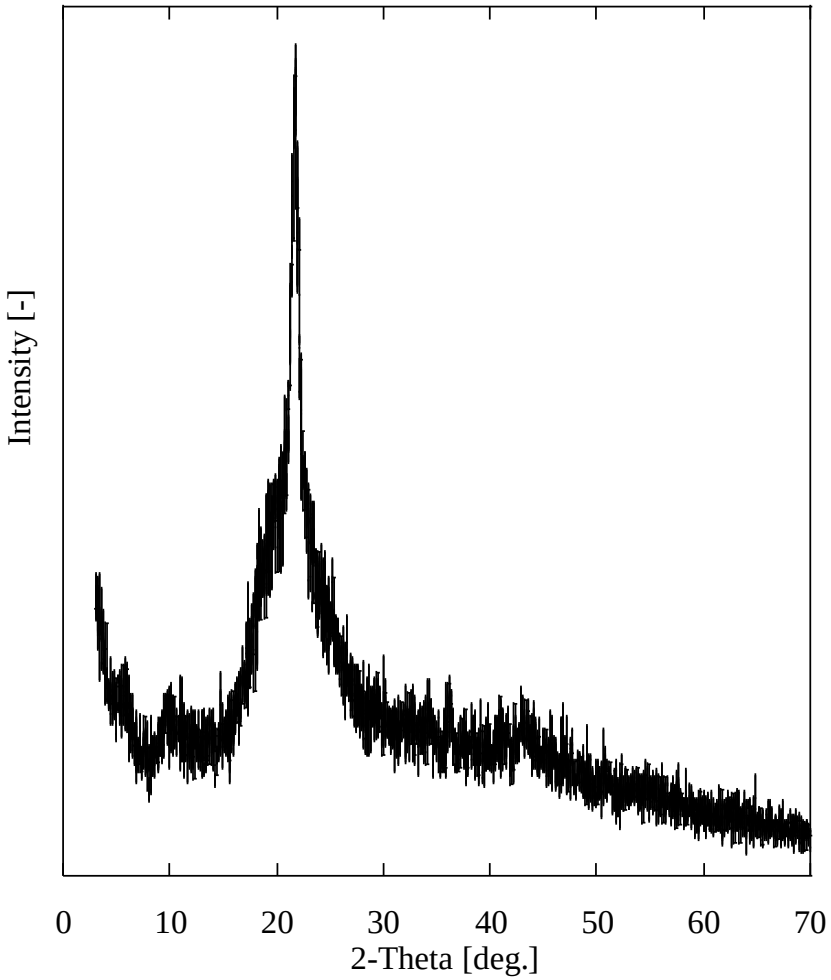

Fig. 14 XRD patterns of spent B-CaO catalyst from post 1st reusability reaction.

3-4. Conclusions

This study demonstrated that by applying such alcohol as grinding-assisted on nano-grinding process was efficient to improve the physicochemical properties and the catalytic features of CaO-based catalyst. After being treated by alcohol-assisted nano-grinding with three kind of alcohol, the CaO-based catalyst with higher SSA, reduced-particle sizes and generated active sites on CaO surface, such as Ca-oxide, Ca-hydroxide and Ca-alkoxide, and the presence of Lewis acid sites on surface catalyst was obtained.

The the CaO-based catalyst treated show high catalytic activity on WCO transesterification with methanol. The catalysts: M-CaO, E-CaO and B-CaO were able to complete the transesterification of WCO having up to 10 wt% FFA and 0.11 wt% moisture content and gave ME yields 98.6 % for M-CaO catalyst, 99.9 % for E-CaO catalyst and 99.7% for B-CaO catalyst in 2 h reaction. The high performance of the catalysts due to large surface area that could serve the reaction, high dispersion of catalyst and the presence of Lewis acid sites on the catalyst surface. Contribution of dispersibility of catalysts imply the importance of active sites to promote the dispersion of CaO catalyst in both methanol and WCO.

The the CaO-based catalyst treated exhibited high tolerance with moisture content due to the presence alkoxy-shielding on the surface of catalysts that could reduce the polarity of catalyst surface. However, reducing the polarity on surface of catalyst made FFA easy to adsorb on surface catalyst and then deactivate the catalyst by neutralized the basicity of the catalyst. The reusability of the catalyst was so poor, this finding will be taken as challenging for the next study.

References

[1] D. M. Marinkovic, M.V. Stankovic, A.V. Velickovic, J.M. Avramovic, M.R. Miladinovic, *et al*., Renewable and Sustainable Energy Reviews 56 (2016) 1387-1408.

[2] L. Lin, X. Li, F. Cui, H. Zhou, X. Shen, M. Dong, Bioenerg. Res. 5 (2012) 949-957.

[3] D. M. Alonso, F. Vila, R. Mariscal, M. Ojeda, M. Lopez Granados, J. Santamaria-Gonzalez, Catalysis Today 158 (2010) 114-120.

[4] L. Zhao, Z. Qiu, S.M. Stagg-Williams, Fuel Processing Technology 114 (2014) 154-162.

[5] M. R. Avhad, J.M. Marchetti, Catalysis Reviews 58 (2016) 157-208.

[6] L. Jan, B. Ondrusschka, Chem. Eng. Technol. 27 (2004) 1156-1159.

[7] X. Liu, X. Piao, Y. Wang, S. Zhu, J. Phys. Chem. A. 114 (2010) 3750-3755.

[8] I. Poljansek, B. Likozar, Influence of mass transfer and kinetics on biodiesel production process, in: M. El-Amin (Eds.), Mass transfer in multiphase systems and its applications, InTech, 2011, pp 433-458.

[9] Y. Zhang, M. Stanciulescu, M. Ikura, Applied Catalysis A: General 366 (2009) 176-183.

[10] M. L. Granados, M.D.Z. Poves, D.M. Alonso, R. Mariscal, F.C. Galisteo, R. Moreno-Tost, *et al*., Applied Catalysis B: Environmental 73 (2007) 317-326.

[11] M. Kouzu, J. Hidaka, Fuel 93 (2012) 1-12.

[12] F.S. Lisboa, F.R. Silva, C.S. Cordeiro, L.P. Ramos, F. Wypych, J. Braz. Chem. Soc. 25 (2014) 1592-1600.

[13] G. Nawaratna, R. Lacey, S.D. Fernando, Catal. Sci. Technol. 2 (2012) 364-372.

[14] A.P.S. Dias, J. Puna, J. Gomes, M.J.N. Correia, J. Bordado, Renewable Energy,

99 (2016) 622-630.

[15] X. Liu, X. Piao, Y. Wang, S. Zhu, H. He, Fuel 87 (2008) 1076-1082.

[16] W. N. R. Wan Isahak, M. Ismail, J. Mohd. Jahim, J. Salimon, M.A. Yarmo, World Applied Science Journal 9 (2010) 17-22.

[17] A. Buasri, N. Chaiyut, V. Loryuenyong, P. Worawanitchaphong, S. Trongyong, Sci. World J. 2013 (2013) 1-7.

[18] A. N. R. Reddy, A. A. Saleh, Md. S. Islam, S. Hamdan, Md. A. Maleque, Energy Fuels 30 (2016) 334-343.

[19] M. Kouzu, T. Kasuno, M. Tajika, S. Yamanaka, J. Hidaka, Applied Catalysis A: General 334 (2008) 357-365.

[20] X. Liu, X. Piao, Y. Wang, S. Zhu, Energy & Fuels 22 (2008) 1313-1317.

[21] N. Kaur, A. Ali, RSC Adv. 5 (2015) 13285-13295.

[22] D. Kumar, A. Ali, Energy Fuels 27 (2013) 3758-3768.

[23] W. Thitsartan, S. Kawi, Green Chem. 13 (2011) 3423-3430.

[24] M. Kim, C. DiMaggio, S. Yan, S. O. Salley, K. Y. S. Ng, Green Chem. 13 (2013) 334-339.

[25] H. J. Berchmans, S. Hirata, Bioresource Technology 99:6 (2008) 1716-1721.

[26] J. Posom, P. Sirisomboon, Biosystems Engineering 130 (2015) 52-59.

[27] F. R. Panjaitan, S. Yamanaka, Y. Kuga, Advanced Powder Technology, In Press.

[28] S. Yamanaka, A. Suzuma, T. Fujimoto, Y. Kuga, J of Nanoparticle Research 15:1573 (2013) 1-8.

[29] T. Lopez, R. Gomez, Journal of Sol-Gel Science and Technology 13 (1998) 1043-1047.

[30] N. Kaur, A. Ali, Renewable Energy 81 (2015) 421-431.

[31] A. Kawashima, K. Matsubara, K. Honda, Bioresour. Technol. 100 (2009) 696-

700.

[32] C. Plank, E. Lorbeer, J. of Chromatography A 697 (1995) 461-468.

[33] T. Watanabe, J. Liao, M. Senna, J. of Solid State Chemistry 115 (1995) 390-394.

[34] P. Jakson, G.D. Parfitt, J. Chem. Soc., Faraday Trans. 1, 68 (1972) 1443-1450.

[35] S. Cai, K. Sohlberg, Journal of Molecular Catalysis A: Chemical 193 (2003) 157-164.

[36] M. Weibel, R. K. Mishra, ZKG 6 (2014) 29-39.

[37] X. Liu, H. He, Y. Wang, S. Zhu, X. Piao, Fuel 87 (2008) 216-221.

[38] A. P. S. Diaz, J. Puna, M. J. N. Correia, I. Nogueira, J. Gomes, J. Bordado, Fuel Processing Technology 116 (2013) 94-100.

[39] Y. Yanagisawa, S. Kashima, Surface Science 454-456 (2000) 379-383.

[40] H. Hattori, Chem. Rev. 95 (3) (1995) 537-558.

[41] J. Kondo, Y. Sakata, K. Maruya, K. Tamaru, T. Onishi, Applied Surface Science 28 (1987) 475-478.

[42] M. M. Branda, A. H. Rodriguez, P. G. Belelli, N. J. Castellani, Surface Science 603 (2009) 1093-1098.

[43] R. Ladera, E. Finocchio, S. Rojas, J.L.G. Fierro, M. Ojeda, Catalysis Today 192 (2012) 136-143.

[44] B. Moulin, L. Oliviero, P. Bazin, M. Daturi, G. Coctentin, F. Mauge, Phys. Chem. Chem. Phys. 13 (2011) 10797-10807.

[45] S. K. Moothedath, S. C. Ahluwalia, Powder Technology 71 (1992) 229-237.

[46] S. L. A. Hennart, W. J. Wildeboer, P. van Hee, G. M. H. Meesters, Chemical Engineering Science 64 (2009) 4123-4130.

[47] S. H. Teo, U. Rashid, Y. H. Taufiq-Yap, Energy Conversion and Management 87 (2014) 618-627.

[48] W. Wu, R. F. Giese, C. J. Van Oss, Powder Technology 89 (1996) 129-132.

[49] M. Senna, Advanced Powder Technol. 13 (2) (2002) 115-138.

[50] T. Lopez, R. Gomez, J. Navarrete, E. Lopez-Salinas, Journal of Sol-Gel Science and Technology 13 (1998) 1043-1047.

[51] G. Busca, Phys. Chem. Chem. Phys. 1 (1999) 723-736.

[52] C. Rodriguez-Navarro, I. Vettori, E. Ruiz-Agudo, Langmuir 32 (2016) 5183-5194.

[53] M. K. Dongare, A. P. B. Sinha, Thermochimica Acta 57 (1982) 37-45.

[54] D. Cornu, H. Guesmi, G. Laugel, J. Krafft, H. Lauron-Pernot, Phys. Chem. Phys. 17 (2015) 14168-14176.

[55] K. S. Kim, M. A. Barteau, Langmuir 4 (1988) 533-543.

[56] C. Angelici, M. E. Z. Velthoen, B. M. Weckhuysen, P. C. A. Bruijnincx, Catal. Sci. Technol. 5 (2015) 2869-2879.

[57] H. Kahlert, G. Meyer, A. Albrecht, ChemTexts 2 (2016) 7-35.

[58] L. Leon-Reina, A. Cabeza, J. Rius, P. Maireles-Torres, A. C. Alba-Rubio, Journal of Catalysis 300 (2013) 30-36.

[59] M. Kouzu, T. Kasuno, M. Tajika, Y. Sugimoto, S. Yamanaka, J. Hidaka, Fuel 87 (2008) 2798-2806.

[60] M. Juarez, C. Osawa, M. Acuna, N. Samman, Food Control 22 (2011) 1920-1927.

APPENDIX A

Fig.S1 FTIR spectra of the samples: M-CaO, E-CaO and B-CaO evacuated in an air-ventilated oven at 300 ^{o}C.

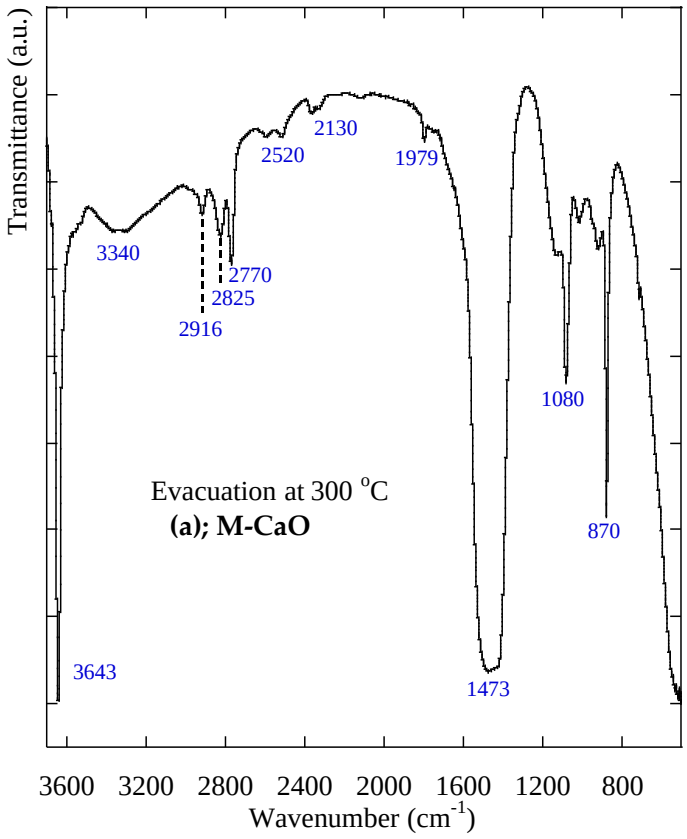

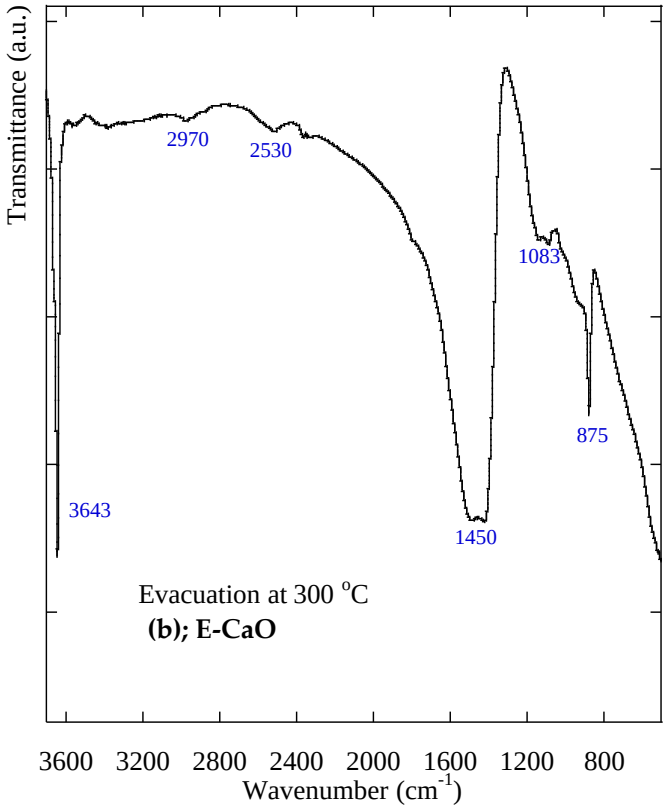
Transmittance (a.u.)
2970
2530
1083
875
3643
1450
Evacuation at 300 °C
(b); E-CaO
3600 3200 2800 2400 2000 1600 1200 800
Wavenumber (cm-1)

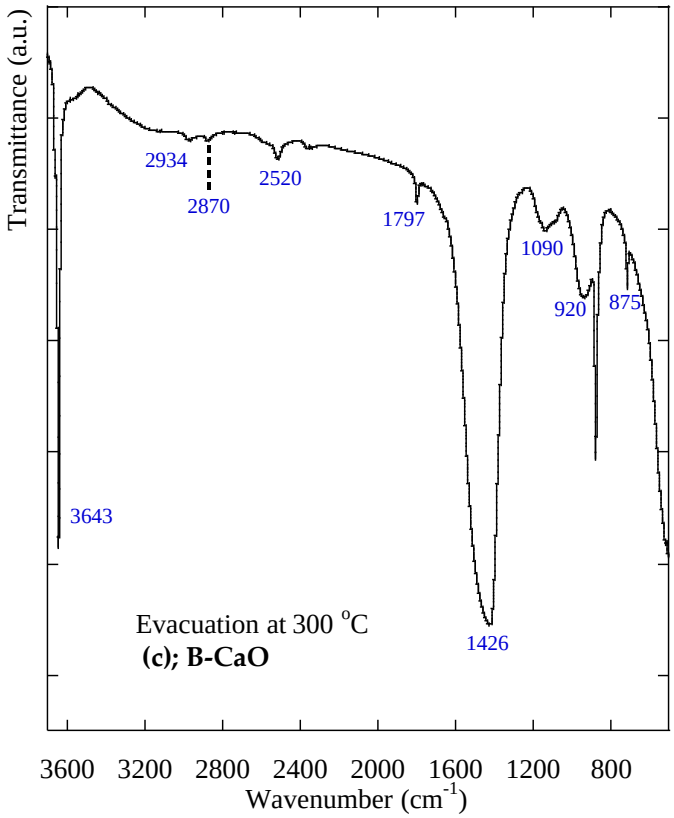
Transmittance (a.u.)
2934
2870
2520
1797
1090
920
875
3643
1426
Evacuation at 300 °C
(c); B-CaO
3600 3200 2800 2400 2000 1600 1200 800
Wavenumber (cm-1)

APPENDIX B

Fig.S2 XRD patterns of the samples evacuated in 300 ºC; (1) Ca-oxide, ICDD file 04-1497; (2) Ca-hydroxide, ICDD file 04-0733; (3) Ca-alkoxide refer to [15]; (4) $CaCO_3$, ICDD file 47-1743.

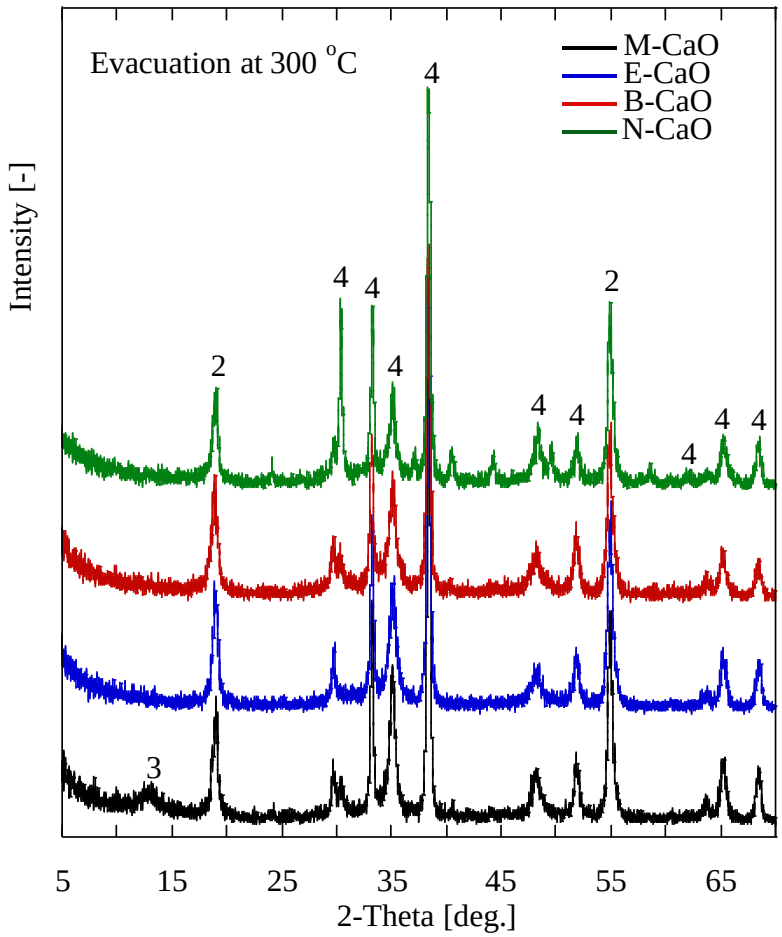

APPENDIX C

Fig.S3 Optical microscopy for catalyst dispersion after 3 mins mixing with magnetic stirrer at 800 rpm for catalysts M-CaO, E-CaO, B-CaO and N-CaO; Inserted photographs are product after 180 mins transesterification reaction time, centrifuged at 4000 rpm and 10 min: (a) methanol-assisted, (b) ethanol-assisted, (c) 1-butanol-assisted, and (d) bare grinding-assisted.

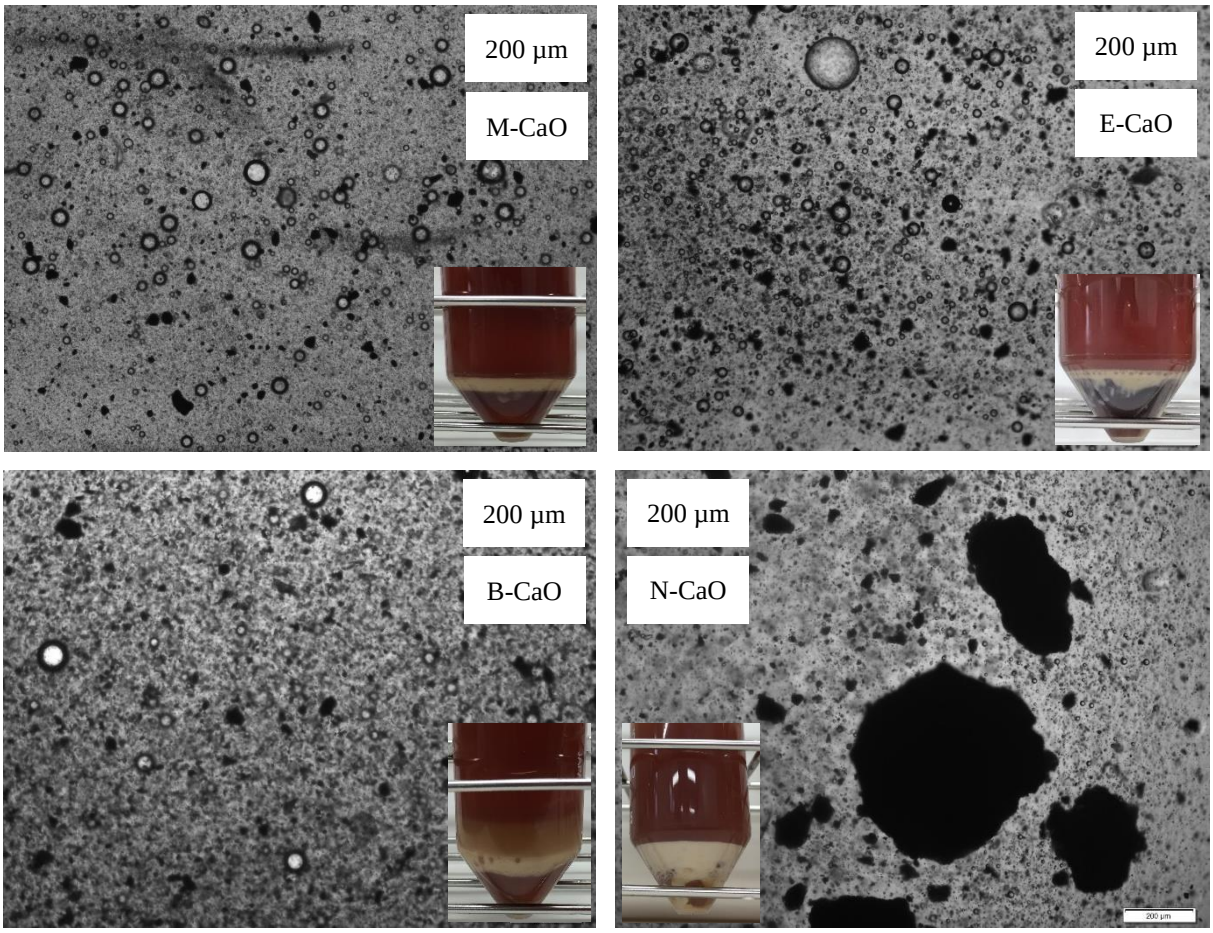

Chapter 4

Effect of the free fatty acids and water content on CaO-based catalyst activity on different vegetable oils transesterification (Catalyst prepared by 1-butanol-assisted nano-grinding)

4-1 Introduction

Application of waste cooking oil, unrefined oil, low-grade edible oil and non-edible oil could be advantageous in reducing the biodiesel production cost to make the price competitive with petroleum fuel and prevent from a fuel versus food situation [**1, 2, 3**]. As reported by Haas et al. [4] the cost of oil feedstock book for ~ 88% of biodiesel production. Although such feedstocks being cheap than edible oil, these oils usually having high free fatty acids (up to 12 wt%) and moisture (up to 3 wt%) [**2**]. Transesterification reaction commonly required refined oil feedstock with high quality such free fatty acid (FFA) should be lesser than 0.5 wt% and water content lesser than 0.06 wt% [**4, 5, 6, 7**].

The presence of FFA and water in oil feedstock deactivates the catalyst due to the saponification. FFA content in oils not only deactivates the homogeneous alkali catalyst through saponification but also found to reduce the activity of heterogeneous catalysts [**8, 9, 10, 11**]. Commonly, biodiesel production with high FFA oil feedstock is carried out in two stage of process, first is esterification of FFA content using acid catalysts, and second is transesterification of triglycerides using basic catalyst which increases the production cost [**12**].

CaO is very susceptive to FFA and moisture or water content. CaO surface easily gets covered with moisture when exposed to ambient air resulted $Ca(OH)_2$. Certain water content in reaction medium also led hydration of CaO to $Ca(OH)_2$ [**13, 14, 15**]. A numerous investigation have conducted for the upper limits of FFA and water contents in calcium-based catalysts transesterification catalyzed. CaO reagent (commercial-available) drop its catalytic performance in transesterification when acidity of oil feedstock increased because of neutralization of catalyst basic sites by FFA and promoting catalyst loss in the formation soap [**16, 17**]. Calcined clamshell (M.

mereterix) was utilized for transesterification low acid value oil feedstock (0.73 mg KOH/g) and obtained 89.91% yield of ME at 3 h. The catalyst deterioration reported being neutralized by the FFA content [**18**].

To increase the resistance of pure CaO towards FFA and water contents, the pure CaO catalyst doped or loaded onto other oxides. Authors in [**19**] demonstrated the application of nanocrystalline Li^+ impregnated CaO as a solid base on waste cottonseed oil transesterification with 15 wt% moisture and 6 wt% FFA and achieved the completion reaction in short reaction time. The K/CaO was found high catalytic activity towards 8.4 wt% FFA and 0.28 wt% moisture contents [**3**]. Kaur and Ali [**20**] investigated Zr/CaO catalyst high tolerance to 15 wt% moisture and 6 wt% FFA. The Zr/CaO catalyst was effective to yield 99% methyl ester (ME) at methanol to oil molar ratio of 15:1 at 65 ^oC and 5 wt% catalyst concentration. High performance also found in CaO/Al2O3 which having tolerance up to 2.49 mg KOH/g of palm oil, 94.3 % ME was obtained [**21**]. Catalyst MgO/CaO prepared by the coprecipitation method achieving conversion close to 60% within 3 h, whereas pure MgO is inactive [**22**].

In order to achieve the practical use also in continuation to the earlier work (Chapter 3) to develop neat CaO catalyst for the transesterification of high FFA containing and moisture (or water) content, catalyst application of the best performance in Chapter 3 was applied in three types of feedstock oil transesterification. The oil feedstocks were refined soybean oil (SBO), un-refined, low-grade crude palm oil (U-CPO) and waste cooking oil (WCO) based rapeseed oil. CPO has the highest average oil yield of any oil crop, thus considerably as oil feedstock for long term production of biodiesel [**23**]. CPO composition was: (a) neutral lipid: triglyceride (~93%), diglyceride (~4.5%), monoglyceride, and FFA (~1.5%); (2) polar lipid (ppm total lipid): phospholipid (1143 ppm) and glycolipid (438 ppm). In case of low-grade CPO, the FFA

content could be reached up to 5 – 7.5% [**24**]. WCO also has a potential as source for biodiesel production. By repeated of it uses as a cooking oil, elevated acidity and increased specific heat. The different cooking conditions also resulted variation of salt and water contains in WCO [**25**].

The physicochemical study of CaO-based catalyst treated by alcohol-assisted nano-grinding in Chapter 3, the catalysts tolerance to waste cooking oil (WCO) having 10 wt% and 0.11 wt% water content in the first batch transesterification reaction. Although after 2nd consecutive transesterification reaction the catalysts suffering seriously deactivation due to lower crystallinity, the yield of methyl ester (ME) almost compete the NaOH catalyst performance in the first batch transesterification reaction.

The objective of this study is to investigate the effects of FFA, water or moisture on CaO-based catalyst structure activities. The CaO-based catalyst was prepared by 1-butanol-assisted nano-grinding.

4-2 Experimental Section

4-2-1 Materials

Scallop shell powder was purchased from Tokoro-cho Industry (Kitami, Japan) which composed of calcite crystals and a small quantity of organic matter. U-CPO was donated by Indonesian Oil Palm Research Institute (Indonesia). WCO was obtained from cafeteria of Muroran Institute of Technology (Japan). Soybean oil (reagent grade), methanol (>99.8%), 1-butanol (99%), dichloromethane (solvent grade), HCl (p.a.) were purchased from Kanto Chemical (Japan). Hexane (HPLC grade), 2-propanol (>99.5%) 1-Oleoyl-rac-glycerol (monoolein, ≥99%), dioleoyl glycerol (diolein, ≥99%), glyceryl trioleate (triolein, ≥99%), pyridine (HPLC grade) as buffer in sample analysis preparation were purchased as standard from Sigma Aldrich (St. Luis, USA).

Tetrahydrofuran (reagent grade) and KOH standard solution (8 mol/L) were purchased from Wako Pure Chemical Industries Ltd. (Japan). Heptane (anhydrous 99%) as solvent, N-Methyl-N-(trimethylsilyl)-trifluoracetamide (synthesis grade) as agent of derivatization of OH groups in sample analysis preparation were purchased from Sigma Aldrich (St. Luis, USA). Glyceryl tridecanoate (≥99%) as internal standard for quantity analysis was purchased from Sigma Aldrich (St. Luis, USA).

The FFA content in waste cooking oil was estimated in terms of KOH in milligrams in order to neutralize 1 g of fatty acid according to the procedure described elsewhere [**1, 26**]. A 2 g of the waste cooking oil diluted with 50 ml of 95% ethanol and diethyl ether in a 1:1 molar ratio were thoroughly mixed in a conical flask using magnetic stirrer. The mixture was titrated against 0.1 of KOH drop wisely using phenolphthalein solution (0.05 g of phenolphthalein to 50 ml of 95% pure ethanol and diluted to a 100 ml using distilled water) until the color turned pink and lasted for 10 s. The measurement repeated two times for accuracy and the FFA content was measured at 10 wt%. Determination of the moisture content (% wet basis) of waste cooking oil was measured as described in literature [**27**]. A 2 g of oil were placed in aluminium can which previously dried and tared. The moisture content were measured using an oven at 105 ^{o}C. After sitting in desiccator for 1 h to cool, the sample was weighed every 6 h until the weight remained constant.

4-2-2 CaO-based catalyst preparation

CaO was obtained from the calcination of scallop shell powder at 1000 °C for 3 h. 1-butanol-assisted nano-grinding was carried out in the planetary ball mill (P-7 premium line, Fritsch, Germany), which was equipped with two zirconia pots of 80 cm^3 volume, each containing 100 g of yttria-stabilized zirconia milling beads (3 mm

diameter). Bead-filling ratio relative to the pot volume, J^a, was 0.35 and sample loading ratio to void fraction of the beads, U^b, was 0.27. The nano-grinding was conducted in batchwise method for 5 h. During the nano-grinding operation was stopped for 15 min after every 1 h of grinding to prevent the inside of the milling pot from overheating. Revolution speed kept at 900 rpm and 1-butanol addition was 1.25 g per 10 g of CaO.

4-2-3 Catalyst characterization

The SSA of the powders was determined from nitrogen gas adsorption by using the five-point BET method (Microtrac, Adsotrac DN-04). Prior to measurement, samples were degassed at 473 K for 2 h. The X-ray powder diffraction (XRD) measurements were performed by a Multi Flex-120 NP Rigaku (Japan) equipped with a Cu-Kα anode (λ = 1.5418 Å), operated at a tension and current of 40 kV and 20 mA, respectively. Measurements were recorded at room temperature over the 2θ range 3–70°, with a 0.02° step size. Crystalline phases were identified by comparison with ICDD data files. Fourier-transform infrared (FTIR) spectra were recorded using a JASCO FTIR-460 PlusK spectrometer, and catalyst was measured as KBR pellets. Measurements were conducted over the range 4000–400 cm^{-1} with a 4 cm^{-1} resolution. A scanning electron microscope (SEM) analysis was carried out in JEOL JSM-6380A with an acceleration voltage of 20 keV. Prior to analysis, the sample was covered a carbon film.

Total basic sites (f_m) of the catalysts were evaluated by measuring the acidity conjugate acid, by titration method. In a typical experiment, 25 mg catalyst CaO ground was dissolved in 25 mL of 0.1 M HCl and resulting mixture was stirred for an hour. The catalyst would neutralize HCl equivalent to its basicity. The resulted solution was titrated against standard NaOH solution to determine the exact concentration of excess

HCl. The amount of HCl neutralized by the catalyst was determined and represented as basicity of the catalyst as mmol of HCl/g of catalyst [**20**].

4-2-4 Transesterification

The transesterification was carried out at 60±1 °C with a methanol-to-oil molar ratio of 9:1 and catalyst concentration of 3 wt% with respect to the oil mass. The stirring rate was held at 800 rpm. The transesterification was carried out with three type of oil feedstock: (1) WCO having 10 wt% FFA and 0.11 wt% moisture; (2) U-CPO having 5.6 wt% FFA and 0.16 wt% moisture; and (3) SBO having 0.04 wt% FFA and 4 wt% water content. The water content of oil feedstock type (3) obtained by adding 4 wt% (respect to oil) of water to the SBO.

Prior to analysis, samples (1 ml) were removed from the reaction mixture and immediately treated using a procedure detailed elsewhere [28]. The quantities of esters, monoglyceride, diglyceride, and triglyceride were analyzed using a gas chromatograph (Shimadzu GC-14B) equipped with a flame ionization detector (FID), on a DB-5HT capillary column (14 m × 0.25 mm, 0.1 μm film thickness). The analytical work was performed with the following heating regime: holding at 50 °C for 1 min, followed by three separate steps of temperature increase, firstly to 180 °C at a rate of 10 °C/min, then to 230 °C at 7 °C/min, and lastly to 380 °C at 10 °C/min, at which point the temperature was held for 10 mins. Quantitative analysis was carried out following a procedure described in detail elsewhere [**29**].

4-3 Result and discussion

4-3-1 Bulk and surface characterization of catalysts

The morphology of the sample of ground B-CaO and post reaction sample was examined by SEM (**Fig 1 (a)-(d)**). The ground B-CaO showed irregular-shaped smaller than 5 μm and cloud like aggregate. The micrographs after the transesterification reaction samples show that samples changing in characteristic morphology. The spent B-CaO catalysts, as the **Fig. 1 (b), (c)** and **(d)** shown, the shapes can be identified as Ca-methoxide (flower like cluster shape), CaDg with rectangular shape and some like aggregate of spheroids which can be identified as Ca-hydroxide [**30, 31**]. Some aggregation and disordered shapes also can be observed on samples of the spent catalysts that can be ascribable to the effect of vigorous of stirring on transesterification reaction medium.

The total basicity (f_m) of the catalysts value was 5.02 mmol g^{-1} of catalyst which was evaluated by titration method. The basicity of the CaO-based catalyst treated by 1-butanol-assisted nano-grinding was increased compare to the initial basic strength. This behavior agree with author in [**32**]. The basicity increased due to mechano-chemistry reaction between 1-butanol with the CaO during the nano-grinding. The SSA of the catalyst was 64.5 m^2g^{-1}. This was advantage of 1-butanol-assisted which can led to a reduced-energy state, thus can reduce the agglomeration energy during the nano-grinding [**33**].

The XRD pattern (**Fig.2**) for fresh B-CaO after the nano-grinding suggested the presence of crystallite of Ca-hydroxide, while the major crystallite was Ca-oxide. The crystalline active sites were indexed and matched to known materials: Ca-oxide (ICDD file 04-1497), and Ca-hydroxide (ICDD file 04-0733). Before the 1-butanol-assisted nano-grinding, the main phase of calcined scallop shell (as a starting material CaO

catalyst) was CaO. The formation of Ca-hydroxide was due to the partial hydration of CaO by 1-butanol during the nano-grinding.

The FTIR spectra analyses to characterize the surface species after the 1-butanol-assisted nano-grinding. The vibrational features of the sample presented in **Fig. 3**. The sharp peak at 3642 cm^{-1} can be assigned to hydroxyl groups of $Ca(OH)_2$ [**15**]. The spectra of alcohol chemisorbed on the surface of catalyst were observed at bands 2960 cm^{-1}, 2934 cm^{-1}, 2870 cm^{-1} which ascribable to C-H stretching of Ca-alkoxide [15**,** 34]. In the region 1500–1400 cm^{-1}, the bands attributed to deformation of C–H modes of alkoxy groups and presence of carbonate groups mostly overlap [**15, 35**].

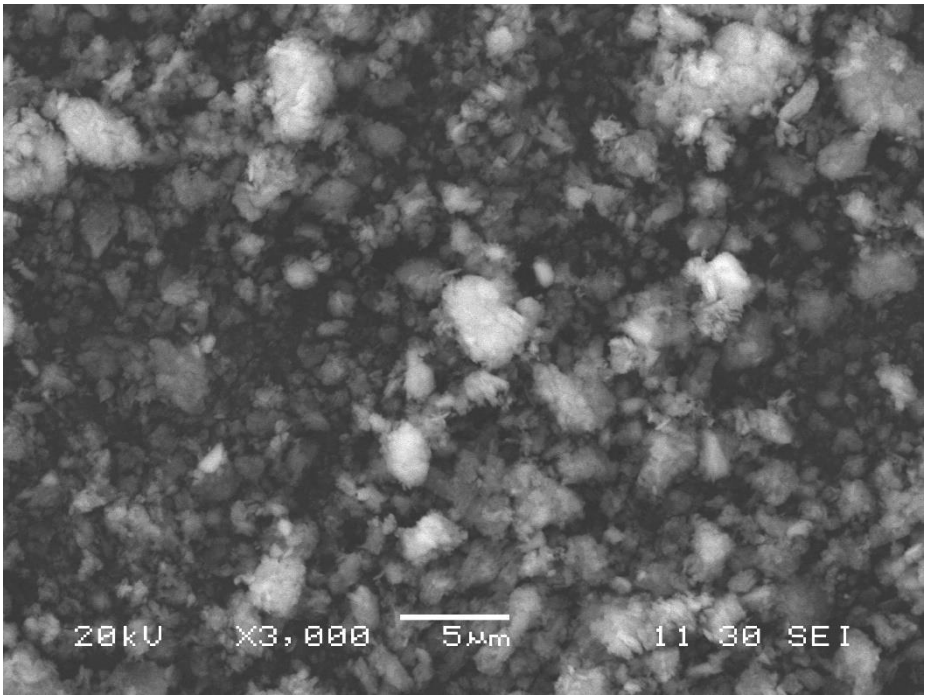

Fig. 1 (a) SEM micrograph of B-CaO catalyst

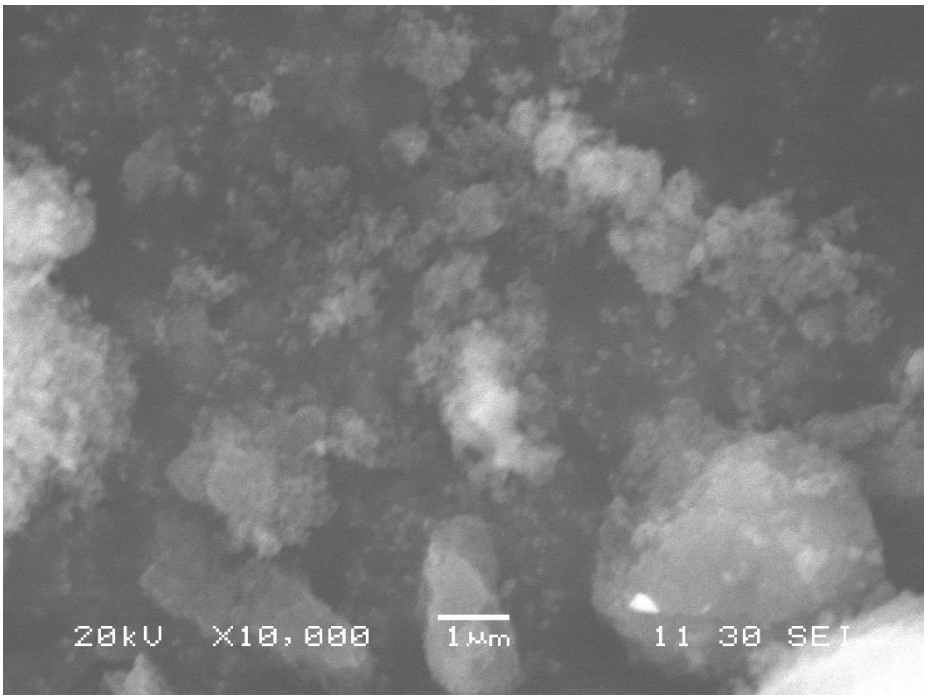

Fig. 1 (b) SEM micrograph of spent B-CaO catalyst using WCO having 10 wt% FFA and 0.11 wt% moisture content.

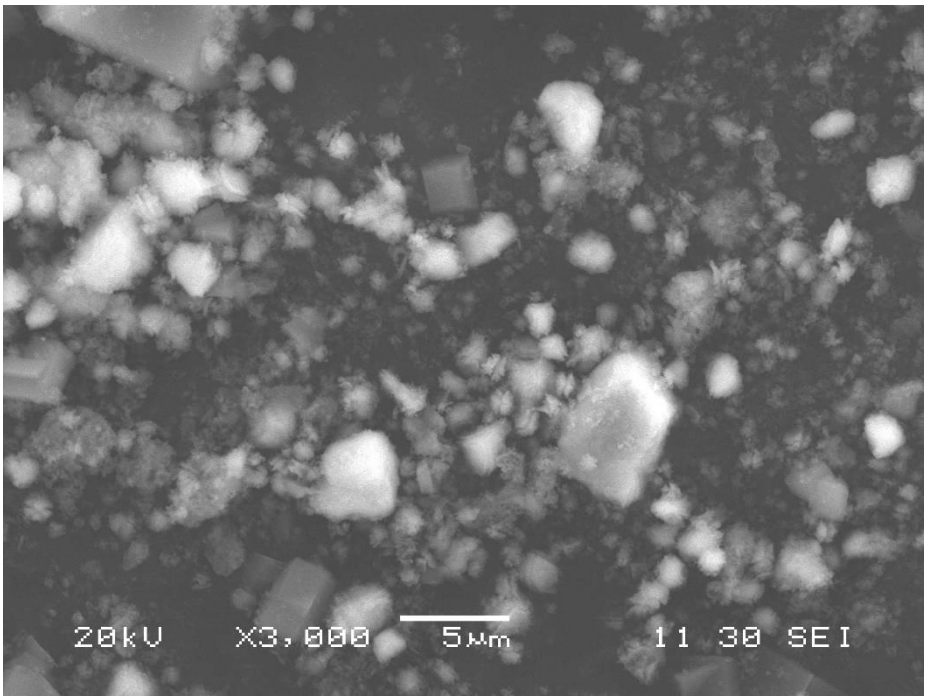

Fig. 1 (c) SEM micrograph of spent B-CaO catalyst using U-CPO having 5.6 wt% FFA and 0.16 wt% moisture content

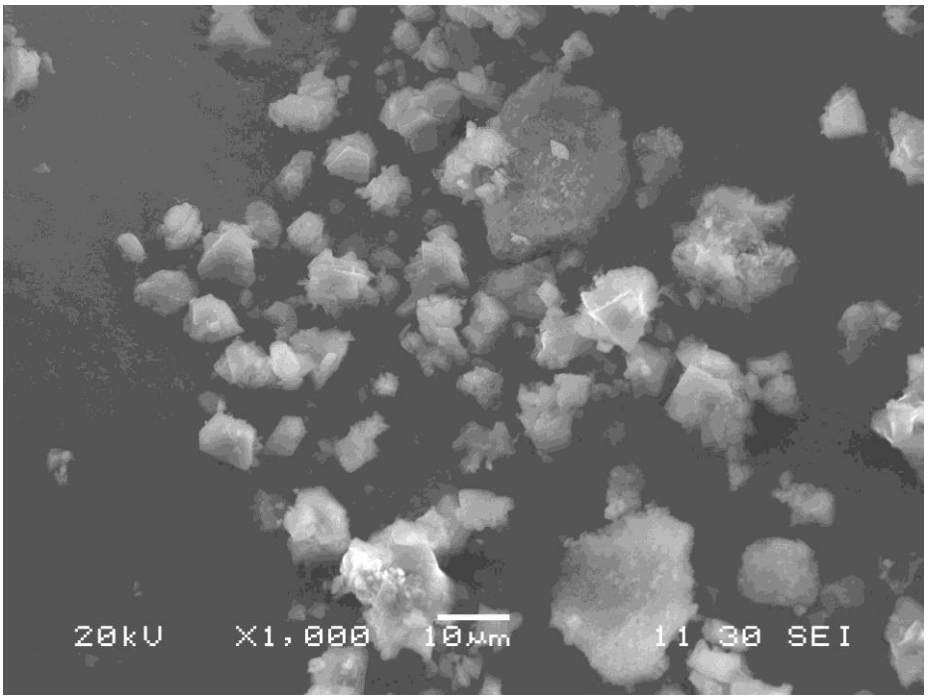

Fig. 1 (d) SEM micrograph of spent B-CaO catalyst using SBO having 0.04 wt% FFA and 4 wt% water content

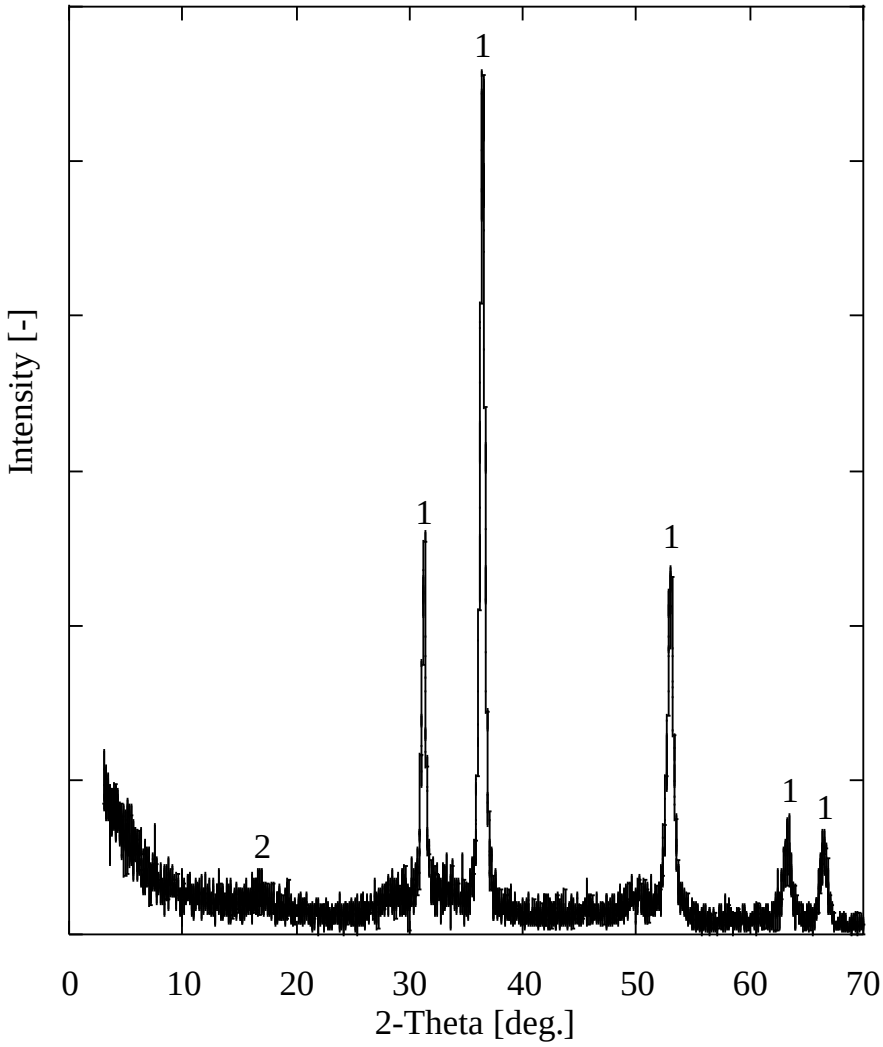

Fig. 2 XRD pattern of the B-CaO catalyst after 5 h nano-grinding with batchwise method. The 1-butanol-assisted used was 1.25 g. (1) Ca-oxide, ICDD file 04-1497; (2) Ca-hydroxide, ICDD file 04-0733.

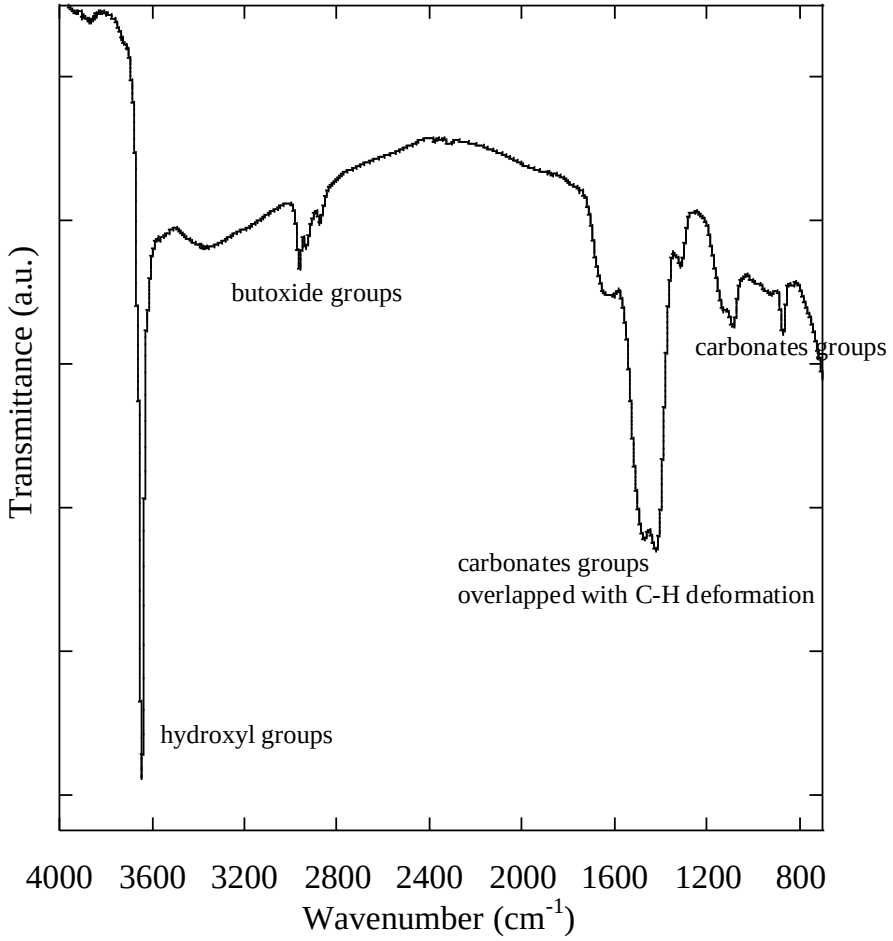

Fig. 3 FTIR spectra of the B-CaO catalyst after 5 h nano-grinding with batchwise method. The 1-butanol-assisted used was 1.25 g.

4-3-2 Catalytic Activity

The catalytic activity as the fresh B-CaO catalyst was tested at methanol reflux at 60^{o}C with three kind of oil feedstocks: (1) WCO having 10 wt% FFA and 0.11 wt% moisture; (2) U-CPO having 5.6 wt% FFA and 0.16 wt% moisture; and (3) SBO having 0.04 wt% FFA and 4 wt% water content. The transesterification reaction carried out in conditions: methanol-to-oil molar ratio of 9:1 and catalyst concentration of 3 wt% with respect to the oil mass. After the reaction period (3 h) the catalyst was removed by filtration and washed with 2-propanol. The spent catalyst from WCO and U-CPO reaction was observed like gel formation. This behavior results from neutralization of surface of basicity of catalyst via saponification reaction between FFA and calcium [**7**].

ME yield were obtained depicted in **Fig. 4**, in the view of the previous experiment in Chapter 3, FFA and moisture content affected the catalyst activity. The same phenomenon was observed in this study, nonetheless the B-CaO catalyst can completed the reaction. The B-CaO catalyst exhibited high catalytic activity, ME yield obtained above 98.5 % in 2 h.

FFA and water content have an obvious influence on the B-CaO catalytic activity (**Figs**. **5** and **6**). Although the ME yield was above 98.5 % in 2 h, the appreciable time in data at 10 min the ME was only above 8 % (**Fig. 4**). This behavior explained that the catalyst need induction time to start the transesterification reaction. As has described in Chapter 3, the surface properties of B-CaO catalyst is hydrophobic and less polar because the existence of hydrocarbon tails of alkoxy-shielding. Possibly, this caused a competition of reaction on transesterification medium. The high SSA of catalyst induced competitiveness reaction between oil, FFA, water and methanol in the basicity sites on catalyst surface. This might be a reason, the yield of ME resulted in low conversion below 60 min of reaction.

Taken a fact that CaDg was the true catalyst in transesterification reaction catalyzed by CaO [**30**], the succeeding of transformation CaO active phase into CaDg played important role to boost the rate of reaction. Seemingly, the FFA and water content on oil feedstocks extended the time of CaO the transformation into CaDg.

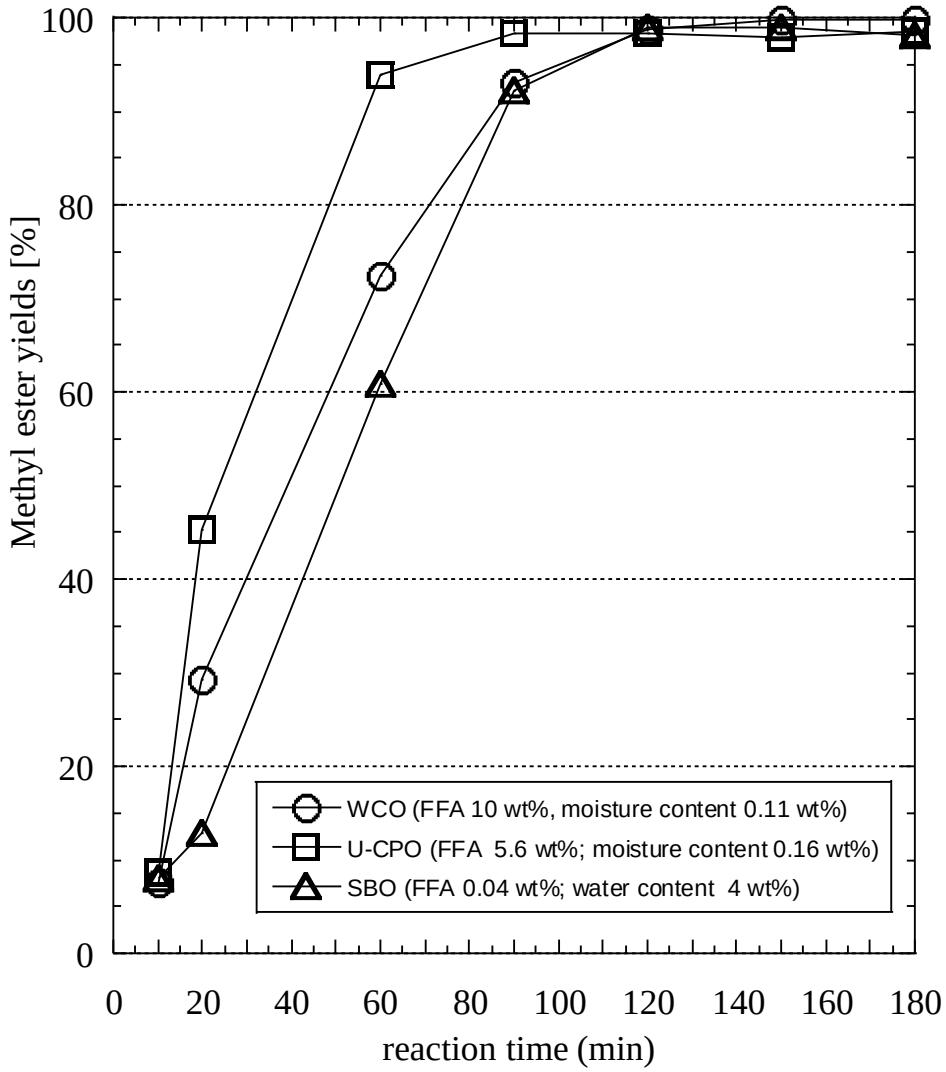

Fig.4 The influence of FFA and water content. Reaction conditions: Methanol/oil molar ratio = 9:1; catalyst amount = 3 wt%, temperature = 65 ^{o}C)

4-3-3 The effects of FFA and water content on the catalyst

Considering the using low-quality oil (often contained FFA and water) on transesterification reaction to biodiesel production, the structural changes of the catalyst in the reaction medium were evaluated. The XRD patterns in **Fig. 5** show different level of deterioration of the CaO catalyst. FFA on oil feedstock damaged the CaO catalyst, it can be seen that catalyst seriously suffer a fast decay due to neutralization. This phenomenon agreed with the authors in [**17, 18**]. The CaO catalyst in neat form that they used decay when used oil with 2 wt% FFA and 0.73 mg/KOH oil acidity. The decay of CaO catalyst behavior confirm by SEM micrographs in **Fig. 1 (b)-(c)**. The morphologies can be identified as Ca-methoxide (flower like cluster shape), and some like aggregate of spheroids which can be identified as Ca-hydroxide [**30, 36**]. The low crystallite shape of rectangular CaDg displayed weak. The B-CaO catalyst seems to be tolerance with water content in oil feedstock. It can be explained by the changing of surface chemical of B-CaO catalyst during the nano-grinding from hydrophilic to hydrophobic. The crystallite intensity in **Fig. 5** still can be defined as crystallite of CaDg. This behavior also confirmed in SEM micrograph in **Fig 1 (d)**, the shape of rectangular CaDg can be seen clearly.

FTIR spectra of the spent catalyst as shown in **Fig. 6** that moisture or water content has negative effect on the surface of the catalysts treated by alcohol-assisted nano-grinding with the absence of band of hydroxyl features. Inversely, FFA content has strong effect on the surface of the catalysts treated by alcohol-assisted nano-grinding. It can be attributed to the presence alkoxy-shielding on the surface of catalysts after the nano-grinding. FTIR spectra in **Fig. 6** explaind the decay of surface of B-CaO catalyst by FFA content. The features in 2923 cm^{-1} and 2854 cm^{-1} are assigned to C-H stretching of Ca-methoxide [**10**]. The presence a band at 1577 cm^{-1} can be ascribed as the existence

of carbonyl adsorbed species of FFA [**36**]. This was an evident to the catalyst basic site neutralization by FFA.

Overall, the catalytic activity of B-CaO catalyst on those three oil feedstocks was high. The ME yield was above 98.5 % at 2 h of reaction. The presence of the Lewis acid sites (as has described in Chapter 3) has significant contribution in FFA conversion into ME. Lewis acids was effectively in transforming FFA into ME [**37**].

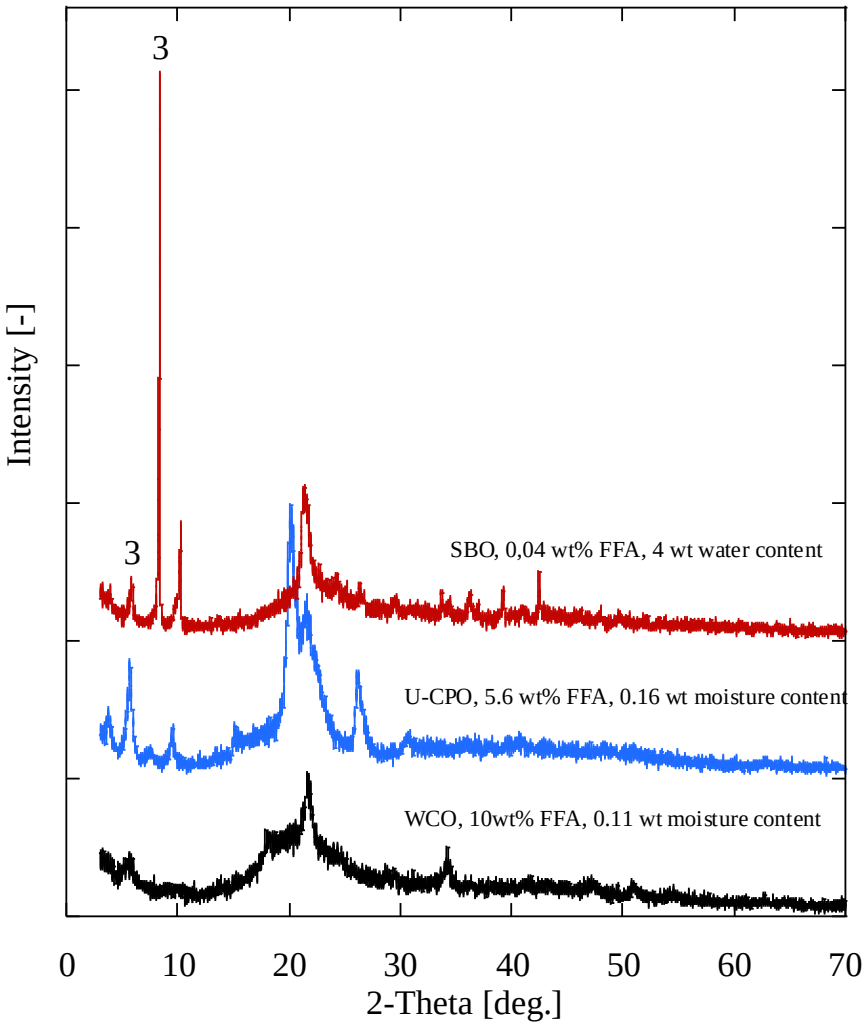

Fig. 5 XRD patterns of spent B-CaO catalyst with different oil feedstocks; (3) CaDg was taken from [**16**]

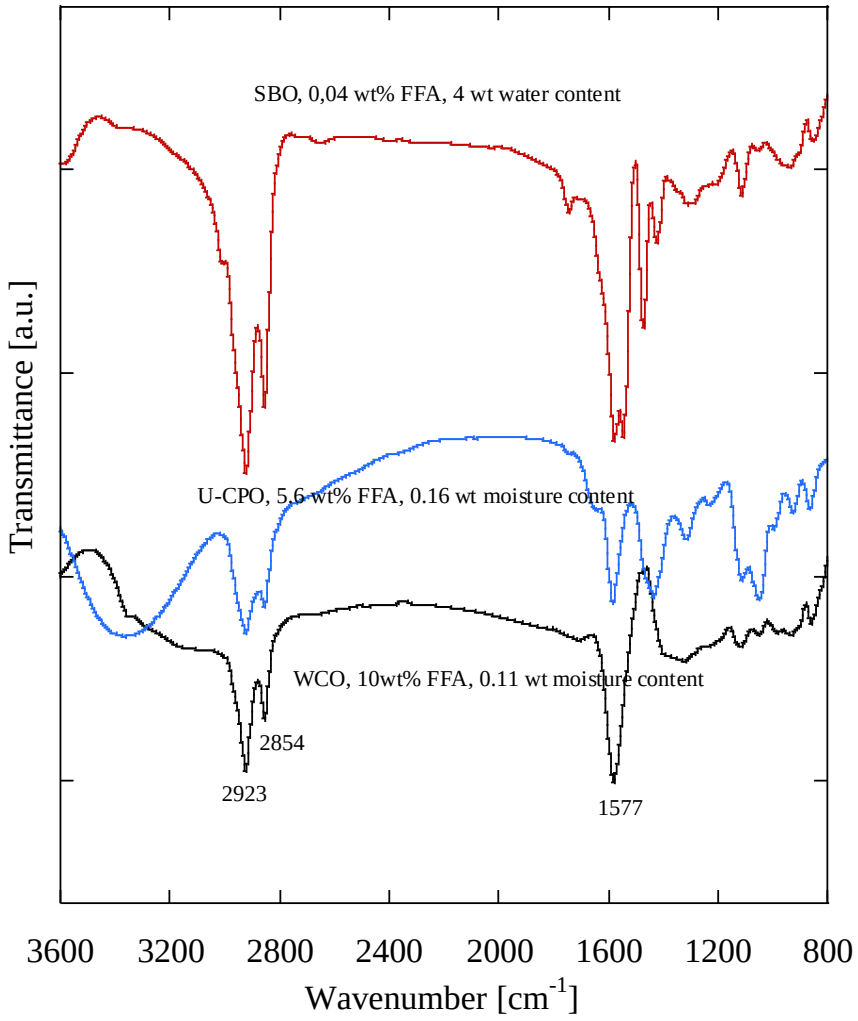

Fig. 6 FTIR spectra of spent B-CaO catalyst with different oil feedstocks.

4-4 Conclusions

This study evaluated the tolerance of CaO catalyst treated with 1-butanol-assisted nano-grinding to FFA and water content. The the CaO-based catalyst treated show high catalytic activity on WCO transesterification with methanol. The catalyst was able to complete the transesterification: 98.7% for WCO, 98.4% for U-CPO and 99% for SBO with 4 wt% water content. The high catalytic activity of the catalyst due to large SSA that could serve the reaction, high dispersion of catalyst and the presence of Lewis acid sites on the catalyst surface. Contribution of dispersibility of catalysts imply the importance of active sites to promote the dispersion of CaO catalyst in both methanol and oil feedstocks.

The CaO catalyst treated with 1-butanol-assisted nano-grinding, exhibited high tolerance with moisture or water content up to 4 wt%, due to reducing of polarity of CaO catalyst surface by alkoxy hydrocarbon tails. However, reducing of polarity on surface of catalyst made FFA strongly reacted with basic species on surface catalyst and then deactivate the catalyst by saponification reaction. However, in the batch reaction, the yield of methyl ester is above 98.5 % in the first batch transesterification reaction in 2 h. Deterioration of CaO catalyst treated with 1-butanol-assisted nano-grinding was mainly by FFA neutralization on surface of catalyst. By using this catalyst, which is relatively inexpensive because of low raw materials and production cost, greatly decreases the production cost of biodiesel.

References

[1] A. N. R. Reddy, A. A. Saleh, Md. Saiful Islam, S. Hamdan, Md. Abdul Maleque, Energy Fuels 30 (2016) 334-343.

[2] D. Kumar, A. Ali, Energy Fuels 27 (2013) 3758-3768.

[3] D. Kumar, A. Ali, Biomass and Bioenergy 46 (2012) 459-468.

[4] M. J. Haas, A. J. McAloon, W. C. Yee, T. A. Foglia, Bioresour. Technol. 97 (2006) 671-678.

[5] B. Freedman, E. H. Pryde, T. L. Mounts, J. Am. Oil Chem. Soc. 61 (1984) 1638–1643.

[6] B. Sajjadi, A.A.A. Raman, H. Arandiyan, Renewable and Sustainable Energy Reviews, 63 (2016) 62-92.

[7] M. J. Haas, A.J. McAloon, W.C. Yee, T.A. Foglia, Bioresource Technology, 97:4 (2006) 671-678.

[8] C. D. M. de Araujo, C.C., de Andrade, E. de Souza e Silva, F.A. Dupas, Renewable and Sustainable Energy Reviews, 27 (2013) 445-452.

[9] N. Kaur, A. Ali, RSC Adv. 5 (2015) 13285- 13295.

[10] S. Yan, M. Kim, S. O. Salley and K. Y. S. Ng, Appl. Catal., A 360 (2009) 163-170.

[11] A. P. S. Diaz, J. Puna, M. J. N. Correia, I. Nogueira, J. Gomes, J. Bordado, Fuel Processing Technology 116 (2013) 94-100.

[12] H. Berchmans, S. Hirata, Bioresource Technology 99 (2008) 1716-1721.

[13] J. Zhang, S. Chen, R. Yang, Y. Yan, Fuel 89 (2010) 2939-2944.

[14] B. Yoosuk, P. Udomsap, B. Puttasawat, P. Krasae, Bioresource Technology 101 (2010) 3784-3786.

[15] M. L. Granados, M. Z. D. Poves, D. M. Alonso, R. Mariscal, F. C. Galisteo, R.

M. Tost, et al., Appl. Catal. B. Environ 73 (2007) 317-326.

[16] M. Kouzu, T. Kasuno, M. Tajika, Y. Sugimoto, S. Yamanaka, J. Hidaka, Fuel 87 (2008) 2798-2806.

[17] A. P. S. Diaz, J. Puna, M. J. N. Correia, I. Nogueira, J. Gomes, J. Bordado, Fuel Processing Technology 116 (2013) 94-100.

[18] P. Nair, B. Singh, S. N. Upadhyay, Y. C. Sharma, Journal of Cleaner Production 29-30 (2012) 82-90.

[19] D. Kumar, A. Ali, Energy Fuels 24(3) 2010 2091-2097.

[20] N. Kaur, A. Ali, Fuel Processing Technology 119 (2014) 173-184.

[21] S. Benjapornkulaphong, C. Ngamcharussrivichai, K. Bunyakiat, Chem Eng J 145 (2009) 468-474.

[22] M.C.G. Albuquerque, D.C.S Azevedo, C.L Cavalcante Jr., J. Santamaria-Gonzalez, J.M. Merida-Robles, R. Moreno-Tost, et al., J Mol Catal A. Chem 300 (2009) 19-24.

[23] A. Johari, B. B. Nyakuma, S. H. Mohd Nor, R. Mat, H. Hashim, A. A., Zaki Y. Zakaria, T. A. T. Abdullah, Energy 81 (2015) 255-261.

[24] S. George, C. Arumughan, JAOCS 69 (3) (1992) 283-287.

[25] A. da Silva Cesar, D. E. Werderits, G. L. de Oliveira Saraiva, R. C. da Silva Guabiroba, Renewable and Sustainable Energy Reviews 72 (2017) 246-253.

[26] H. Berchmans, S. Hirata, Bioresource Technology 99 (2008) 1716-1721.

[27] J. Posom, P. Sirisomboon, Biosystems Engineering 130 (2015) 52-59.

[28] A. Kawashima, K. Matsubara, K. Honda, Bioresour. Technol. 100 (2009) 696-700.

[29] C. Plank, E. Lorbeer, J. of Chromatography A 697 (1995) 461-468.

[30] M. Kouzu, T. Kasuno, M. Tajika, S. Yamanaka, J. Hidaka, Applied Catalysis A.

General 334 (2008) 357-365.

[31] S. H. Teo, U. Rashid, Y. H. Taufiq-Yap, Energy Conversion and Management 87 (2014) 618-627.

[32] T. Watanabe, J. Liao, M. Senna, J. of Solid State Chemistry 115 (1995) 390-394.

[33]. M. Weibel, R. K. Mishra, ZKG 6 (2014) 29-39.

[34] P. Jakson, G.D. Parfitt, J. Chem. Soc., Faraday Trans. 1, 68 (1972) 1443-1450.

[35] R. Ladera, E. Finocchio, S. Rojas, J.L.G. Fierro, M. Ojeda, Catalysis Today 192 (2012) 136-143.

[36] M. Juarez, C. Osawa, M. Acuna, N. Samman, Food Control 22 (2011) 1920-1927.

[37] N. U. Soriano Jr., R. Venditti, D. S. Argyropoulos, Fuel 88 (3) (2009) 560-565.

APPENDIX Chromatogram of Methyl Esters

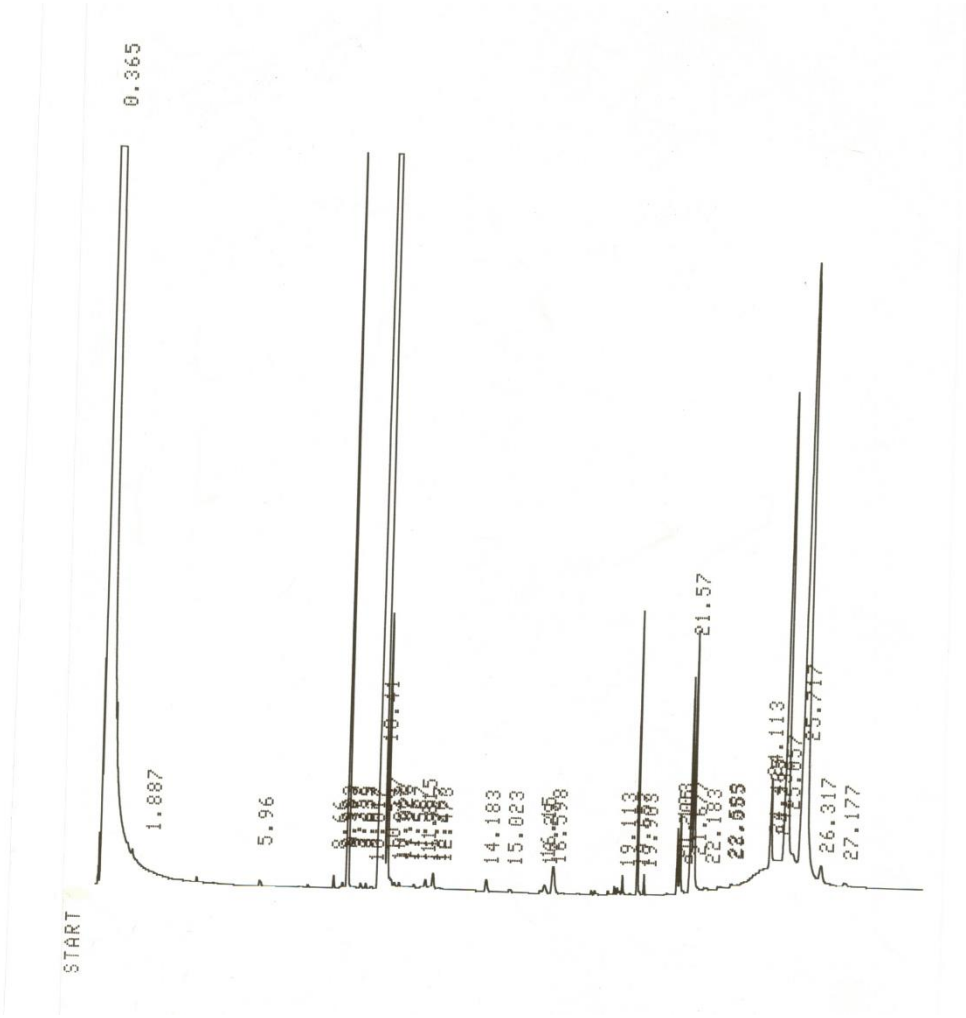

Fig. S1 Chromatogram ME with oil feedstock soybean oil

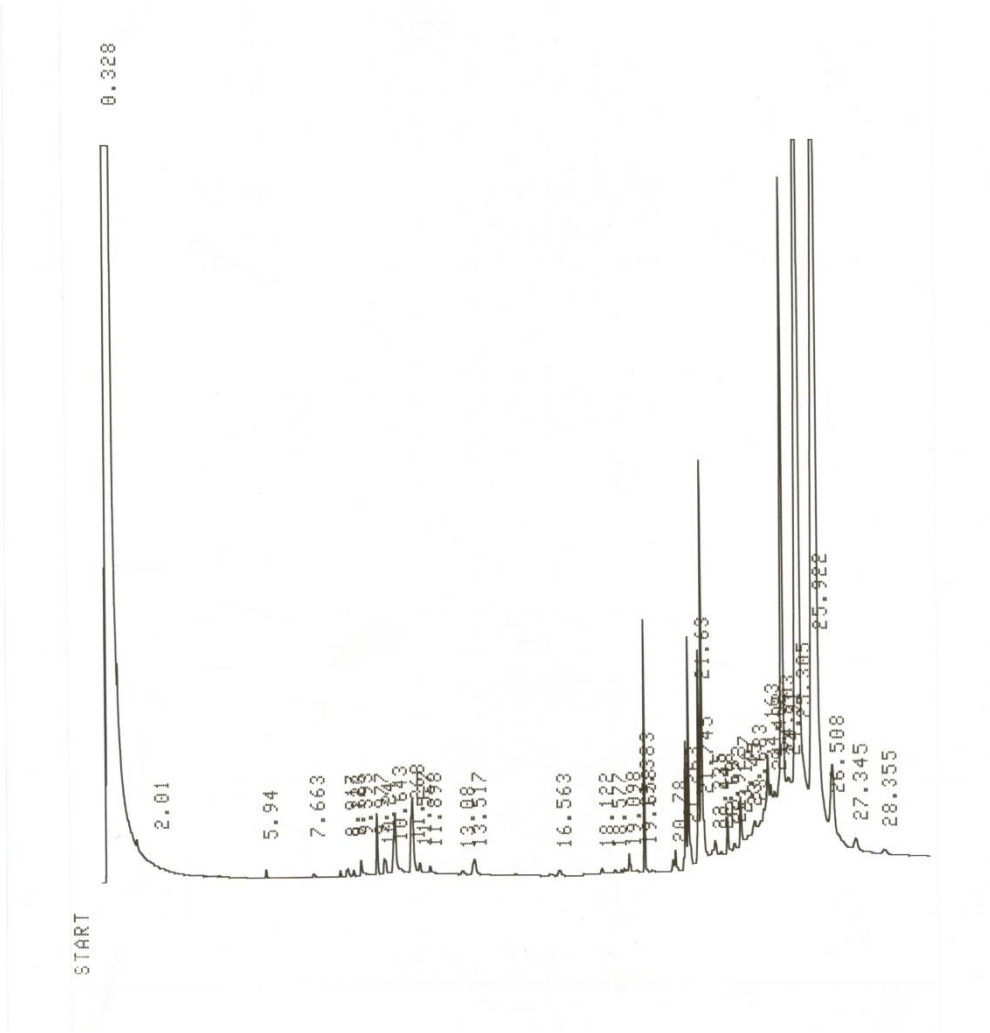

Fig. S2 Chromatogram ME with oil feedstock waste cooking oil

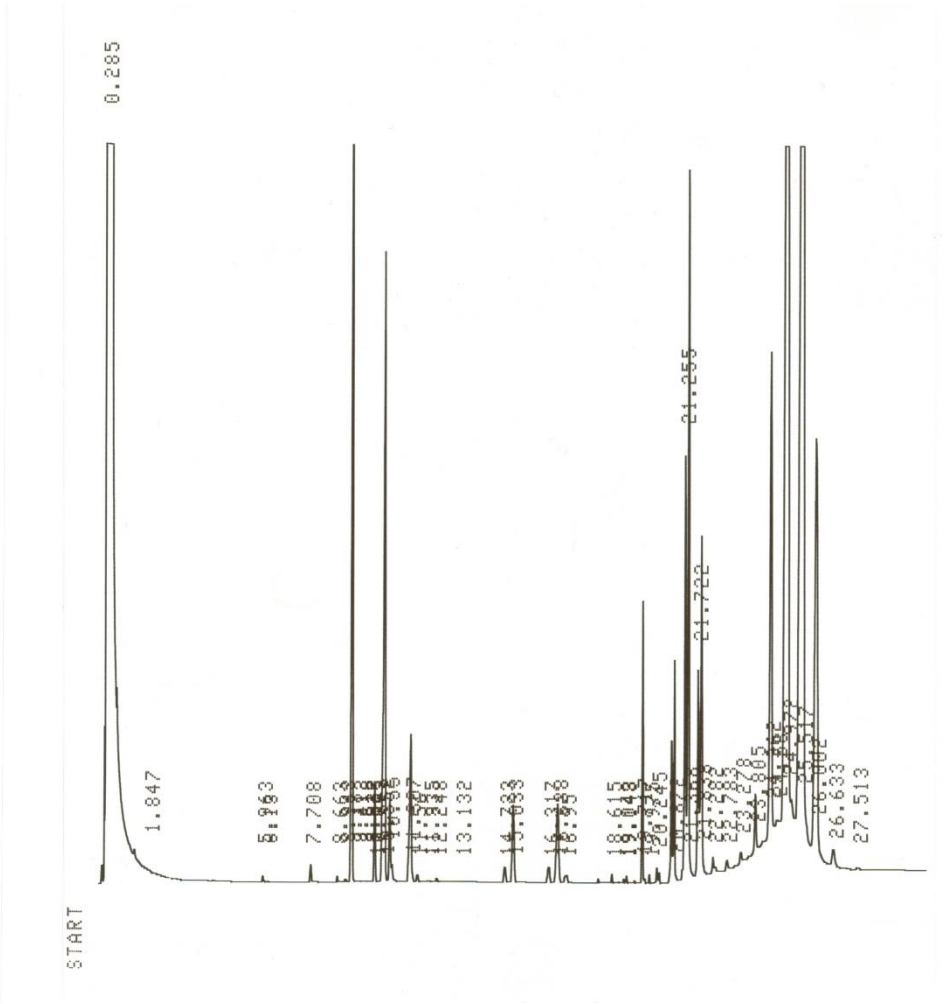

Fig. S3 Chromatogram ME with oil feedstock crude palm oil

Chapter 5

Concluding Remarks

This dissertation considers CaO-based catalyst used in transesterification reaction of oil feedstocks in wide range quality. The fact, CaO-based catalyst has many drawbacks, such low reaction rate, requires long time to achieve the maximal ME production, requirement of high methanol to oil ratio and very susceptive to free fatty acid and water content. Looking for the optimum of structure of CaO-based catalyst to improve its catalytic activity and stability and allow its long-term usage still remains a challenge. This dissertation is dedicated to developing an intensified nano-grinding method for improving physicochemical properties of CaO-based catalyst derived from scallop shell for biodiesel production.

In chapter 2, clarifying true catalytic active site on CaO catalyzed transesterification reaction to biodiesel was studied. The finding was the important of reduction in calcium diglyceroxide formation time during the early stages of the transesterification. Calcium diglyceroxide was a true catalytic active site on transesterification catalyzed by CaO-based catalyst. Reduction of transformation CaO active site into calcium diglyceroxide was arising from the combination of high SSA and effective active phase composition on the catalyst surface. To prepare the catalyst, CaO derived from scallop shells processed using the methanol-assisted dry nano-grinding technique. It is found that this technique, assisted by methanol, was able to enhance the specific surface area, as well as altering the composition of active phases on the surface of the catalyst: using different grinding conditions, also detected that calcium oxide, calcium methoxide, and calcium hydroxide could form during the process. Another finding found that changing the active surface phase composition of CaO-ss could modify the basicity in either direction, and from the results, it can be concluded that combining high SSA with Ca hydroxide surface phase composition is an effective strategy for reducing the mass transfer limitations during the initial stages

of reaction. This was indicated by the rapid formation of calcium diglyceroxide at the beginning of the reaction: this species plays an important role in the methanolysis reaction in two ways, firstly by promoting miscibility between the oil and methanol, and secondly, its function as a highly active catalyst for ester formation. The reusability of the catalyst was up to 5 cycles.

In chapter 3, enhancing scallop shell-derived CaO catalyst activity on biodiesel producing from waste cooking oil by alcohol-assisted nano-grinding was studied. This study demonstrated alcohol-assisted on nano-grinding process was efficient to improve the physicochemical properties and the catalytic features of CaO-based catalyst. After being treated by alcohol-assisted nano-grinding with three kind of alcohol, the CaO-based catalyst with higher SSA, reduced-particle sizes and generated active sites on CaO surface, such as Ca-oxide, Ca-hydroxide and Ca-alkoxide, and the presence of Lewis acid sites on surface catalyst was obtained. The catalysts were able to complete the transesterification of WCO having up to 10 wt% FFA and 0.11 wt% moisture content and gave ME yields above 98.5 % in 2 h reaction. The high performance of the catalysts due to large surface area that could serve the reaction, high dispersion of catalyst and the presence of Lewis acid sites on the catalyst surface. Contribution of dispersibility of catalysts imply the importance of active sites to promote the dispersion of CaO catalyst in both methanol and WCO.

The CaO-based catalyst treated exhibited high tolerance with moisture content due to the presence alkoxy-shielding on the surface of catalysts that could reduce the polarity of catalyst surface. However, reducing the polarity on surface of catalyst made FFA easy to adsorb on surface catalyst and then deactivate the catalyst by neutralized the basicity of the catalyst and the reusability of the catalyst was so poor.

In chapter 4, effect of the free fatty acids and water content on CaO-based catalyst

activity on different vegetable oils transesterification was studied. This studied investigated the effect of FFA and water content in oil feedstock on CaO transesterification catalyzed. The CaO-based catalyst treated by 1-butanol-assisted nano-grinding was used. The CaO-based catalyst treated exhibited high tolerance with moisture content due to the presence alkoxy-shielding on the surface of catalysts that could reduce the polarity of catalyst surface. However, reducing the polarity on surface of catalyst made FFA easy to adsorb on surface catalyst and then deactivate the catalyst by neutralized the basicity of the catalyst. The yield of methyl ester is above 98.5 % in the first batch transesterification reaction in 2 h.

In conclusion, this research dissertation had succeed to develop an improved CaO catalyst with high catalytic activity by properly design of physicochemical properties of CaO derived from scallop shell. Novel alcohol-assisted nano-grinding was used to design and modify physicochemical properties of CaO derived from scallop shell, namely SSA, basicity, size, hydrophobicity, Lewis acid-sites and catalyst dispersibility. According to the catalytic testing that carried out in this study, the catalyst tolerates to FFA (up to 10 wt%) and water content (up to 4 wt%) in oil feedstock. CaO catalyst that produced by novel alcohol-assisted nano-grinding seem to gradually near the practical level. Although the planetary ball mill technology that used in nano-grinding method need a conditional solution for making the alcohol-assisted nano-grinding became feasible technology to produce high activity of CaO catalyst in large scale, the essential of properties of design high catalytic activity CaO catalyst was established in this research dissertation. Finally, it should be noted that CaO catalyst developed by alcohol-assisted nano-grinding is a significant technology to achieve the utilization of CaO catalyst for the industrial biodiesel production, because this catalyst tolerable to FFA and water content.

List of Publications

Frisda R. Panjaitan, Shinya Yamanaka, Yoshikazu Kuga, Soybean oil methanolysis over scallop shells-derived CaO prepared via methanol-assisted dry nano-grinding, Advance Powder Technology, In press.

Frisda R. Panjaitan, Shinya Yamanaka, Yoshikazu Kuga, Enhancing scallop shell-derived CaO catalyst activity on biodiesel producing from waste cooking oil by alcohol-assisted nano-grinding, Fuel Processing Technology, submitted.

Frisda R. Panjaitan, Shinya Yamanaka, Yoshikazu Kuga, Effect of the free fatty acid and water content on structural changes of CaO catalyst prepared by alcohol-assisted nano-grinding on low-grade oils transesterification, Powder Technology, submitted.

Acknowledgements

I would like to express my sincere gratitude to my advisor, Dr. Shinya Yamanaka, for his continuous support and guidance in research and study. His mentorship, insight and encouragement will continue to inspire me both personally and professionally. I would like to acknowledge Prof. Yoshikazu Kuga for his valuable time, helpful guidance and critical of this doctoral dissertation. I would also like to thank Indonesian Oil Palm Research Institute for providing me the scholarship. I would also like to express my thanks to Oiso Takahiro for his tutorship during my study in Muroran city, to Yurna Yenni, my senior in Indonesian Oil Palm Research Institute for her spirit encouragement in my study. Finally, I want to thank my parents, my sisters and my brothers, and to all the laboratory member since 2014-2016 in Laboratory Surface and Chemical Engineering, Muroran Institute of Technology. I thank you all, for supporting me to accomplish my doctoral study in Muroran Institute of Technology.